EXPERIMENTS ON NON-EQUILIBRIUM SUPERSONIC FLOW SHOCK STAND-OFF DISTANCE OF SPHERES CARRIED OUT IN A NEW TYPE OF INTERMITTENT WIND TUNNEL

George Buzyna and Peter P. Wegener
Department of Engineering and Applied Science
Yale University

May 1969

ARNOLD ENGINEERING DEVELOPMENT CENTER
AIR FORCE SYSTEMS COMMAND
ARNOLD AIR FORCE STATION, TENNESSEE

NOTICES

When U. S. Government drawings specifications, or other data are used for any purpose other than a definitely related Government procurement operation, the Government thereby incurs no responsibility nor any obligation whatsoever, and the fact that the Government may have formulated, furnished, or in any way supplied the said drawings, specifications, or other data, is not to be regarded by implication or otherwise, or in any manner licensing the holder or any other person or corporation, or conveying any rights or permission to manufacture, use, or sell any patented invention that may in any way be related thereto.

Qualified users may obtain copies of this report from the Defense Documentation Center.

References to named commercial products in this report are not to be considered in any sense as an endorsement of the product by the United States Air Force or the Government.

EXPERIMENTS ON NON-EQUILIBRIUM SUPERSONIC FLOW SHOCK STAND-OFF DISTANCE OF SPHERES CARRIED OUT IN A NEW TYPE OF INTERMITTENT WIND TUNNEL

George Buzyna and Peter P. Wegener

Department of Engineering and Applied Science
Yale University

FOREWORD

The work reported herein was conducted under Program Element 62201F, Project 8952, Task 08.

The present technical report #1 on Contract AF 40(600)-1133 with Yale University, "Non-equilibrium Flow in Supersonic Aerodynamics", principal investigator: Peter P. Wegener, covers one completed phase of the work outlined in the first proposal directed to DCS - Research, AEDC. This proposal by Yale University, Department of Engineering and Applied Science, was dated 3 February 1965 and carried the same title as the above quoted contract. The project monitor was Captain Harold L. Rogler, USAF Advanced Plans Division, Directorate of Plans and Technology. The work was carried out in the period 1 July 1965 to 31 December 1966, covering problem c. of page 4 of the proposal, and it was submitted on August 15, 1967. In addition, the design, construction and theoretical and experimental performance of a new type of intermittent wind tunnel is described. This facility was built in lieu of the straight shock tube described in the proposal. Because of the interest in this facility, an informal 44 page progress report entitled "A New Facility for Non-equilibrium Flow Studies and Preliminary Results on Flow about Spheres", by George Buzyna and Peter P. Wegener, dated 15 July 1966, had previously been submitted to DCS - Research. Other than some firing range data in Section IV, all material in this progress report has been incorporated in the present report #1 which therefore supersedes the older publication. In this way the phases discussed have now been completely reported.

Helpful discussions and advice by Drs. B. T. Chu, I. J. Eberstein, and G. Wortberg are gratefully acknowledged.

This technical report has been reviewed and is approved.

Harold L. Rogler
Captain, USAF
Advanced Plans Division
Directorate of Plans
and Technology

Edward R. Feicht
Colonel, USAF
Director of Plans
and Technology

ABSTRACT

An experimental investigation of the non-equilibrium behavior of the shock stand-off distance ahead of spheres is described. Wind tunnel experiments using a well understood reacting model gas mixture with a single relaxation process are performed. A marked variation of the dimensionless shock stand-off distance as a function of a non-equilibrium parameter patterned after that proposed by Damköhler is observed. Qualitatively, the results are found to be in agreement with theoretical predictions in the literature.

A new application of the Ludwieg tube intermittent supersonic wind tunnel to the study of non-equilibrium flow is presented in the process of this work. The behavior of the intermittent tunnel as a tool in non-equilibrium flow research is calculated in some detail. Experimental results on the facility performance are included for comparison.

TABLE OF CONTENTS

		Page
List of Illustrations		vi
List of Symbols		viii
I.	Introduction	1
II.	Background: Ideal Inviscid Gas Flow	3
III.	Background: Real Inviscid Gas Flow	9
IV.	Experimental Approach	13
V.	Experimental Equipment	15
VI.	Experimental Results	22
VII.	Analysis of Experimental Results	35
VIII.	Summary	46
Appendix I.	Properties of the Model Reacting Gas Mixture	49
Appendix II.	Properties, Calibration, and Detailed Description of the Tube Wind Tunnel and the Experimental Procedure	54
Appendix III.	Equilibrium Flow Analysis in the Tube Wind Tunnel	72
Appendix IV.	Non-Equilibrium Flow Analysis in the Nozzle and Non-Equilibrium Flow Through a Shock Wave	79
Appendix V.	Reduction of Experimental Data	85
Appendix VI.	Numerical Calculations	90
References		96

LIST OF ILLUSTRATIONS

		Page
Figure 1	A schematic diagram of the supersonic flow field near the forward portion of a sphere at free stream Mach number M=2	3
Figure 2	Dimensionless stand-off distance as a function of free stream Mach number and specific heat ratio, γ, for a sphere of radius R	5
Figure 3	Dimensionless stand-off distance as a function of the free stream Mach number for a sphere of radius R in air, $\gamma = 1.4$	6
Figure 4	Dimensionless stand-off distance as a function of the density ratio across the normal shock wave and the specific heat ratio γ for a sphere of radius R (after Van Dyke and Gordon 1959)	8
Figure 5	Freeman's (1958) representation of the dimensionless shock stand-off distance as a function of a non-equilibrium parameter Λ	11
Figure 6	A simplified representation of the dimensionless stand-off distance as a function of Mach number with non-equilibrium effects	12
Figure 7	Schematic drawing of Ludwieg's tube wind tunnel and the wave diagram of the flow	16
Figure 8	Schematic drawing of the present tube wind tunnel and the wave diagram of the flow	18
Figure 9	Pressure vs. velocity - an approximate representation of the flow in the tube wind tunnel	20
Figure 10	Sharp focus shadowgraphs of the flow fields about 1/32 (on the left) and 1/2 (on the right) inch diameter spheres in dry nitrogen at $M_\infty = 1.5$. The flow is from left to right.	23
Figure 11	Dimensionless stand-off distance as a function of sphere diameter	30
Figure 12	Sharp focus shadowgraph of the non-equilibrium flow field about a 1/2 inch diameter sphere at $M_\infty = 1.36$ ($\omega_o = 0.301$). The flow is from left to right.	32

Page

Figure 13 Static pressure trace of the flow in the nozzle side wall, oscilloscope trace (ω_o = 0.215, T_4 = 298.8°K, p_4 = 876 mm Hg). The arrow indicates the time at which the sharp focus shadowgraph is taken. 33

Figure 14 Static pressure trace of the starting process and testing time in the nozzle side wall, oscilloscope trace (ω_o = 0.215, T_4 = 298.8°K, p_4 = 876 mm Hg). The arrow indicates the time at which the sharp focus shadowgraph is taken. 33

Figure 15 Dimensionless stand-off distance as a function of the Damköhler parameter 38

Figure 16 Dimensionless stand-off distance as a function of the density ratio across the normal shock wave for a sphere 40

Figure 17 Dimensionless stand-off distance as a function of the Damköhler parameter 41

Figure 18 Dimensionless stand-off distance as a function of the Damköhler parameter 44

Figure 19 Dimensionless stand-off distance as a function of the Damköhler parameter 45

LIST OF SYMBOLS

Commonly used symbols are defined below. All other symbols are defined where needed.

A	cross-sectional area of nozzle
a	speed of sound
D	Damköhler's non-equilibrium parameter
h	enthalpy
K_p	equilibrium constant in pressure units
k_D	dissociation rate constant
k_R	recombination rate constant
L	length of pressure tube
M	Mach number = u/a
p	pressure
R	radius of sphere
R	universal gas constant
r	tube radius
r_D	dissociation rate
r_R	recombination rate
T	temperature
T*	characteristic temperature defined by Equation (I.2)
t	time coordinate
u	velocity
x	distance coordinate
α	degree of dissociation of NO_2
γ	ratio of specific heats

Δ	stand-off distance
δ	boundary layer thickness
δ^*	boundary layer displacement thickness
Λ	Freeman's non-equilibrium parameter
ω_i	mass fraction of ith species
ω_o	total reactant mass fraction
τ	characteristic time scale
ρ	density
ρ_*	characteristic density defined in Equation (I.2)
μ	molecular weight
[i]	concentration of ith species
$\Delta h_{N_2O_4}$	heat of dissociation of N_2O_4 per gram of N_2O_4

Subscripts

e	equilibrium state
f	frozen state
s	condition immediately behind the shock wave
o	stagnation condition
1	undisturbed state of the gas in the dump tube
2	state of the gas behind the right facing shock wave in the dump tube
3	state of the gas between the contact surface and the left facing shock wave or expansion fan in dump tube
3'	state of the gas between the left facing shock wave or expansion fan in the dump tube and the exit of the nozzle
4	undisturbed state of the gas in the pressure tube
4'	state of the gas between the expansion fan in the pressure tube and the entrance of the nozzle

∞ free stream condition in the test section

Primed variables denote dimensional quantities.

INTRODUCTION

Flight at hypersonic speeds, such as is encountered during entry of planetary atmospheres, gives rise to high temperature flow fields about the vehicle. At such high temperatures, vibrational excitation, dissociation, chemical reaction, ionization, etc. of the constituents of the atmosphere may occur. Excitation of these degrees of freedom and the establishment of thermodynamic equilibrium requires a certain amount of time. If the characteristic time to establish thermodynamic equilibrium in a gas is comparable to the time it takes for a fluid particle to pass through any region of interest in the flow, non-equilibrium states will occur in these regions. The existence of such non-equilibrium states has an appreciable effect on the flow field.

The occurrence of non-equilibrium states in the flow fields about bodies during the entry into planetary atmospheres has led to an extensive study of the non-equilibrium flow fields about blunt bodies. Blunt bodies form an important class of aerodynamic shapes and are of great practical importance in that they maintain low aerodynamic heating of the body during the entry of the atmosphere.

The flow field about a blunt body is characterized by a detached bow shock wave at some distance ahead of the body. The distance between the bow wave and the body along the stagnation stream line, the stand-off distance, is strongly affected by non-equilibrium states in the flow field, and reflects the non-equilibrium behavior of the flow about the body. The present research is directed towards the study of the shock stand-off distance as a function of the extent to which the flow is out of equilibrium in the region between the shock wave and the body.

A considerable amount of work on the non-equilibrium flow about blunt bodies has been reported in the literature. This work has been largely of approximate-analytical (e.g. Ref. 1), analytical-numerical (e.g. Ref. 2), and purely numerical (e.g. Ref. 3) nature. In general, the most successful methods have been numerical. Despite the large number of methods in existence, none of these can be considered as completely successful (4). The solution of the flow about a blunt body, and particularly the non-equilibrium flow, still remains one of the more difficult problems in aerodynamics.

Relatively little experimental work of fundamental nature has been reported on the non-equilibrium behavior of the stand-off distance. Experiments have been performed in pure gases with vibrational excitation (5) and non-equilibrium dissociation (6), and in multi-component gas mixtures such as air (7) with more than one non-equilibrium mode. Although these experiments demonstrate the effect of a non-equilibrium flow on the stand-off distance, they do not separate the non-equilibrium behavior

from other relevant parameters of the flow field, e.g. the Mach number. The behavior of the stand-off distance as a function of the extent to which the flow is out of equilibrium with all other relevant parameters maintained constant is not directly demonstrated.

In the present study of the non-equilibrium behavior of the stand-off distance, an experimental approach is adopted. The dimensionless stand-off distance is studied as a function of a non-equilibrium parameter (the ratio of a characteristic flow time to a characteristic time required for the establishment of thermodynamic equilibrium from an excited state) with all other relevant parameters of the flow field maintained constant. A flow field is considered which exhibits only a single non-equilibrium mode, i.e. dissociation, and whose rate process and thermodynamic properties are known.

II
BACKGROUND: IDEAL INVISCID GAS FLOW

A blunt body moving at supersonic speed will exhibit a detached bow shock wave some distance ahead of it. The stand-off distance, i.e. the shortest distance between the shock wave and the stagnation point, is a characteristic feature of such a flow. A schematic representation of an axisymmetric supersonic flow past a sphere is shown in Figure 1. The flow behind the shock wave is subsonic in a small region near the stagnation point and it accelerates through sonic to supersonic speeds as the fluid in the shock layer, i.e. the fluid between the shock wave and the body expands around the body. This mixed flow field consisting of the subsonic, transonic and supersonic regions is also a characteristic feature of a blunt body flow.

Although the stand-off distance can be recorded and measured experimentally with relative ease, its analytic calculation remains one of the more difficult problems in aerodynamics. The difficulty arises as a consequence of the nature of the mixed flow and the unknown location

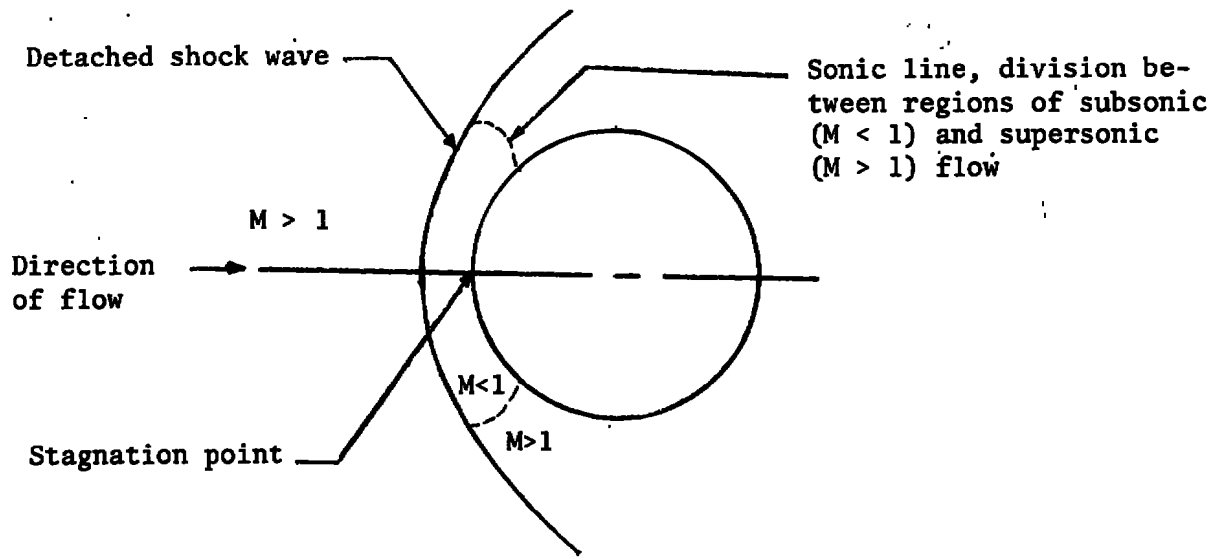

Fig. 1 A schematic diagram of the supersonic flow field near the forward portion of a sphere at free stream Mach number M = 2

of the boundaries, i.e. the shock wave and the sonic region. A number of analytical and semi-analytical methods have been developed in recent years to calculate axisymmetric flow fields. These methods, however, suffer from poor convergence (4) and generally require simplifying assumptions that limit their application to hypersonic flow. Analytical methods, thus far, have not been successful over the entire supersonic-hypersonic range. A number of approximate analytical results for hypersonic flow, expressed in terms of the density ratio across the normal shock, are available (see Refs. 8 and 9). A review of analytical treatments can be found in Ref. 10 and a comprehensive treatment of many methods in Ref. 9.

The most accurate calculation of the subsonic flow field and of the shock stand-off distance has been obtained from numerical solutions. Many of these numerical methods, however, cannot be regarded as successful because they rely unduly on human insight, are insufficiently automated, and require much computing effort (4).

The behavior of the shock stand-off distance with respect to its variables may be conveniently represented by considering a dimensionless stand-off distance with respect to some characteristic length of the body. For an inviscid, thermally and calorically perfect gas flow the dimensionless shock stand-off distance depends only on the free stream Mach number M (ratio of the velocity of a fluid element or the speed of the body to the local sound speed) and the specific heat ratio of the gas. The variation of the dimensionless shock stand-off distance with Mach number and specific heat ratio for a sphere is shown in Figure 2. Van Dyke and Gordon's numerical results (11) and Kendall's experimental work (12) are shown here. Van Dyke's numerical calculations give an excellent representation of the shock stand-off distance variation, and these calculations are in good agreement with experimental results and other numerical results. Note that the stand-off distance decreases rapidly with increasing Mach number M for low values of M and remains relatively independent of the Mach number at hypersonic speed, $M > 5$. As the Mach number grows larger, the stand-off distance approaches asymptotically towards a limiting value. This is a consequence of the fact that for a thermally and calorically perfect gas the density ratio across the normal shock wave reaches a limiting value as $M \to \infty$, and the stand-off distance is a strong function of the density ratio. A noticeable change in stand-off distance is also observed with a change in the specific heat ratio at constant Mach number.

An expanded region of the dimensionless stand-off distance at low Mach numbers for a sphere is shown in Figure 3. This range is of interest to the present work. Note that at low Mach numbers the stand-off distance is strongly dependent on the Mach number and disagreement between authors increases as the Mach number decreases.

The shock stand-off distance may also be represented graphically as a function of the density ratio across the normal shock wave on the

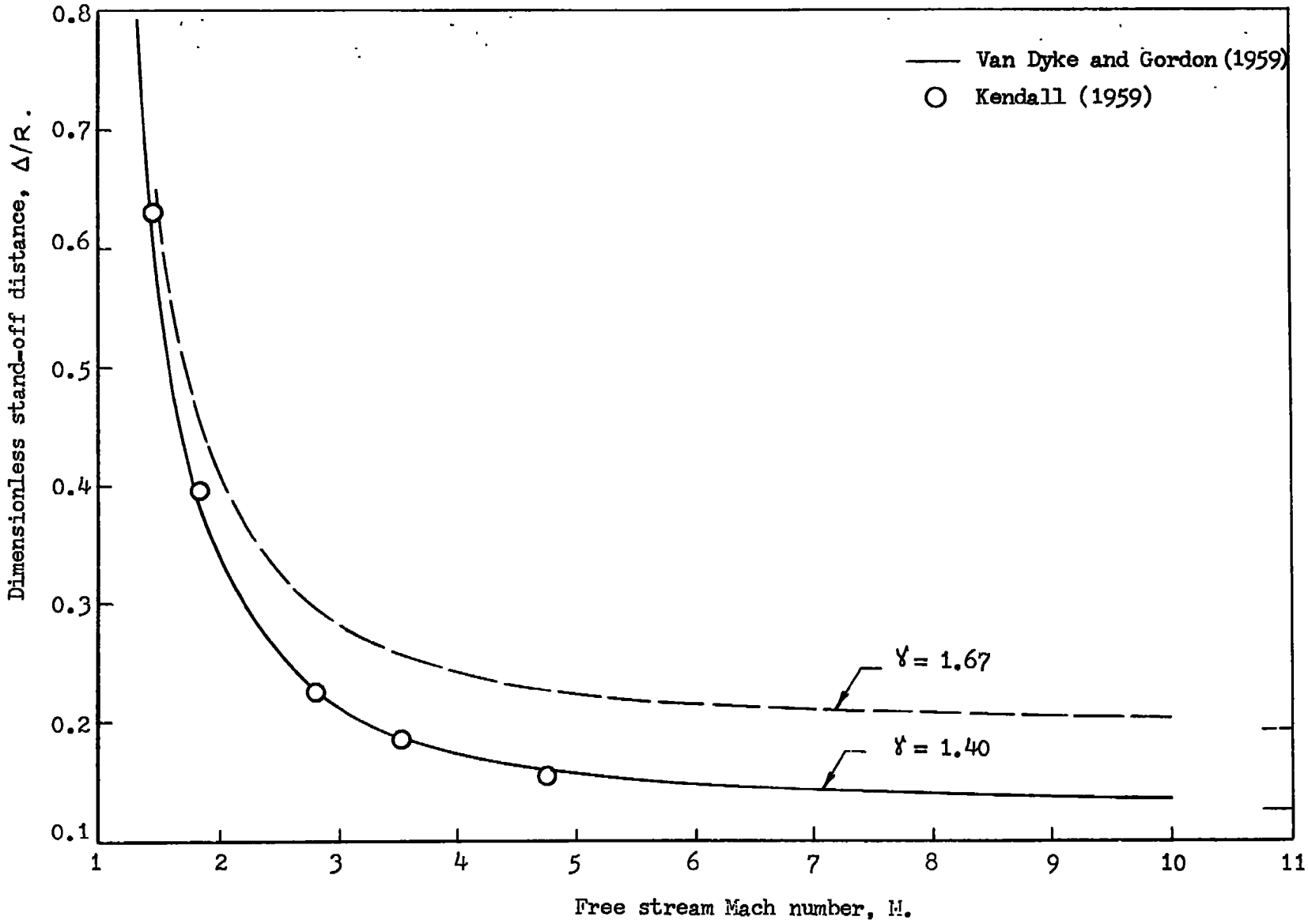

Fig. 2 Dimensionless stand-off distance as a function of free stream Mach number and specific heat ratio, γ, for a sphere of radius R

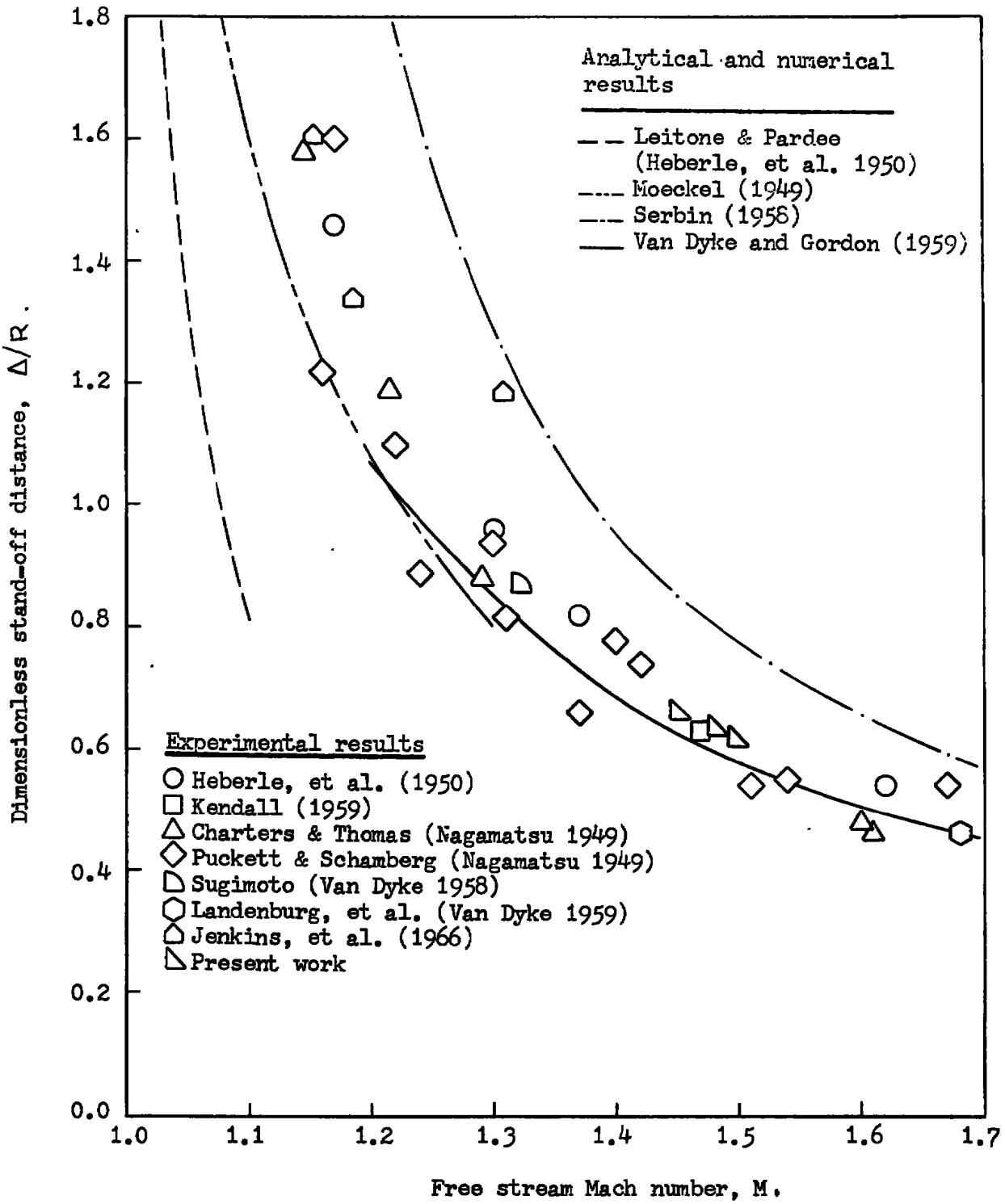

Fig. 3 Dimensionless stand-off distance as a function of the free stream Mach number for a sphere of radius R in air, $\gamma = 1.4$

stagnation streamline. In such a representation the dependence on the specific heat ratio becomes weak. The variation of the dimensionless stand-off distance with the density ratio taken from numerical calculations of Van Dyke and Gordon (11) for a sphere is shown in Figure 4. Here, the logarithm of the dimensionless stand-off distance, $\log(\Delta/R)$, is given as a function of the logarithm of the ratio of the density jump across normal shock wave to the free stream density, $\log((\rho_s-\rho_\infty)/\rho_\infty)$. This particular representation is useful in that short segments of the curve can be approximated by straight lines.

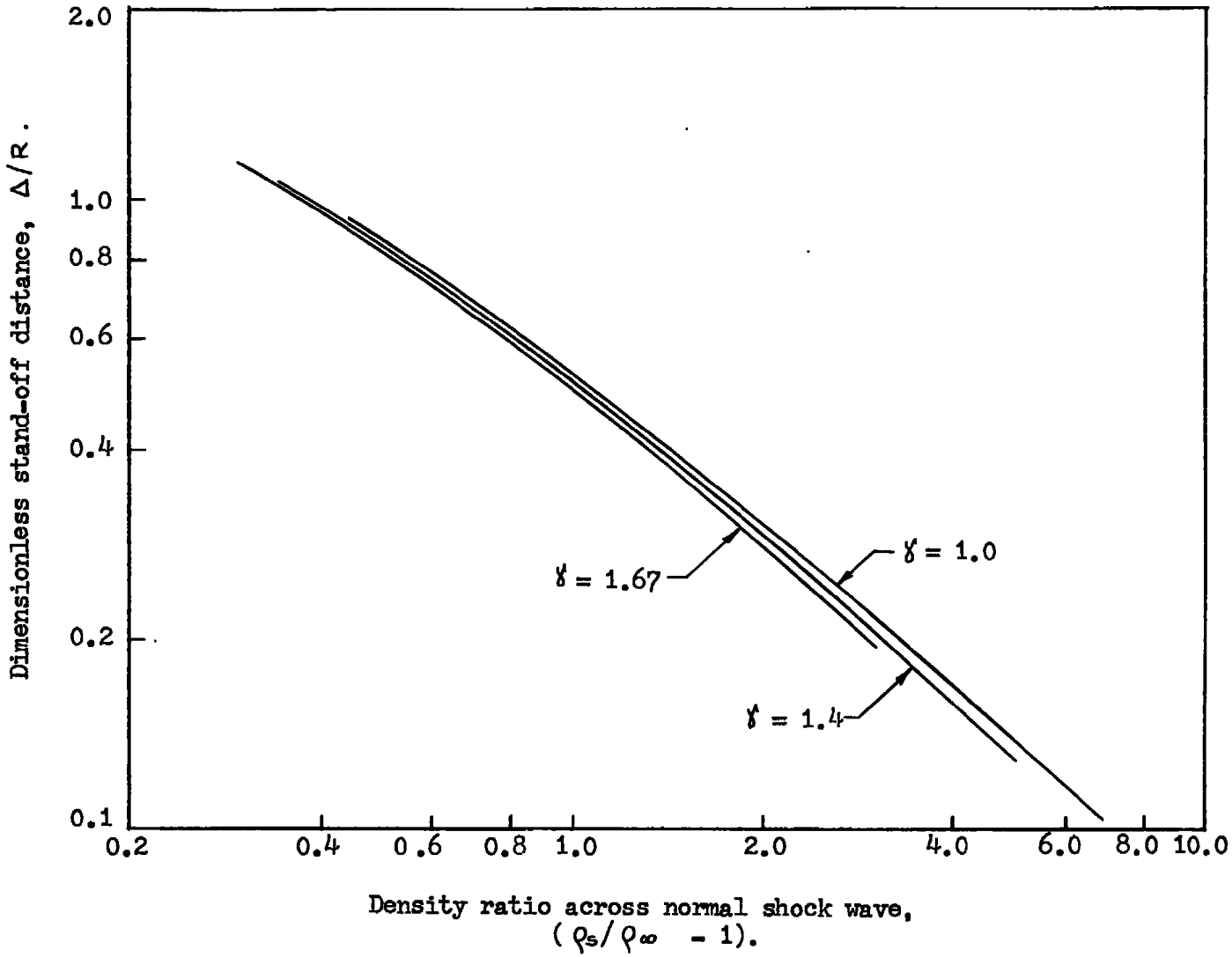

Fig. 4 Dimensionless stand-off distance as a function of the density ratio across the normal shock wave and the specific heat ratio γ for a sphere of radius R (after Van Dyke and Gordon 1959)

III
BACKGROUND: REAL INVISCID GAS FLOW

The development of flight at hypersonic speeds has led to the study of real gas effects in blunt body flows. In such high speed flows the temperature attained behind the strong bow shock wave is high enough that the internal degrees of freedom (rotation, vibration, dissociation, chemical reaction, ionization, etc.) of the constituents of the gas may become excited. For air, for example deviation from ideal gas behavior can be noticed at a temperature of approximately 2,500°K where vibrational relaxation becomes important and oxygen begins to dissociate. This temperature corresponds to a free stream Mach number of approximately six in air at standard conditions. At a temperature of 4,000°K, oxygen dissociation is complete and the dissociation of nitrogen begins, while at 8,000°K nitrogen dissociation is complete and ionization of atoms begins (9). Excitation of these internal degrees of freedom and the establishment of equilibrium requires a certain amount of time. The characteristic times to establish equilibrium for the various degrees of freedom frequently differ appreciably from each other. Equilibrium in the translational degree of freedom, the external degree of freedom, is established most quickly, and the characteristic time is of the order of the average time between molecular collisions. For example, in air at standard conditions the characteristic time is of the order of 10^{-10} sec. (13). Establishment of equilibrium in the internal degrees of freedom requires considerably more time. For oxygen if the time to establish equilibrium in the translational degree of freedom is t_c, then the characteristic time to establish equilibrium in the rotational mode is of the order of 10 to 10^2 t_c, and in the vibrational mode is of the order of 5×10^5 t_c (14). If the time it takes for a fluid element to traverse a region of interest in a flow is of the order of the characteristic times required for the establishment of thermodynamic equilibrium, non-equilibrium states will occur in the flow. In general, the existence of non-equilibrium thermodynamic states has an appreciable effect on the flow field. The non-equilibrium flow behavior can be conveniently described by Damköhler's first parameter (15), given as the ratio of a characteristic flow time to a characteristic time which describes the rate process. If the characteristic time of the rate process is much smaller than the characteristic flow time, the flow field will be in equilibrium, and if the characteristic time of the rate process is much larger than the characteristic flow time the flow is denoted as a frozen flow.

A considerable amount of analytical work has also been done on the non-equilibrium flow about a blunt body. However, the addition of a rate equation to the governing equations further complicates the already difficult calculation of the inviscid flow without excited internal degrees of freedom. Numerical methods here have also been generally more successful.

The non-equilibrium behavior of the dimensionless stand-off distance with a single non-equilibrium mode may be conveniently described in terms of an ideal dissociating gas postulated by Lighthill (16) and extended to non-equilibrium conditions by Freeman's rate equation (1). Viscosity, thermal conduction and diffusion are neglected. For high speed flow with a strong shock wave the functional relationship between the dimensionless stand-off distance, Δ/R, and its relevant dimensionless parameters can be expressed by (17)

$$\frac{\Delta}{R} = \frac{\Delta}{R}\,(M_d,\ \eta,\ \alpha_\infty,\ D), \tag{1}$$

where R denotes a characteristic dimension, M_d the ratio of the kinetic energy of the flow to the dissociation energy of the gas, η the ratio of the free stream density to a characteristic dissociation density, α_∞ the free stream degree of dissociation, and D a non-equilibrium or Damköhler parameter. A qualitative study of the variation of the dimensionless stand-off distance with a non-equilibrium parameter for the above dissociating gas has been conducted by Freeman (1). He considered analytically the non-equilibrium flow about a sphere with the aid of a modified Newtonian theory of hypersonic inviscid flow. Freeman's computed results for $M_d = 1$, $\eta = 10^{-6}$ and $\alpha_\infty = 0$ is shown in Figure 5. The non-equilibrium parameter Λ used by Freeman is the ratio of the sphere size to the characteristic length scale of the dissociation process and is essentially equivalent to the Damköhler parameter. The overall effect of the excitation of the internal degree of freedom, in this case dissociation, of the molecules is to absorb some of the energy associated with the active degrees of freedom and thereby reduce the translational temperature of the gas. In a hypersonic blunt body flow the change in pressure in the shock layer due to non-equilibrium effects is relatively small (1). The main effect of the excitation of the internal degree of freedom is to further increase the density behind the shock wave. The increased density in the shock layer will tend to decrease the distance between the shock and the body due to the contraction of stream tubes and thus, the equilibrium stand-off distance is smaller than the corresponding frozen stand-off distance. Since the density in the shock layer is sensitive to non-equilibrium changes, the stand-off distance is also a sensitive parameter. The greatest variation in the stand-off distance occurs near the frozen limit and the approach to the equilibrium limit is asymptotic, Figure 5. It is shown by Freeman that the stand-off distance for an ideal dissociating gas flow can change by as much as 50 percent between the limits of a gas with constant specific heats and a dissociated gas in thermodynamic equilibrium. For more complicated gases such as air with a number of coupled chemical reactions, a variation between the limits is also calculated to be as high as 50 percent (18). Since Freeman's work, the non-equilibrium variation of the stand-off distance for other gas models has been demonstrated by Lick (3) with the use of a numerical method, by (2) with a semi-analytical method and by other authors with different variations of these methods. In general, the results of these authors show the same qualitative behavior of the stand-off distance with a non-equilibrium parameter.

Relatively little experimental work concerned with the non-

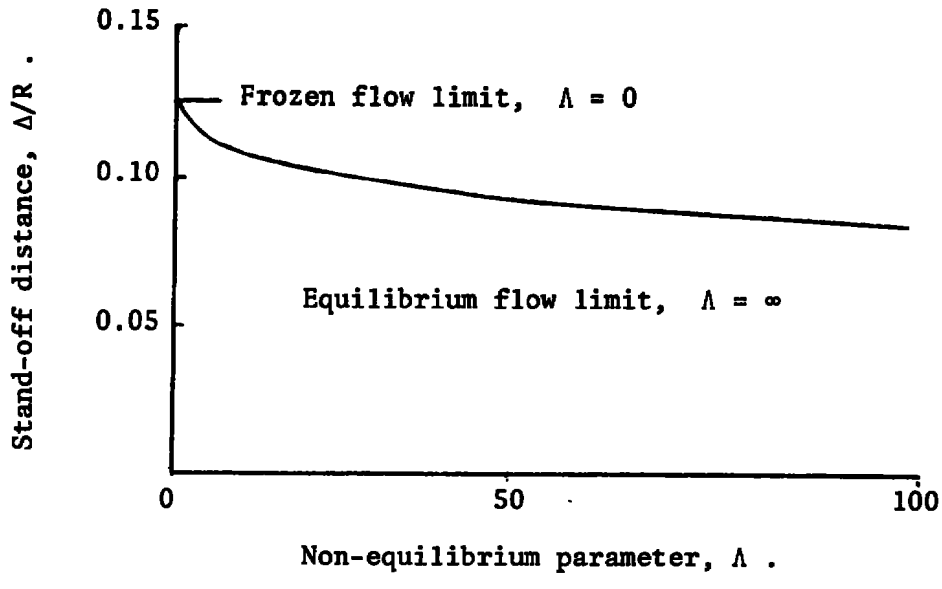

Fig. 5 Freeman's (1958) representation of the dimensionless shock stand-off distance as a function of a non-equilibrium parameter Λ

equilibrium behavior of the shock stand-off distance has been reported in the literature. A qualitative representation of the experimental work simplified to the behavior with one internal mode is shown in Figure 6. At low speeds, or Mach numbers, the temperature behind the detached shock is too low for the internal mode to become activated. As the speed of the body is increased, the excitation of the internal mode begins to take place and the shock stand-off distance begins to depart from its frozen curve toward another curve where the speed and temperature are high enough for the equilibration of the internal mode to take place immediately behind the shock wave. The transition region between these curves represents non-equilibrium flow. The behavior described above is essentially what has been observed by Schwartz and Eckerman in their experiments with vibrational excitation in chlorine gas (5). Similar behavior has also been observed with dissociation of oxygen (6) and dissociation of the components of air (7). Eckerman (6) used the fact that the stand-off distance is sensitive to non-equilibrium states to deduce the dissociation reaction rates of oxygen. Although experiments have demonstrated the effects of non-equilibrium flow on the stand-off distance, they do not show an explicit behavior of the stand-off distance as a function of a non-equilibrium parameter alone as expressed, for example, in Figure 5 or implied by Equation (1). Generally, the non-equilibrium effect is produced by a change in the free stream conditions or the speed of the projectile and therefore, other relevant parameters of the flow field are varied simultaneously with the non-equilibrium parameter.

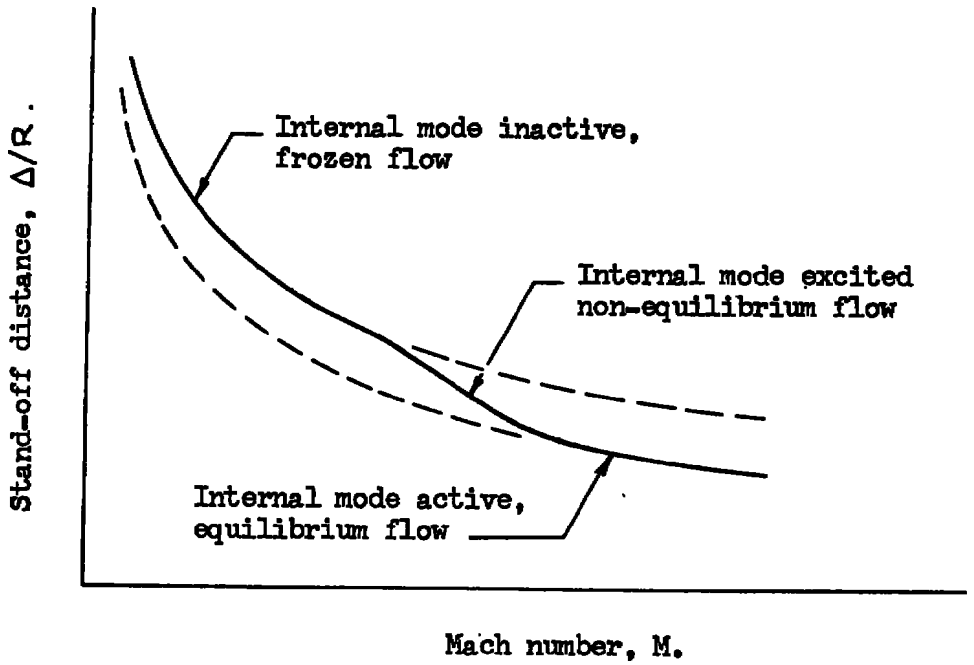

Fig. 6 A simplified representation of the dimensionless stand-off distance as a function of Mach number with non-equilibrium effects

IV
EXPERIMENTAL APPROACH

In the present study of the non-equilibrium behavior of the stand-off distance an experimental approach is adopted. It is assumed that only one non-equilibrium mode is present as also discussed by Wood and Kirkwood (19) and that viscosity, thermal conduction and diffusion can be neglected. The non-equilibrium mode is represented by a dissociation process and is given by a reacting gas mixture of nitrogen tetroxide and dioxide carried at low concentration in inert nitrogen, and is given by

$$N_2 + N_2O_4 \rightleftarrows N_2 + 2NO_2 \tag{2}$$

where the mole fraction of reactants is less than $n_R = 0.20$. It is assumed that the individually taken participating components of the mixture are thermally and calorically perfect gases. The thermodynamic properties of this model gas mixture are known at equilibrium (20) and its rate mechanism is known from shock tube experiments (21) and non-equilibrium nozzle flow experiments (22). The above reaction is well understood and has been used previously as a model for aerodynamic studies in nozzles (23) and a ballistic range (24). A further advantage of this reaction is that it occurs at room temperature and strong shock waves are not required to cause significant dissociation and departure from equilibrium. The physical properties and a detailed description of the model gas mixture are given in Appendix I.

The non-equilibrium flow about a blunt body in the above model gas mixture can be described in terms of four independent parameters. A functional relationship between the dimensionless stand-off distance Δ/R and its relevant dimensionless parameters may be expressed in the form

$$\frac{\Delta}{R} = \frac{\Delta}{R}(M_\infty, \omega_o, \alpha_\infty, D) \quad , \tag{3}$$

where M_∞ is the free stream Mach number with respect to the free stream frozen sound speed, ω_o the mass fraction of reactants, α_∞ the degree of dissociation of reactants in the free stream, and D the Damköhler parameter. These parameters are deduced from the dimensionless form of the governing equations and boundary conditions which describe the inviscid non-equilibrium flow about a blunt body (the variables are non-dimensionalized with respect to the physical properties of the model gas). The significance of the reactant mass fraction is that it determines the physical properties of the model gas mixture. In particular, it determines the heat of reaction of the gas mixture, and the characteristic reaction time or relaxation time for a given free stream and shock strength.

It is evident from Equation (3) that a study of the dimensionless stand-off distance solely as a function of the Damköhler parameter requires all other parameters to be constant (c.f. Ref. (1) and Figure (5)). The Damköhler parameter may be varied either through the characteristic reaction time or through the characteristic flow time. In the present experimental approach only the variation of the characteristic flow time is feasible. The characteristic reaction time can not be varied since it is dependent upon the free stream conditions and the reactant mass fraction, and these, in turn, can not be varied without simultaneously varying the other parameters of the problem. The characteristic flow time is taken as the time required by a fluid element to flow through the stand-off distance, and the sphere is taken as the blunt body. One recalls that for a flow in an ideal gas at a constant Mach number and a given specific heat ratio, the dimensional stand-off distance for a sphere is directly proportional to its radius. A change in the sphere radius results in a corresponding change of the stand-off distance and thus, a corresponding change of the characteristic flow time. Note that the sphere radius appears only in the Damköhler parameter and not in any of the other parameters expressed in Equation (3). The experimental approach therefore, consists of a set of experiments with a number of different sphere diameters (a number of different characteristic flow times) conducted in identical and known equilibrium free-streams (fixed characteristic reaction time), and these experiments are conducted in a supersonic wind tunnel.

V
EXPERIMENTAL EQUIPMENT

The experimental work is conducted in an intermittent supersonic wind tunnel which has been designed and fabricated for this work. A wind tunnel has been selected since it is most suited for the adopted approach, i.e. free streams in the test section can be kept constant and the sphere sizes can be easily interchanged. Preliminary experiments have been tried in a ballistic range. However, the range has been found to be impractical since body size could not be easily varied.

The intermittent supersonic wind tunnel is modeled after the device originally suggested by Ludwieg (Refs. (25) and (26)) in conjunction with a contest to devise an inexpensive supersonic wind tunnel for educational purposes. Ludwieg's tunnel is essentially a blow down wind tunnel in which the supply tanks are replaced by a long tube. The length of this tube governs the duration of the operation. A schematic of such a tunnel is shown in Figure 7. The supply tube is closed at one end and at the opposite end a convergent-divergent nozzle with test section is attached. In principle, the supply tube could be curled up for increased length. The tube is filled with a compressed gas and the nozzle flow is initiated by releasing a quick opening valve, as suggested by Ludwieg, or rupturing a diaphragm as employed here. Expansion waves travel from the diaphragm into the tube and accelerate the gas toward the nozzle. As soon as the nozzle throat becomes choked, as determined by the ratio of nozzle throat to tube area, the strength, or pressure ratio, of the expansion fan becomes fixed. Thus, for an inviscid gas a region of constant pressure, density, temperature and velocity is created between the expansion fan and the nozzle inlet. This region serves as the supply condition for a steady flow expansion through the nozzle exactly like a constant pressure and temperature reservoir for an ordinary intermittent wind tunnel. The duration of steady nozzle flow is determined by the length of the tube, i.e., the time required for the expansion fan to reach the end wall of the tube and return to the nozzle.

An idealized schematic diagram of the described one-dimensional flow in the t - x plane is also shown in Figure 7. The discharged gas may be dumped into a tank or the atmosphere in case the test section pressure is higher than the ambient air pressure. Two such tunnels, one in Germany (27) and the other in England (28) are described in the literature and are in operation.

The tunnel built here is similar to Ludwieg's except for the portion of the tunnel into which the gas is discharged. The dump tank in this case is another tube, of approximately the same length as the pressure tube, attached to the tunnel at the diaphragm section. Although the flow in the pressure tube is identical to the tube proposed by Ludwieg, the entire tunnel is operated as a shock tube with a nozzle at the diaphragm

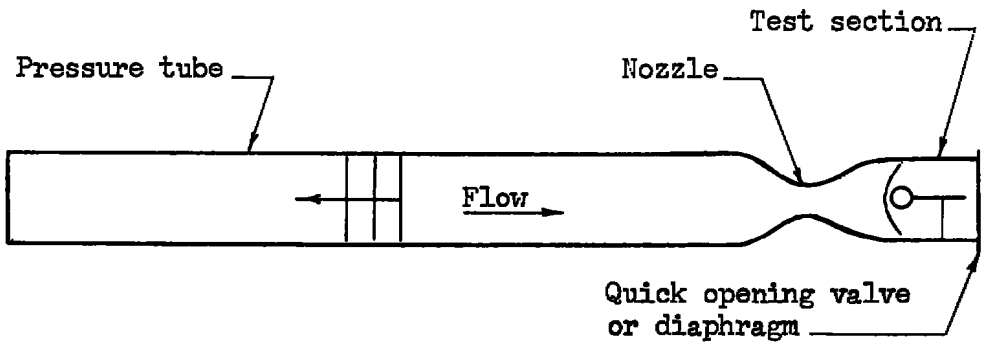

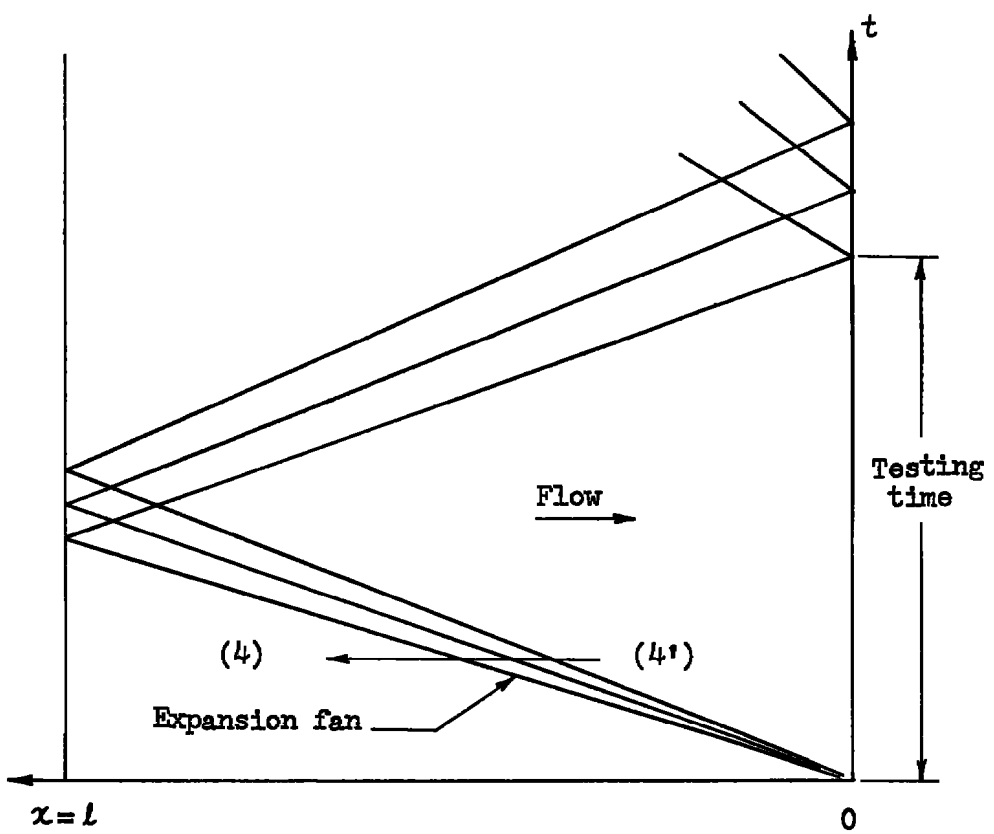

Fig. 7 Schematic drawing of Ludwieg's tube wind tunnel and the wave diagram of the flow

section. The details of the design and construction of the tube as well as the apparatus for the preparation of the model gas mixture are shown in Appendix II.

The operation of the tunnel is as follows. The pressure tube is filled to the desired pressure with dry air, nitrogen, or the carefully prepared reacting mixture. The dump tube is evacuated to the appropriate pressure level or to lower pressure. The cellophane diaphragm is ruptured and the flow is initiated. Expansion waves travel into the pressure tube and accelerate the gas toward the nozzle while a shock wave travels into the dump tube.

In order to simplify the discussion of the theory of the tube tunnel, at first an ideal operation will be assumed similar to that applied to shock tubes. The gas is assumed to be thermally and calorically perfect and inviscid. Since the nozzle section of the tube is short compared with the overall length, it is assumed that the nozzle is located at the diaphragm section and is very narrow, i.e., the area changes at the diaphragm are discontinuous. One can thus speak of the tunnel as if it were a shock tube with a nozzle at the diaphragm (29). A schematic of such a tube is given in Figure 8.

In the case of a shock tube the flow at the diaphragm section is steady, thus, by an addition of a nozzle at this location a steady expansion is possible if both tube ends are of infinite length. Thus, if the throat is sonic, the Mach number ahead of the nozzle M_4, and the Mach number at the nozzle exit M_3, is uniquely fixed by the geometry of the tube, i.e., by the cross-sectional area ratios of driver tube to nozzle throat and dump tube to nozzle throat, respectively (29). The Mach number M_4, is given by the subsonic portion of the steady flow and M_3, by the supersonic portion. A wave diagram of the above flow is also shown in Figure 8.

After diaphragm rupture, left facing waves travel into region (4) of the high pressure tube or driver section. The strength of the expansion wave is determined and fixed by the geometry of the tube. Region (4') behind the expansion becomes fixed and has uniform thermal and flow properties. A right facing shock wave passes into region (1) of the low pressure end of the tunnel. A contact surface follows the shock wave. In the region between the contact surface and the exit of the nozzle, two modes of operation are possible. In the case of high pressure-tube to dump-tube pressure ratios, p_4/p_1, a left facing expansion wave separates regions (3') and (3). Whereas for low ratios of p_4/p_1, a left facing shock wave separates the two regions. The entire tunnel flow, as well as the two possibilities between region (3) and (3') is clearly shown in a p/p_1 vs. u/a_1 graph, Figure 9. Steady nozzle flow time is determined by the time it takes the expansion fan to leave the nozzle, reflect from the end wall of the tube, and return to the nozzle.

The use of the high pressure tube and nozzle as an intermittent wind tunnel has been suggested as stated previously by Ludwieg. The

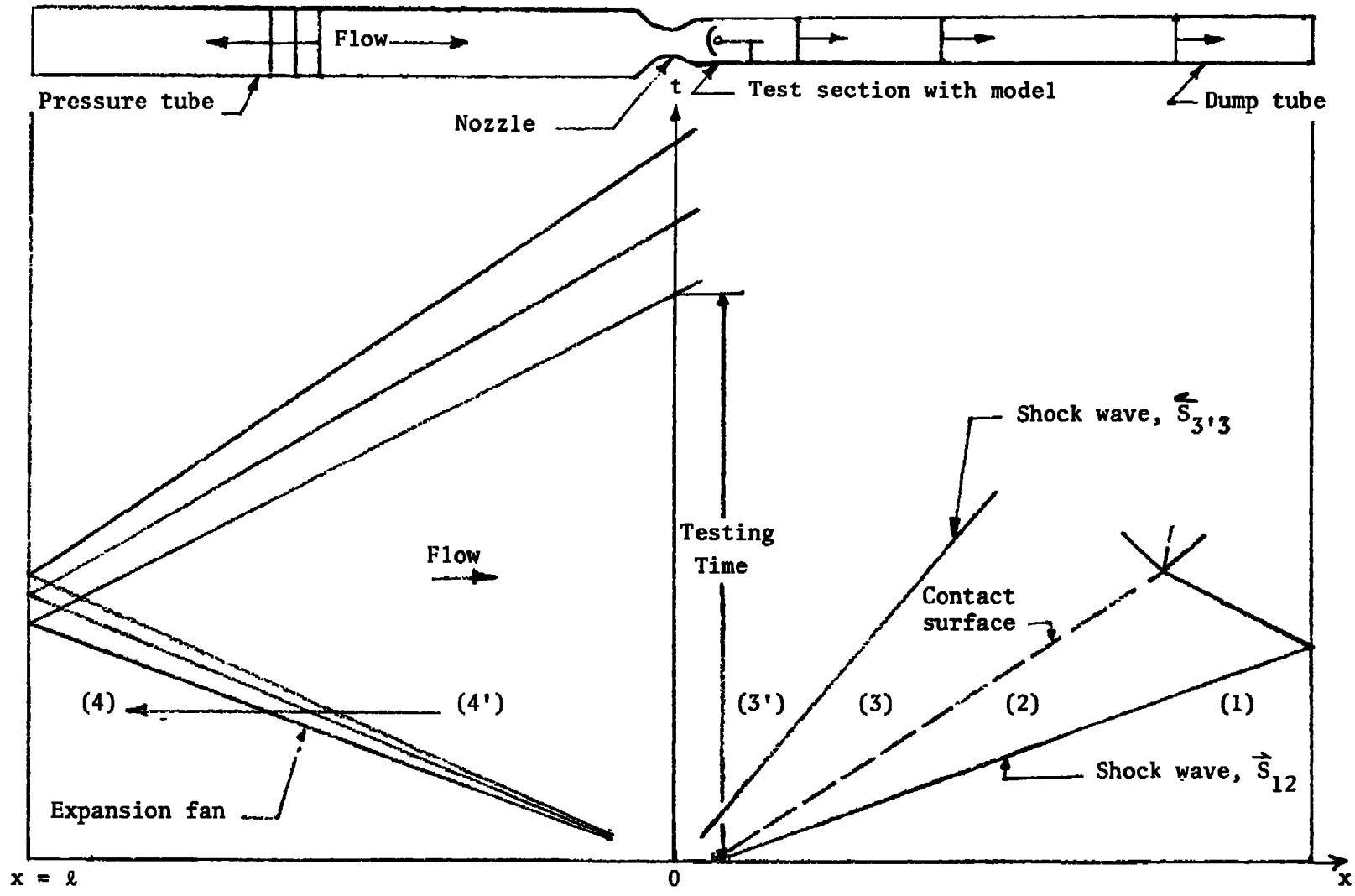

Fig. 8 Schematic drawing of the present tube wind tunnel and the wave diagram of the flow

tunnel constructed here is the same in principle except for the nature of the dump tank and its attendant operation. The choice to operate the tunnel with a shock tube type dump section and operation has been made in order that one may utilize the property of the shock wave as an accurate, reproducible and experimentally simple trigger for the electronic instrumentation. In this manner flow observation by photograph, movie, interferometry, etc., can be made reproducibly.

The calculation of test time and properties ahead of the nozzle, as well as the stagnation conditions for the nozzle flow, have been discussed by Becker (30) and Cable and Cox (28) for ideal operation with a thermally and calorically perfect gas. These derivations are not repeated here; however, their results are given in Appendix II. For known stagnation conditions, the flow in the nozzle can be obtained from the tables compiled by the Ames Research Staff (31). When the tunnel is operated with the reacting gas mixture, the flow is no longer described by the equations derived for the perfect gas, and a new solution for the flow through an expansion fan and a nozzle must be obtained for each reacting gas mixture and operating conditions. Under these circumstances, the flow is assumed to be in thermal equilibrium, and the solution of the flow is given in Appendix III. The flow in the nozzle undergoes a large and rapid expansion, and it is possible that departure from equilibrium flow may occur here. To insure that the flow in the nozzle and free stream remains in equilibrium, a separate analysis is made which estimates the location in the nozzle where departure from equilibrium may occur. For this purpose the sudden freezing analysis of Bray (32) is adopted, and the calculations for the model gas are given in Appendix IV.

The analysis of the flow in the tunnel and its wave diagram is based on the assumption that the flow is inviscid and that the area change at the nozzle is discontinuous. In a real tunnel flow, however, boundary layers are formed along the tube wall and the nozzle is a large region of gradual area change. The effect of the growth of the boundary layer in the tube is to change the state of the gas ahead of the nozzle with time (33). For the present operating conditions with nitrogen, it is calculated that the effect of the boundary layer is to decrease the supply pressure at the end of the testing time by 1/2 percent of its initial value. Static pressure traces in the nozzle side wall have confirmed this estimate. The drop in the supply temperature will be much less than the drop in the pressure (26). A similar drop in pressure and temperature will also be encountered with reacting flow. Thus, for the present operating conditions it is permissible to assume that the supply conditions in the tunnel remain constant, particularly since a record of the flow is made approximately at the time when the expansion fan is reflected from the end wall of the tube. The effect of the boundary layer in the tube on the operation of the tunnel is discussed in Appendix II.

The effect of the finite size of the nozzle, in relation to the idealized representation of the flow, is to considerably complicate the flow during the initiation and early stages of the flow in the vicinity of the nozzle. The duration of the flow in the test section under idealized operation with nitrogen is estimated to be 20 milliseconds.

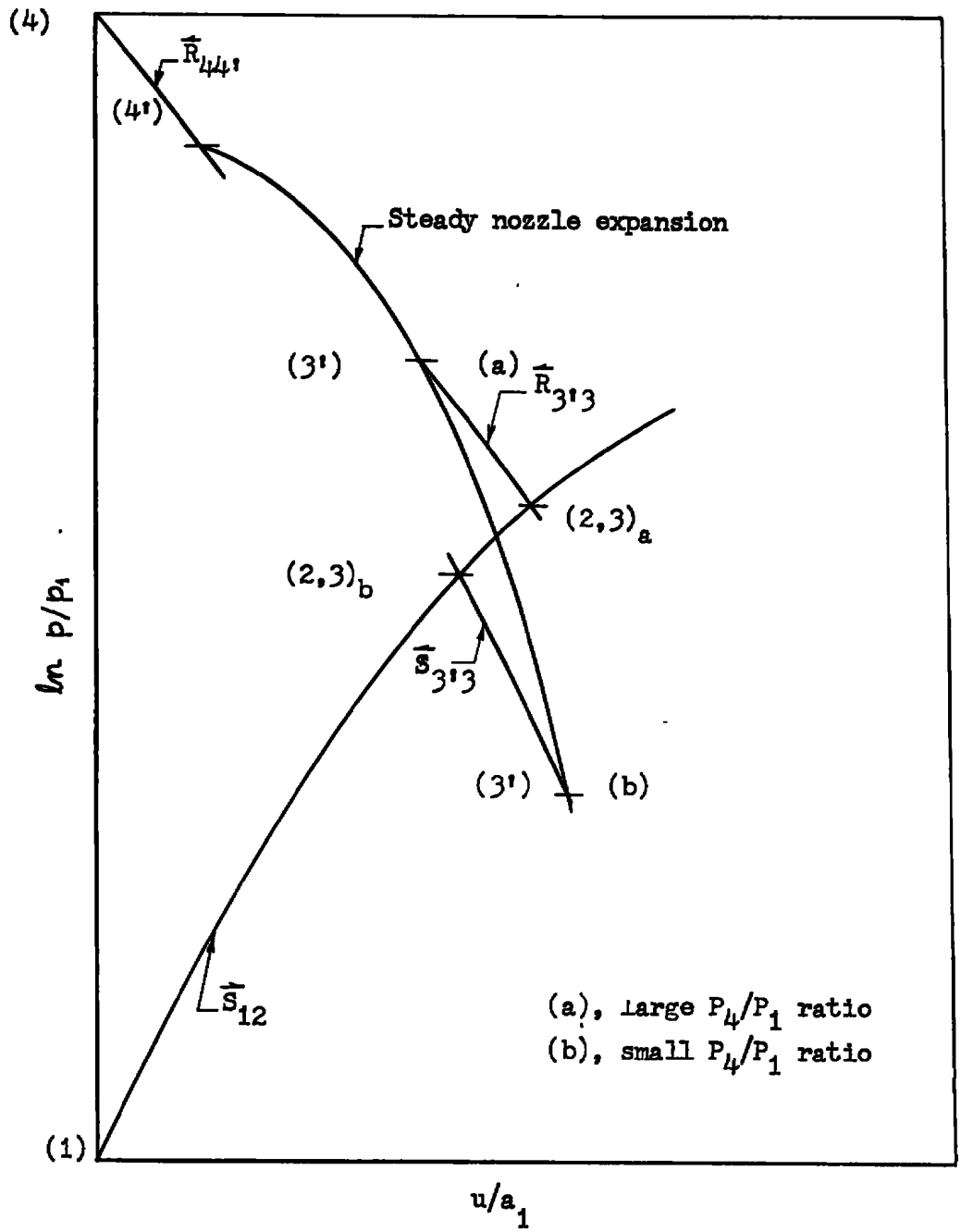

Fig. 9 Pressure vs. velocity – an approximate representation of the flow in the tube wind tunnel

$\overleftarrow{R}_{44'}$ - left facing rarefaction wave between states 4 and 4',
$\overleftarrow{R}_{33'}$ - left facing rarefaction wave between states 3 and 3',
$\overrightarrow{S}_{12}$ - right facing shock wave between states 1 and 2,
$\overleftarrow{S}_{33'}$ - left facing shock wave between states 3' and 3,
(2,3) - conditions at the contact surface.

A static pressure trace in the nozzle side wall also confirms this estimate, but with a major difference, however, only 80 percent of the total running time is steady and approximately 20 percent of the running time is required to establish the steady flow. Essentially the same result has been obtained from a movie film record (5,000 frames per second) of the shadowgraph of the flow field about a sphere in the test section. Details of the performance, calibration and operation of the tunnel are given in Appendix II.

VI
EXPERIMENTAL RESULTS

The experimental method consists of a set of experiments which are conducted in identical free-streams but with different sphere diameters. Measurements of the resulting stand-off distances constitute the experimental data. The flow field about a sphere and its stand-off distance is recorded on Kodak Tri-X Pan film by means of sharp focus shadowgraph photography in parallel light. The film is exposed by a short duration (0.5 microsecond) spark light source at approximately 12 milliseconds after the initiation of the flow in the nozzle. The measurements of the stand-off distance are taken directly from the negatives with the aid of a traveling microscope at a 60 to 1 magnification ratio. The negative is attached to the carriage of the microscope, the direction of the flow (indicated by a reference line on the negative) is lined up with the cross hairs in the microscope sights, and a reading is obtained by advancing the carriage relative to the cross hairs. Sharp focus shadowgraphs of the flow fields about 1/2 and 1/32 in. diameter spheres in nitrogen at a free stream Mach number M = 1.50 are shown in Figure 10. The camera is focused on a plane 0.01 in. from the centerline of the flow in the direction of the camera.

Experiments are conducted at two positions in the nozzle corresponding to two slightly different Mach numbers. One test position is taken at the exit of the nozzle, denoted as the exit test section, and the other 2.5 cm upstream of the exit, denoted as the upstream test section. The nozzle used here is not a parallel flow nozzle. The Mach number gradient with respect to the distance from the throat along the centerline of the nozzle is approximately $\Delta M/\Delta x = 0.015$ cm^{-1}. The largest sphere radius used is approximately R = 0.8 cm.

Stainless steel ball bearings are used as spheres and each set of experiments includes six different sphere diameters. At the exit test section, 1/32, 1/16, 1/8, 1/4, 1/2 and 5/8 in. diameter spheres are used, and at the upstream test section, 1/32, 1/16, 1/8, 1/4, 3/8 and 1/2 in. diameter spheres are used. The smallest diameter represents the smallest sphere about which the flow field can be observed with the present optical and photographic system. In the sharp focus shadowgraphs of the flow field about the smallest sphere, the shock wave image becomes faint and the definition of the sphere edge becomes important with respect to the stand-off distance. The 5/8 in. and 1/2 in. spheres in the two different testing positions represent the largest sizes which do not block the flow in the nozzle. Hence, size changes by factors of 20 and 16 are possible in the two testing positions respectively.

Experiments have been first conducted in dry nitrogen. It is recalled that for non-reacting flow, for a given Mach number and specific heat ratio, the dimensionless stand-off distance is constant. The

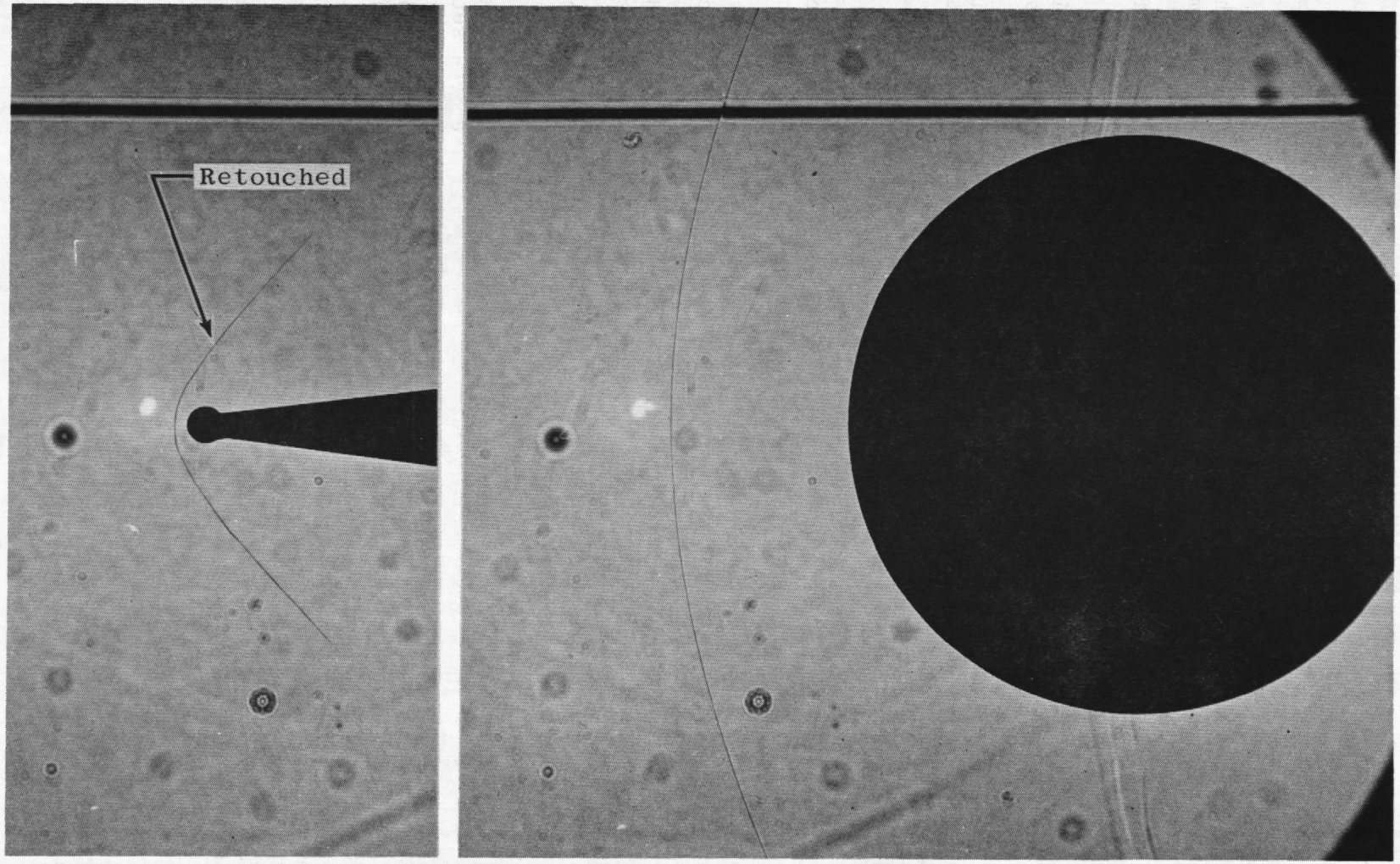

Fig. 10 Sharp focus shadowgraphs of the flow fields about 1/32 (on the left) and 1/2 (on the right) inch diameter spheres in dry nitrogen at M_∞ = 1.5. The flow is from left to right.

nitrogen experiments, therefore, are intended as calibration experiments of the flow in the test section. Each sphere is placed on the centerline of the flow and positioned so that the tip of the detached shock wave is located at approximately the same point in the nozzle free stream. A representative set of experiments conducted in dry nitrogen at the exit test section is shown in Table I. The reduction and interpretation of the raw data is given in Appendix V. The stand-off distance is read along the direction of the flow from the tip of the sphere to the center of the shock wave image, and is non-dimensionalized with respect to the measured sphere radius. The resulting dimensionless stand-off distance Δ/R is shown in the third column of Table I. Each value given in Table I, as well as in all subsequent tables, represents an average value of five readings of the same negative. Errors in the non-dimensional stand-off distances arise primarily due to reading errors of the negatives (Appendix V). The smallest sphere has the greatest uncertainty with a fractional deviation of approximately ±2.4 percent. The larger spheres have a proportionally smaller error, the largest sphere having the least uncertainty with a fractional deviation of approximately ±0.2 percent. Reproducibility of experiments, on the average, is of the order of the reading error.

A systematic variation of approximately 2.5 percent is observed in the dimensionless stand-off distance from the smaller to the largest spheres. The major portion of this variation occurs with the larger diameter spheres and can be attributed to the non-uniform flow in the nozzle test section (Appendix V). Some variation in the stand-off distance is also due to viscous effects. An effective displacement of the stand-off distance is caused by a boundary layer on the surface of the sphere. The relative variation in the dimensionless stand-off distance due to viscous effects, however, is considerably less than the variation due to non-uniform free stream between the same sphere sizes (Appendix V).

It is recalled that the approach to the present problem requires the dimensionless stand-off distance to be constant with sphere size for a non-relaxing flow. It is, therefore, desirable for purposes of interpretation to reduce or "calibrate" the variation of the dimensionless stand-off distance which arises as a consequence of the non-uniform flow in the test section. The following method of adjusting for the variation of the dimensionless stand-off distance is adopted. It is assumed that the best representation of the stand-off distance is obtained with the 1/4 in. diameter sphere. It is large enough not to be significantly affected by reading errors and yet small enough not to be significantly affected by the non-uniform free stream. A proportionality factor is then found for the other spheres which reduces the dimensionless stand-off distance to the value of the 1/4 in. diameter sphere. The dimensionless stand-off distance compensated in this manner is denoted by $(\Delta/R)^*$, or

$$\left(\frac{\Delta}{R}\right)^* = f \cdot \frac{\Delta}{R} , \qquad (4)$$

where f is an appropriate proportionality factor which compensates for non-uniform free stream and does not vary greatly from one. The result

Table I. Dimensionless stand-off distance measurements in pure nitrogen at Mach number M = 1.50

Experiment Number	Nominal Sphere Dia. (in.)	$\frac{\Delta}{R}$	$(\frac{\Delta}{R})^*$
240	1/32	0.628	0.623
241	1/16	0.629	0.624
242	1/8	0.628	0.623
243	1/4	0.623	0.623
244	1/4	0.623	0.623
245	1/2	0.617	0.624
246	1/2	0.616	0.623
247	5/8	0.614	0.623

Δ - Stand-off distance
R - Sphere radius

of the above reduction for the set of nitrogen experiments is shown in the last column of Table I.

The optical-photographic errors, viscous effects and non-uniform flow in the nozzle which appear in the nitrogen experiments also appear in the experiments conducted with the reacting gas mixtures. The reacting gas mixtures are dilute mixtures of NO_2 and N_2O_4 in nitrogen, and the physical properties of the mixture do not differ greatly from the properties of nitrogen. It is assumed that the errors encountered in the experiments with reactants are of the same order as encountered in dry nitrogen, and that the method of compensating for these errors in nitrogen flows can also be used in reacting flows. It is worth noting that the method of reducing the results with the use of Equation (4) is arbitrary and it is used here only as a means by which variations in the dimensionless stand-off distance not due to non-equilibrium effects can be minimized or excluded.

Experiments with the reacting gas mixtures are conducted at a number of different reactant concentrations. At the exit test section, sets of experiments are performed with mass fractions of ω_o = 0.216, 0.301 and 0.400, and at the upstream test section with reactant mass fractions of ω_o = 0.215 and 0.301. The reactant gas mixture can be prepared with an accuracy of less than 0.5 percent in the reactant mass fraction, and model gas mixtures are reproducible to the same accuracy. The raw measurements, dimensionless stand-off distance, Δ/R, and the

dimensionless stand-off distance compensated for the non-uniform free stream $(\Delta/R)^*$, are given in Tables II and III for the exit and the upstream test sections, respectively. The average values of the reactant mass fraction ω_o, and the temperature, T_4, and pressure, p_4, of the undisturbed gas in the pressure tube for each set of experiments are also included here. For a given set of experiments the temperature T_4 does not vary by more than 0.5°C from the average. The pressure can be controlled directly and is, therefore, within 2.5 mm Hg of the average. A graphic presentation of the compensated dimensionless stand-off distance as a function of sphere diameter is given in Figure II. Reproducibility of experiments in reacting flow is demonstrated in Table IV for the 1/4 and the 1/2 in. diameter spheres. In general, the reproducibility of the stand-off distance for a given sphere is of the order of the reading error. A sharp focus shadowgraph of reacting flow over a 1/2 in. diameter sphere at $M_\infty = 1.36$ ($\omega_o = 0.301$) is shown in Figure 12. Note the considerable darkening of the flow behind the shock wave in this photograph. This is due to the increased light absorption of the increased concentration of NO_2 behind the shock wave.

A static pressure trace in the nozzle side wall as a function of time is shown in Figure 13. The total running time is approximately 23 msec. which is somewhat longer than the corresponding time in pure nitrogen. A static pressure trace with an expanded time coordinate is shown in Figure 14. Approximately 5 msec. are required to establish steady flow in the nozzle and the flow remains steady for the remainder of the running time as demonstrated by the constant pressure in the trace. Arrows on the traces indicate the time at which sharp focus shadowgraphs are taken.

Free stream conditions for each experiment are obtained from an equilibrium solution of the flow in the tunnel for the given mass fraction of reactants and the undisturbed temperature and pressure of the gas mixture in the pressure tube. The equilibrium flow solution in the tunnel is given in Appendix III. Representative equilibrium flow conditions in the tube wind tunnel from the undisturbed state to the free stream are shown in Table V. On the basis of the approximate non-equilibrium flow analysis in the nozzle, experiments with a reactant mass fraction of $\omega_o = 0.215$ represent the lower limit of the reactant concentration for which equilibrium flow can be assumed within the accuracy of the analysis for the present initial operating conditions. The highest reactant mass fraction used in the experiments is $\omega_o = 0.400$. Experiments at higher reactant concentration are not conducted due to a number of practical considerations. The nitrogen dioxide gas has a deep red-brown color and absorbs light in the range 3,000 to 5,000 Å (34). Thus, as the concentration of reactants is increased, the light absorbed increases, and consequently, the density and contrast of the sharp focus shadowgraphs also decreases. Furthermore, at the higher partial pressures of reactants, and at the temperatures of the gas encountered at the present operating conditions in the nozzle, it is possible to attain conditions at which condensation of reactants may occur. Finally, at higher concentrations the mechanism and rates of the reaction may be in doubt. The above range

of reactant concentrations and their limitations are dependent on the state of the undisturbed gas in the tube, and this range can be changed by selecting other operating conditions. In the present set of experiments it has been convenient to operate the tunnel at room temperature and atmospheric pressure.

Table II. Stand-off distance measurements at exit test section

Experiment Number	Nominal Sphere Dia. (in)	Δ (cm)	$\frac{\Delta}{R}$	$(\frac{\Delta}{R})^*$
207	1/32	0.029	0.720	0.714
203	1/16	0.055	0.698	0.692
205	1/8	0.105	0.667	0.661
204	1/4	0.198	0.633	0.633
206	1/2	0.376	0.600	0.606
208	5/8	0.463	0.592	0.600
ω_o = 0.216, T_4 = 298.9°K, p_4 = 876 mm Hg				
189	1/32	0.028	0.700	0.694
186	1/16	0.053	0.679	0.673
187	1/8	0.100	0.641	0.635
185	1/4	0.191	0.609	0.609
188	1/2	0.366	0.584	0.590
190	5/8	0.451	0.576	0.585
ω_o = 0.301, T_4 = 297.6°K, p_4 = 876 mm Hg				
220	1/16	0.052	0.661	0.655
222	1/8	0.099	0.632	0.627
219	1/4	0.189	0.602	0.602
224	1/2	0.363	0.579	0.586
221	5/8	0.447	0.572	0.581
ω_o = 0.400, T_4 = 296.1°K, p_4 = 700 mm Hg				

Δ - Stand-off distance, R - Sphere radius.
ω_o, T_4, p_4 - average values of the reactant mass fraction and the undisturbed tube temperature and pressure, respectively.

Table III. Stand-off distance measurements at upstream test section

Experiment Number	Nominal Sphere Dia. (in)	Δ (cm)	$\frac{\Delta}{R}$	$(\frac{\Delta}{R})^*$
199	1/32	0.033	0.812	0.804
197	1/16	0.061	0.775	0.767
201	1/8	0.115	0.735	0.728
198	1/4	0.220	0.701	0.701
200	3/8	0.318	0.676	0.683
202	1/2	0.416	0.664	0.674
$\omega_o = 0.215$, $T_4 = 298.3°K$, $p_4 = 876$ mm Hg				
193	1/32	0.031	0.769	0.761
192	1/16	0.059	0.745	0.738
191	1/8	0.112	0.715	0.708
195	1/4	0.212	0.676	0.676
194	3/8	0.310	0.658	0.665
196	1/2	0.405	0.647	0.658
$\omega_o = 0.301$, $T_4 = 295.8°K$, $p_4 = 876$ mm Hg				

Δ - Stand-off distance, R - Sphere radius.
ω_o, T_4, p_4 - average values of the reactant mass fraction and the undisturbed tube temperature and pressure, respectively.

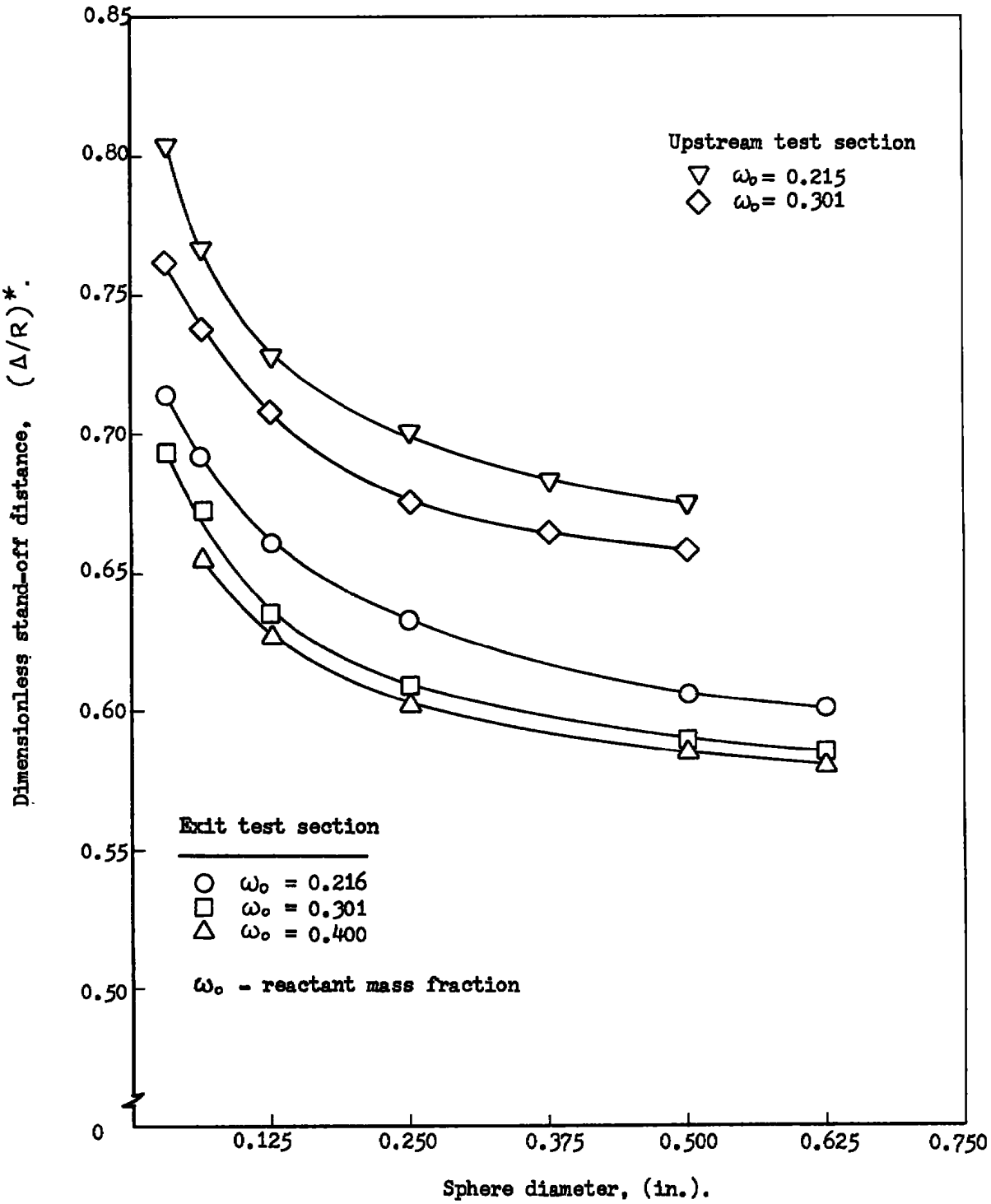

Fig. 11 Dimensionless stand-off distance as a function of sphere diameter

Table IV. Reproducibility of the stand-off distance experiments in reacting flow

Experiment Number	Nominal Sphere Dia. (in)	Δ (cm)	$\frac{\Delta}{R}$
209	1/4	0.198	0.633
210	1/4	0.198	0.633
211	1/4	0.198	0.632
212	1/4	0.198	0.632
ω_o = 0.216,	T_4 = 299.5°K,	p_4 = 876 mm Hg	
118	1/2	0.376	0.601
119	1/2	0.376	0.600
120	1/2	0.376	0.600
ω_o = 0.218,	T_4 = 296.1°K,	p_4 = 875 mm Hg	

Δ - Stand-off distance, R - Sphere radius.
ω_o, T_4, p_4 - average values of the reactant mass fraction and the undisturbed tube temperature and pressure, respectively.

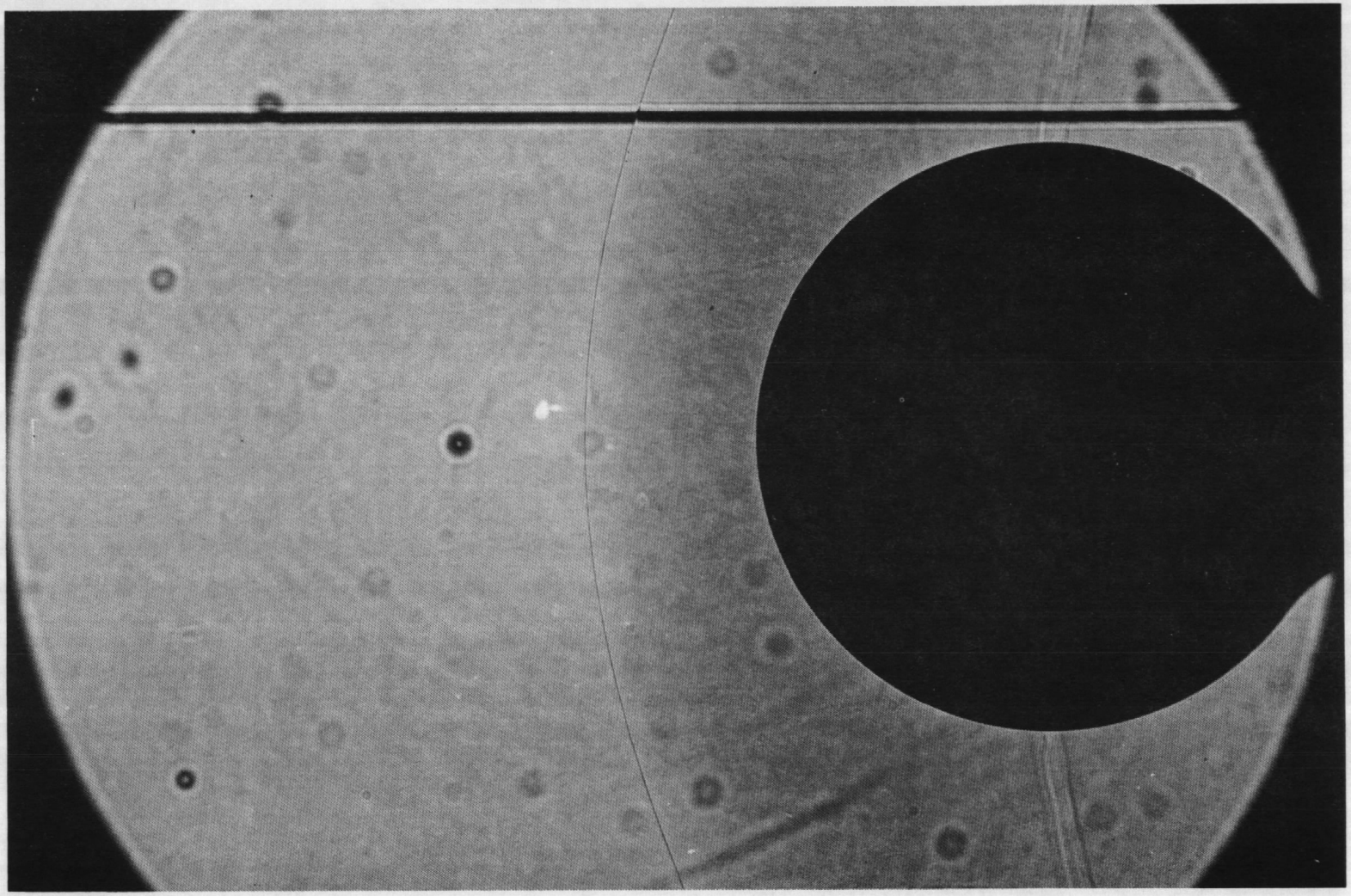

Fig. 12 Sharp focus shadowgraph of the non-equilibrium flow field about a 1/2 inch diameter sphere at $M_\infty = 1.36$ ($\omega_o = 0.301$). The flow is from left to right.

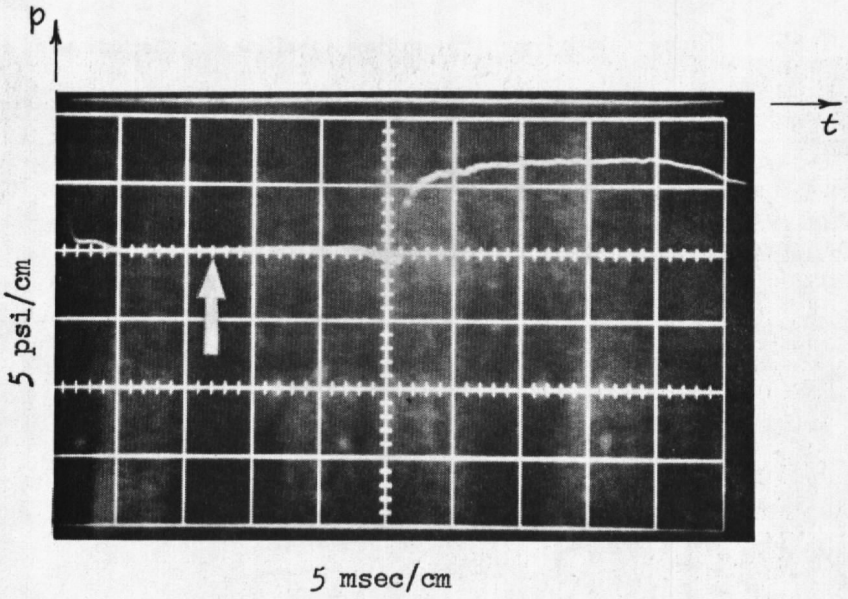

Fig. 13 Static pressure trace of the flow in the nozzle side wall, oscilloscope trace (ω_o = 0.215, T_4 = 298.8°K, p_4 = 876 mm Hg). The arrow indicates the time at which the sharp focus shadowgraph is taken.

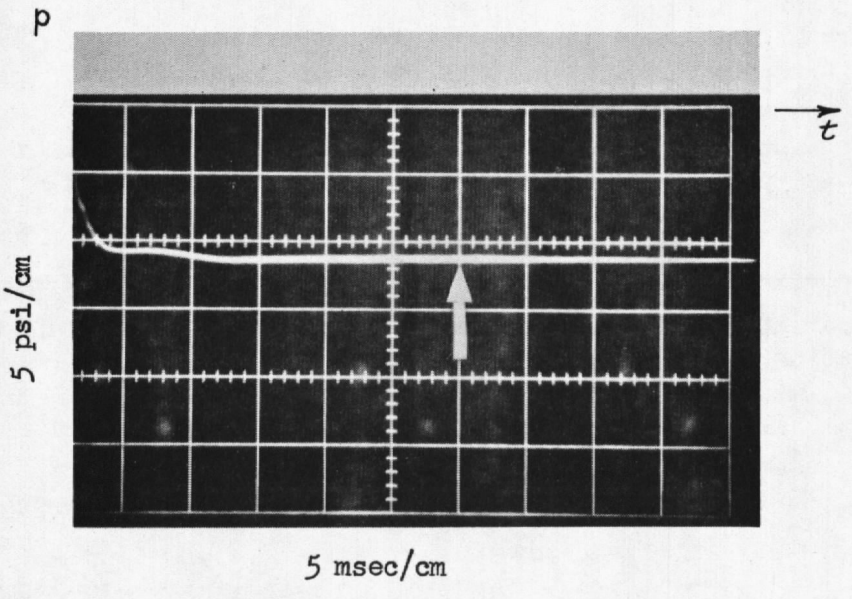

Fig. 14 Static pressure trace of the starting process and testing time in the nozzle side wall, oscilloscope trace (ω_o = 0.215, T_4 = 298.8 °K, p_4 = 876 mm Hg). The arrow indicates the time at which the sharp focus shadowgraph is taken.

Table V. Representative equilibrium flow conditions in the tube wind tunnel

Experiment number: 204
Reactant mass fraction: $\omega_o = 0.216$
Undisturbed initial conditions in the pressure tube:

$T_4 = 298.8°K$
$p_4 = 876$ mm Hg
$\alpha_4 = 0.480$

Induced flow conditions behind the expansion fan:

$M_e = 0.10$
$T_{4'} = 293.0°K$
$\alpha_{4'} = 0.432$

Stagnation conditions for the nozzle flow:

$T_o = 293.3°K$
$p_o = 753$ mm Hg
$\alpha_o = 0.434$

Nozzle throat conditions:

$T^* = 273.4°K$
$\alpha^* = 0.276$

Free stream conditions in the exit test section:

$M_\infty = 1.37$
$T = 252.2°K$
$p = 238$ mm Hg
$\rho = 4.94 \times 10^{-4} g/cm^3$
$\alpha = 0.139$

T - temperature, p - pressure, ρ - density, α - degree of dissociation, M - Mach number.

VII
ANALYSIS OF EXPERIMENTAL RESULTS

The non-equilibrium behavior of the dimensionless shock stand-off distance is described in terms of the Damköhler parameter. One recalls that the Damköhler parameter D is given by the ratio of a characteristic flow time to a characteristic time of the rate process. Since this is a physical parameter, the choice of the characteristic times is not fixed and a number of equivalent representations can be used. In general, however, the limits $D \to \infty$ and $D \to o$ denote equilibrium and frozen flows, respectively.

In the present analysis, the characteristic time is chosen as the time required for a fluid element to flow from the position of the shock wave to the body along the stagnation streamline, i.e. to flow through the stand-off distance Δ. A fluid element flowing along the stagnation streamline will have a finite velocity immediately behind the shock wave, given by the governing frozen shock wave equations, and a zero velocity at the stagnation point. A linear velocity distribution is assumed between the velocity immediately behind the shock wave u_s and the stagnation point, and the average velocity is used to calculate the characteristic flow time. Hence the characteristic flow time τ_Δ is expressed by

$$\tau_\Delta = \frac{\Delta}{\frac{1}{2}u_s} \quad . \tag{5}$$

In a real flow the velocity between the shock and the body falls below a linear distribution (See ref. (12) and (3)). The deviation, however, is not great, and for the purpose of calculating a characteristic flow time it is permissible to assume a linear distribution.

The characteristic time of a rate process depends, in general, on the physical properties and the thermodynamic state of the gas, as well as on the extent of the initial departure from equilibrium. A relaxation time for a rate process can be defined in a few special situations, and in general, it does not have a well-defined physical meaning. Consider the general form of the rate equation as given by Vincenti and Kruger (35)

$$\frac{d\alpha}{dt} = L(p, \rho, \alpha) = \frac{x(p, \rho, \alpha)}{\tau(p, \rho, \alpha)} \quad . \tag{6}$$

In this expression, τ has the units of time and is generally referred to as a local characteristic time of the rate process. For the particular case of small departures from a reference equilibrium state at constant pressure p and density ρ, Equation (6) can be linearized and integrated.

The characteristic time τ appears in the exponential factor and is defined as the relaxation time. The physical meaning of τ is the time required for the deviation from equilibrium to fall to 1/e of its initial value. When the reference state is not at constant pressure and density, and departures from equilibrium are large, the characteristic time τ is referred to as a local relaxation time with respect to a local equilibrium condition (35). A relaxation time is thus associated with small departures from an equilibrium state or a local reference state.

A blunt body flow is characterized by the detached shock wave. Along the stagnation streamline, the normal shock wave is strong and departure from equilibrium is large. In this situation, the meaning of a relaxation time is limited to a small region of the flow and its meaning is not clear for the process as whole. A means of defining a characteristic reaction time for the process as a whole is considered next, and the use of a local relaxation time will be considered later in the analysis.

The state of the gas immediately behind the detached bow shock wave of the blunt body is given by the solution of the flow through the equivalent shock wave with the same free stream. In particular, the flow through the normal portion of the detached shock wave is used to characterize the blunt body flow. In the present situation, the characteristic time which describes the non-equilibrium flow behind a plane shock wave will be assumed to also characterize the non-equilibrium flow behind the normal shock wave of the corresponding blunt body.

A solution of the non-equilibrium flow of the present reacting model gas mixture through a normal shock wave is given in Appendix IV. The rate equation combined with the other governing equations may be expressed in the form

$$\frac{d\alpha}{dt} = F(\alpha), \tag{7}$$

where $F(\alpha)$ is some complicated function of α. This equation is equivalent to Equation (6), and is specialized here for the case of a normal shock wave. The variation of α with time in the non-equilibrium region behind the shock wave is given by

$$t = \int_{\alpha_s}^{\alpha} \frac{d\alpha}{F(\alpha)}, \tag{8}$$

and a characteristic time to reach equilibrium may be conveniently defined, as done by Freeman (1), by

$$\tau_r = \int_{\alpha_s}^{0.95\alpha_e} \frac{d\alpha}{F(\alpha)}, \tag{9}$$

where α_e is the equilibrium value of the degree of dissociation obtained from the equilibrium solution of the shock wave, i.e. from $F(\alpha) = 0$. The characteristic time τ_r is thus a time required to reach 95 percent of the equilibrium degree of dissociation, and may be considered, freely speaking, as a non-linear relaxation time of the non-equilibrium process. With this definition, the Damköhler parameter becomes

$$D = \frac{\tau_\Delta}{\tau_r} , \tag{10}$$

where τ_Δ is the characteristic flow time given by Equation (5). Such a Damköhler parameter is calculated for each experiment in a given set of experiments. For the set of experiments in the exit test section with reactant mass fraction $\omega_o = 0.216$, the characteristic reaction time τ_r has an average value of 14×10^{-6} sec. The characteristic flow time τ_Δ varies from 3×10^{-6} to 40×10^{-6} sec. for the 1/32 and 5/8 in. diameter spheres, and the corresponding Damköhler parameter has a range of values from 0.2 to 2.8, respectively.

The variation of the dimensionless stand-off distance (compensated for the variation of the non-uniform free stream) with the Damköhler parameter for the above set of experiments is shown in Figure 15. A decrease of approximately 16 percent is observed as the Damköhler parameter is increased by an order of magnitude. The vertical bars over the experimental points indicate approximate deviations due to optical, photographic and reading errors of the negatives (Appendix V). These errors become significant only for the smaller diameter spheres, and fall within the symbols representing the experimental points of the larger spheres. The greatest error occurs with the smallest sphere where the deviation is estimated to be ±2 percent and amounts to a deviation of ±13 percent of the total effect observed. Similar errors occur in the Damköhler parameters due to uncertainties in the characteristic times. A deviation of approximately ±2 to ±1 percent is estimated in the Damköhler parameters for the I/32 and 5/8 in. diameter spheres, respectively. These errors are indicated by horizontal bars in Figure 15 and are not significant on the scale of this figure.

The limiting values of the frozen and equilibrium shock positions may be estimated in the following manner. It is recalled that if the dimensionless stand-off distance is plotted as a function of the density ratio across the normal shock, Figure 16, then over a small region of the density ratio, the curve may be represented approximately by a straight line. Furthermore, the variation of the dimensionless stand-off distance with the specific heat ratio at a given density ratio is small and may be assumed negligible. With these facts in mind, a straight line is drawn and extended through the experimental results obtained with dry nitrogen (Figure 16). The frozen and equilibrium density ratios across the normal bow shock waves are obtained from the corresponding frozen and equilibrium plane shock wave solutions (Appendix IV). The range of these density ratios is small so that the straight line representation mentioned above is a good approximation. The limiting stand-off

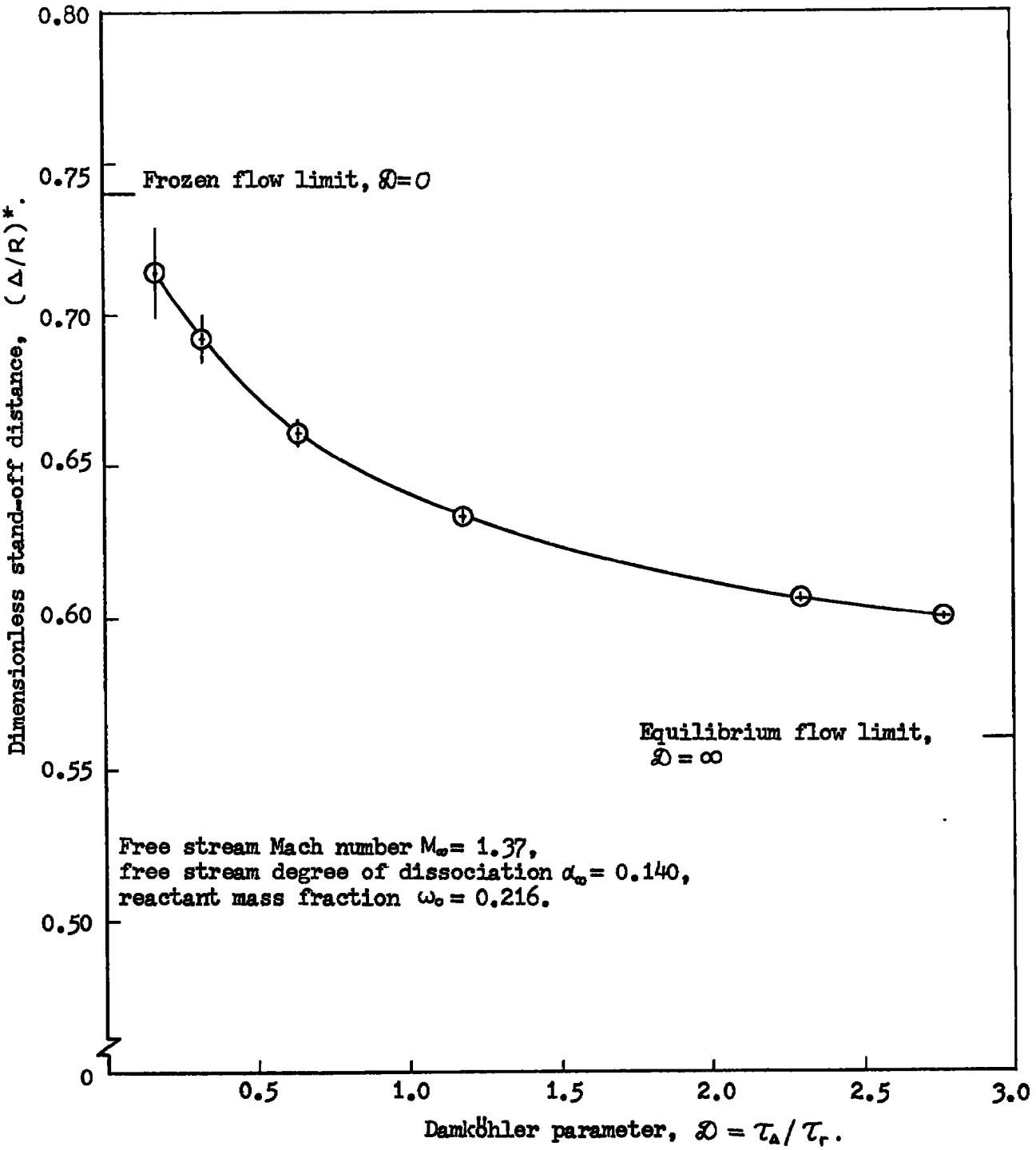

Fig. 15 Dimensionless stand-off distance as a function of the Damköhler parameter

distance values, obtained from their corresponding density ratios, are shown in Figure 15. The change in the dimensionless stand-off distance from the frozen to the equilibrium limit is thus estimated to be 25 percent for the above set of experiments. It is interesting to note that a relatively large change in the dimensionless stand-off distance is observed for an order of magnitude change of the Damköhler parameter and that the limiting frozen and equilibrium behavior is closely approached. This strong dependence on the Damköhler parameter indicates that the experiments were, indeed, conducted in a non-equilibrium regime and that the Damköhler parameter is an appropriate and meaningful parameter. The greatest change in the dimensionless stand-off distance occurs near the frozen limit, and near the equilibrium limit the behavior is weakly dependent on the Damköhler parameter. In this respect, the experimental behavior is in qualitative agreement with Freeman's predictions (1) for the Lighthill ideal dissociation gas extended to non-equilibrium behavior by Freeman's rate equation, and Conti's predictions (2) for a gas mixture of oxygen and nitrogen with nitrogen as an inert diluent and oxygen undergoing dissociation-recombination reaction.

The results of all sets of experiments conducted at three different reactant mass fractions and two different test sections are presented in Figure 17. The reactant mass fraction ω_o, the free stream frozen Mach number M_∞, and the free stream degree of dissociation α_∞, are also shown here. Qualitatively, the behavior of each set of experiments is similar to the set described above and presented in Figure 15.

The experiments conducted at the exit test section are considered first. The variation in the free stream Mach number and the degree of dissociation among the three sets of experiments is slight. The distinguishing feature of each set is its reactant mass fraction which specifies the physical properties of the gas mixture, and in particular, its heat of reaction and characteristic reaction time. An increase in the reactant mass fraction, with all other variables constant, will decrease the characteristic reaction time. Thus, the experiments conducted at higher reactant mass fractions correspond to larger values of the Damköhler parameter, and on the whole are nearer to equilibrium flow. A curve is drawn through the experimental points of the series $\omega_o = 0.301$. Each series taken individually represents non-equilibrium behavior as discussed above.

An interesting feature of these experiments is that the experimental points from the three different sets fall near each other. In a strict sense, a correlation between these sets of experiments is not expected since not all parameters remain constant for each set. However, the variations in M_∞, α_∞ and ω_o are such that the limiting frozen and equilibrium density ratios across the normal shock waves, and therefore, the limiting frozen and equilibrium dimensionless stand-off distances, are nearly the same. The average value of the frozen density ratio across the normal shock wave for each set is 1.66, and across the

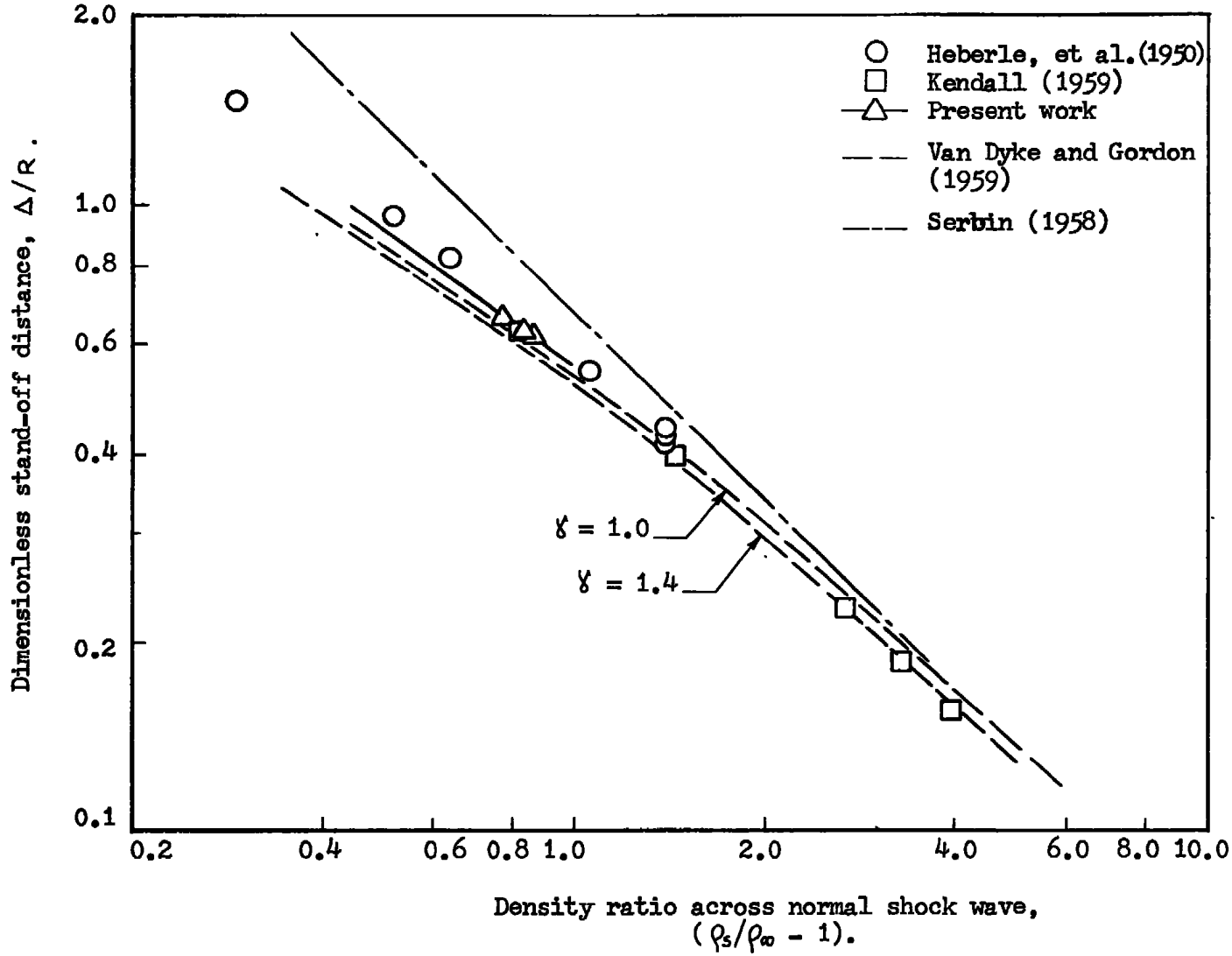

Fig. 16 Dimensionless stand-off distance as a function of the density ratio across the normal shock wave for a sphere

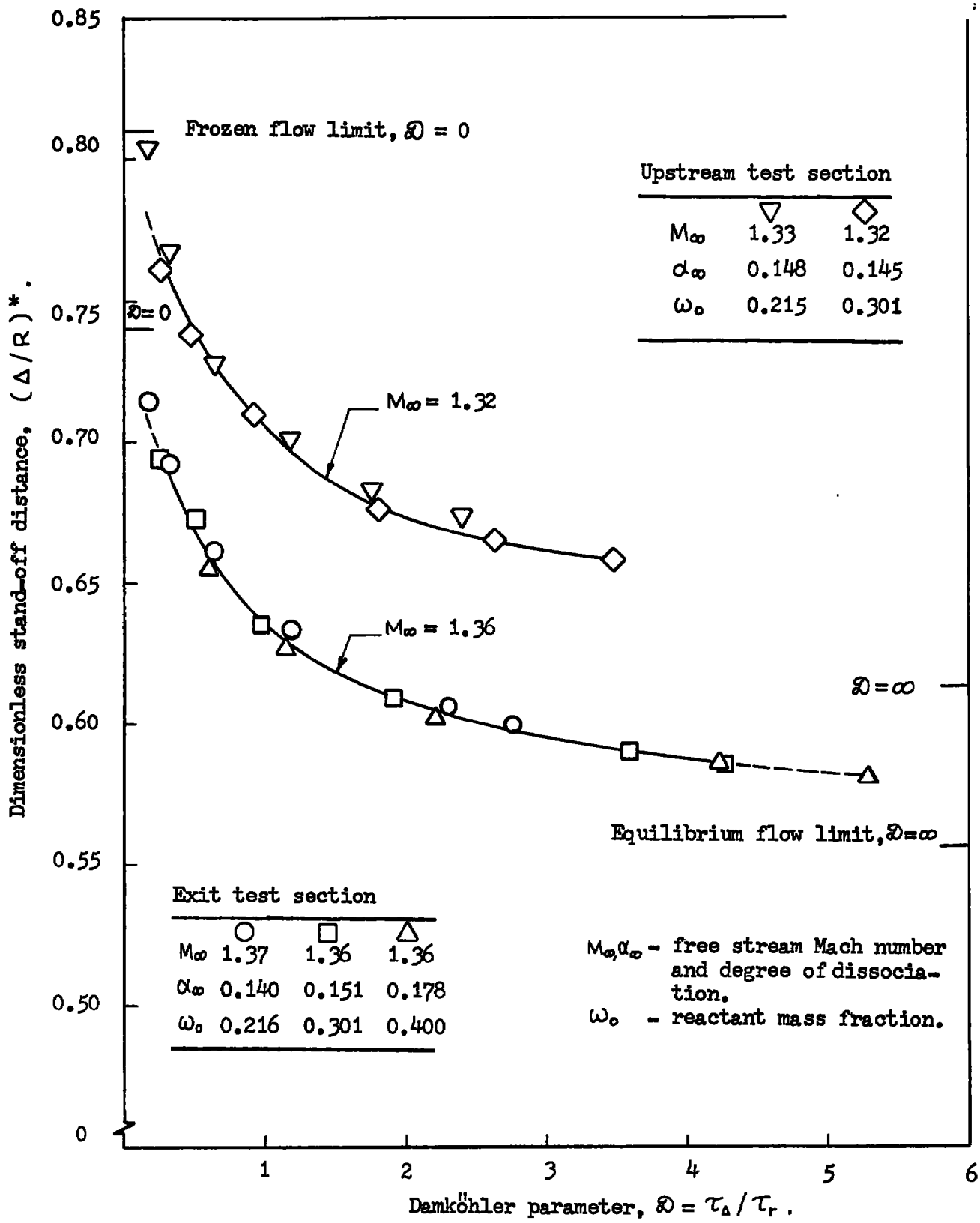

Fig. 17 Dimensionless stand-off distance as a function of the Damköhler parameter

equilibrium shock is 1.96, 1.97 and 1.98 for the sets ω_o = 0.216, 0.301 and 0.400, respectively. The limiting dimensionless stand-off distance values are indicated on the appropriate margins of Figure 17. At the equilibrium limit, only the average value is shown.

In terms of the presentation of Figure 17 and the particular choice of the Damköhler parameter, three parameters, i.e. the frozen and equilibrium density ratios and the Damköhler parameter, dominate and appear to represent the behavior as a whole. The influence of other parameters is weak in terms of this representation. Thus, for given limits of the dimensionless stand-off distance, the gross non-equilibrium behavior is described by the Damköhler parameter. In view of this, the solid curve, Figure 17, through the series ω_o = 0.301 is extended by a dashed curve along the experimental points of the other series, and the entire curve can be considered to represent the non-equilibrium behavior of the three sets of experiments taken as a whole.

The results of the two sets of experiments conducted at the upstream test section, Figure 17, also exhibit the same qualitative behavior as described above in Figure 15. The greatest difference between the experiments at the two test sections is the free stream Mach number, and the limiting values of the density ratios. Here, the frozen density ratios for each set is 1.58 and the equilibrium density ratios are 1.86 and 1.87 for ω_o = 0.215 and 0.301, respectively, and the results of the two different sets of experiments fall near each other between the limiting frozen and equilibrium stand-off distance values. A curve is drawn through the series ω_o = 0.301.

The use of a relaxation time associated with a small departure from a reference state is now considered in the definition of the Damköhler parameter. An expression for the local relaxation time as defined by Equation (6) is given for the model gas mixture in Appendix I and it is evaluated with reference to the frozen state behind the normal shock wave. Since this state is not in equilibrium, a local equilibrium state is assumed to exist. The relaxation time is given by (35).

$$\tau_s = \tau_s(p_s, \rho_s, \bar{\alpha}_s) = - \frac{1}{(\partial L/\partial \alpha)_{p_s,\rho_s}} , \qquad (11)$$

where the subscript s denotes the frozen reference state, and $\bar{\alpha}_s = \bar{\alpha}_s (p_s, \rho_s)$ is the local equilibrium value of α at p_s and ρ_s obtained from the relation

$$x(p_s, \rho_s, \bar{\alpha}_s) = 0, \qquad (12)$$

where $x(p, \rho, \alpha)$ is defined by Equation (6). The characteristic flow time $\tau_{\Delta s}$ is referred to the same reference state, and is given by

$$\tau_{\Delta s} = \frac{\Delta}{u_s} . \qquad (13)$$

The Damköhler parameter is thus given by

$$D_s = \frac{\Delta/u_s}{\tau_s} , \tag{14}$$

and the dimensionless stand-off distance as a function of the Damköhler parameter in this representation is shown in Figure 18 for the experiments conducted at the nozzle test section. The three sets of experiments no longer fall near each other as is the case when the characteristic reaction time is obtained from the reaction profile behind the normal shock wave. The behavior of each set of experiments taken individually, however, is identical with the description given above.

The relaxation time calculated above has a special meaning, i.e. a small departure of α from a reference equilibrium state at p_s and ρ_s. Consider now a more general relaxation time associated with the propagation of a weak disturbance. The governing equations may be linearized about a reference equilibrium state and expressed in terms of a velocity potential ϕ such that $u' = \partial\phi/\partial x$, where u' is the perturbed velocity (35, 36). For one-dimensional flow, the potential equation becomes

$$\tau_\phi \frac{\partial}{\partial t}\left(\frac{1}{a_f^2}\frac{\partial^2\phi}{\partial t^2} - \frac{\partial^2\phi}{\partial x^2}\right) + \frac{1}{a_e^2}\frac{\partial^2\phi}{\partial t^2} - \frac{\partial^2\phi}{\partial x^2} = 0 , \tag{15}$$

and the characteristic relaxation time is given by

$$\tau_\phi = \left(\frac{\tau_s \dfrac{\partial h}{\partial \rho}}{\dfrac{\partial h}{\partial \rho} + \dfrac{\partial h}{\partial \alpha}\dfrac{\partial \bar{\alpha}_s}{\partial \rho}}\right)_s , \tag{16}$$

where τ_s is given by Equation (11). The reference state is again taken as the state behind the frozen shock with a local equilibrium value of $\bar{\alpha}_s$. The relaxation time τ_ϕ is a characteristic time associated with the decay of a weak disturbance. The behavior of the dimensionless stand-off distance as a function of the Damköhler parameter based on τ_ϕ is shown in Figure 19 and the behavior is effectively the same as found when the characteristic reaction time τ_r is used, Figure 17. Generally, a relaxation time deduced from a linear rate equation also characterizes the time scale of the rate of approach to equilibrium in a situation when only the non-linear rate equation is valid (13). Thus, a description in terms of Damköhler parameter based on a relaxation time is essentially similar to a corresponding non-linear representation and different choices of the relaxation time will lead to representations similar to those discussed above.

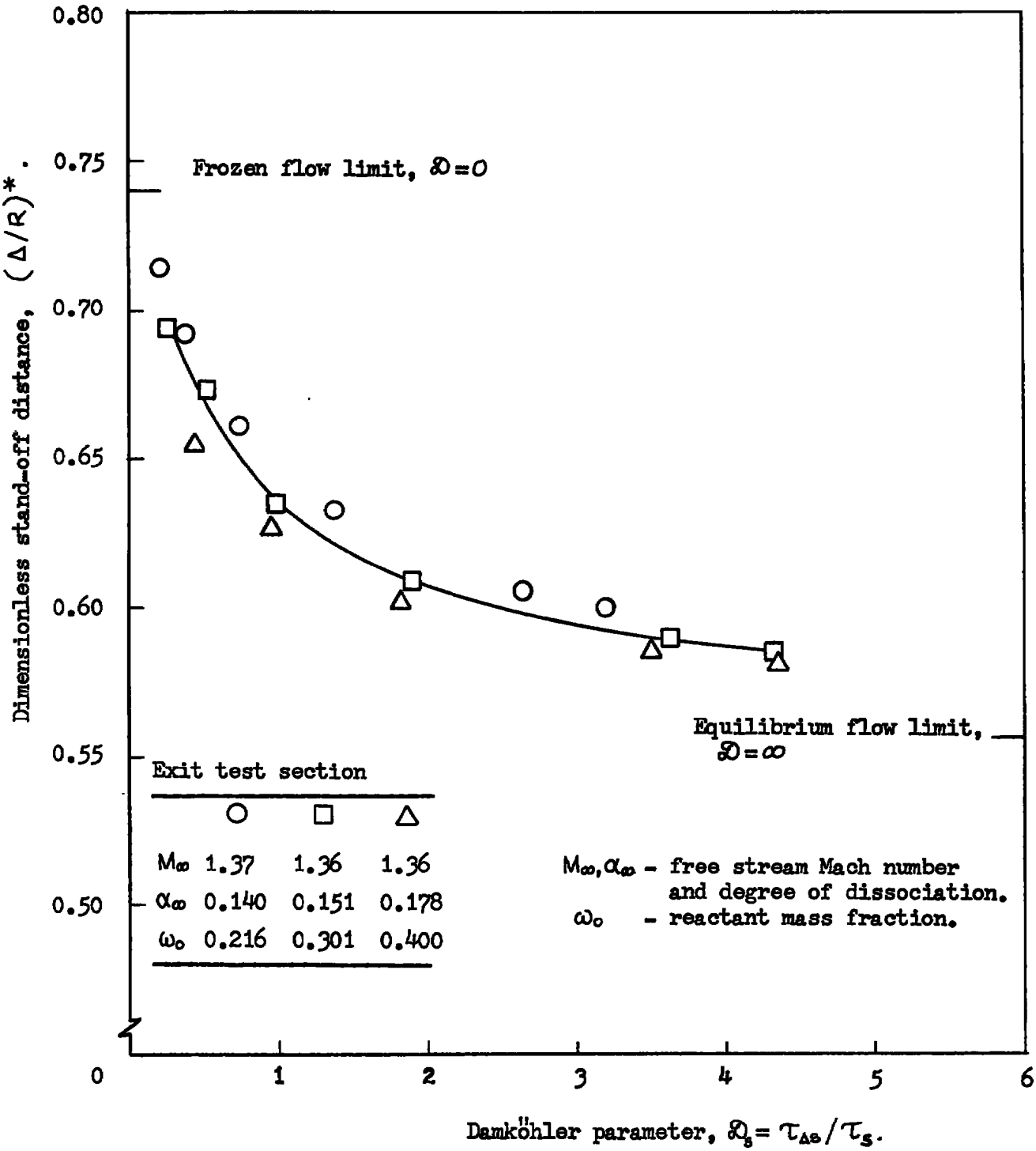

Fig. 18 Dimensionless stand-off distance as a function of the Damköhler parameter

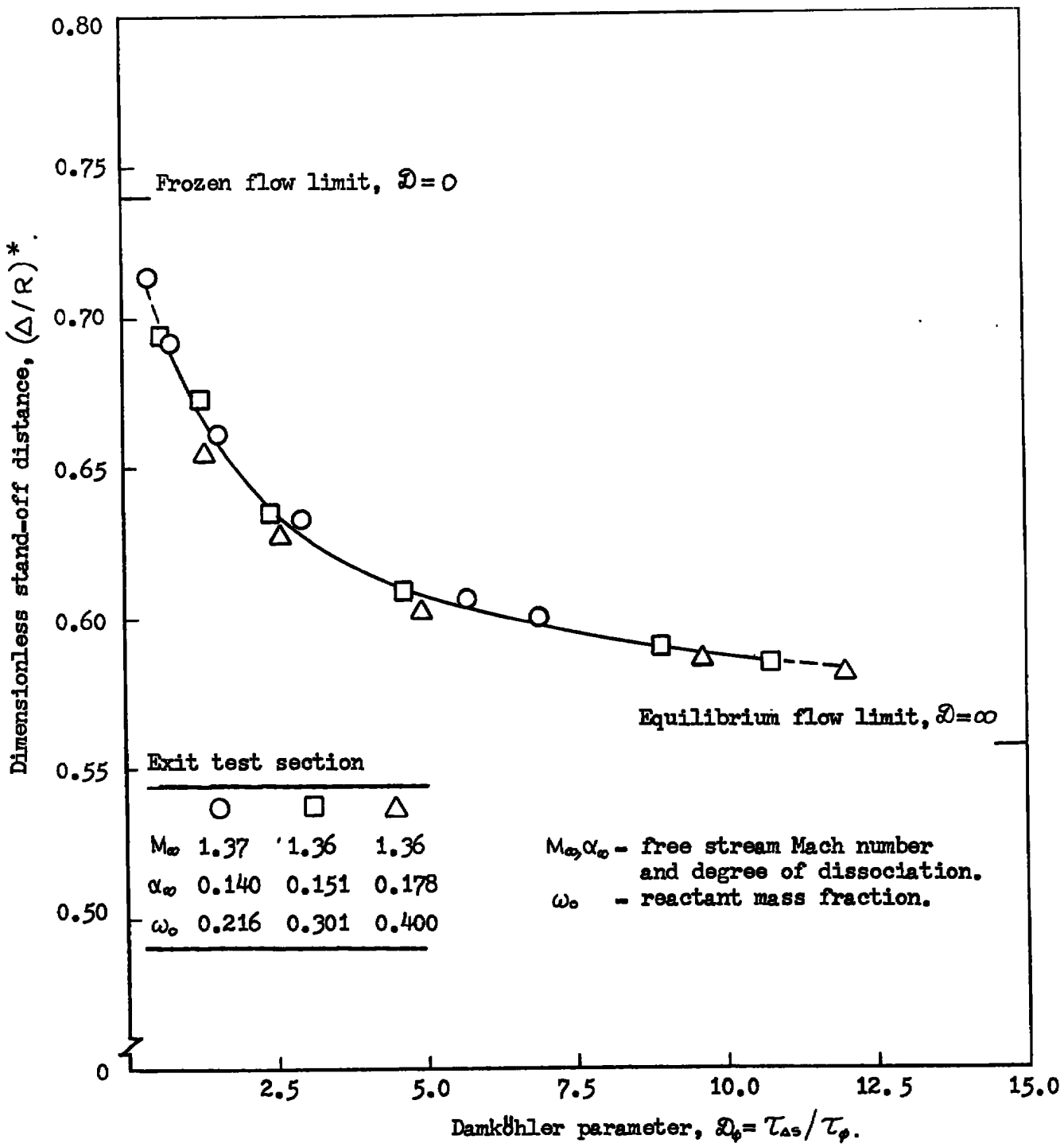

Fig. 19 Dimensionless stand-off distance as a function of the Damköhler parameter

VIII
SUMMARY

The present work is concerned with a fundamental study of the behavior of a fluid dynamic flow field with non-equilibrium thermodynamic states. A study of the shock detachment distance of supersonic blunt body flow is selected because the flow is sensitive to non-equilibrium states and is of current interest in hypersonic aerodynamics. The dimensionless shock stand-off distance is studied from an experimental standpoint as a function of a non-equilibrium parameter, the Damköhler parameter, with all other pertinent parameters of the flow held constant. For a given free stream the non-equilibrium parameter is varied by a variation of the characteristic flow time. A single non-equilibrium mode is represented by the N_2O_4 dissociation reaction whose equilibrium and rate properties are known. The experimental work is conducted in an intermittent supersonic tube wind tunnel which is designed for this work and is patterned after an intermittent tube wind tunnel suggested by Ludwieg (25). The present tunnel, however, is a variation of Ludwieg's tunnel and is operated like a shock tube with a nozzle at the diaphragm section.

Results are obtained over a range of Damköhler parameters, at a number of different reactant concentrations and at slightly different Mach numbers in equilibrium free streams. A marked variation of the dimensionless stand-off distance is observed with the Damköhler parameter for a set of experiments in identical free streams and the qualitative behavior of the dimensionless stand-off distance is in agreement with theoretical predictions in the literature. A variation of approximately 16 percent in the non-dimensional stand-off distance is observed for a change of an order of magnitude in the Damköhler parameter and the maximum variation in the stand-off distance between the frozen and equilibrium limits under these operating conditions is estimated at approximately 25 percent. Results with different equilibrium free streams show that the frozen and equilibrium density ratios across the normal shock and the Damköhler parameter appear to be the dominating parameters and describe these flows as a whole. Two different methods are used to estimate the characteristic time to establish thermodynamic equilibrium and both of these characteristic times result in a meaningful description of the flow in terms of the Damköhler parameter. Thus, when the Damköhler parameter is of the order of one, the flow is, indeed, found to be non-equilibrium. It is hoped that these results will give a new insight into the behavior of the non-equilibrium stand-off distance problem and that they will aid in the interpretation and analysis of more complicated systems.

Flows which exhibit non-equilibrium behavior can, in principle, be used to determine the reaction rates of these processes if the dynamics of the flow field is well known. The applicability of this approach has been demonstrated by Schwartz and Eckerman (5) and Eckerman (6) in their application of the shock stand-off distance to determine reaction rates.

The present experimental technique of varying the characteristic flow time suggests an extension to the existing method. The particular advantage of the present approach is that it provides a number of determinations of the reaction rate at the same free stream conditions and the extent to which the flow is initially out of equilibrium. If the dynamics of the flow field is not explicitly known in terms of the flow variables, as in the present work, it is still possible to obtain a rough estimate of the order of magnitude of the characteristic relaxation time or reaction time of unknown systems. In this situation the present approach also suggests an extension to the technique advanced by Schwartz and Eckerman (5).

The new application of the Ludwieg tube intermittent supersonic wind tunnel, with its present modification, to the study of non-equilibrium flow has proved successful, and it appears to have promise for future studies of non-equilibrium flows. The particular advantages of this tube tunnel, as used here, lies in the ease with which the supply tube may be filled and prepared for a given experiment and the need of only a small quantity of gas, the relatively long duration (20 msec.) of a well-controlled flow, and the low cost of fabrication. The use of the N_2O_4 dissociation reaction has once again demonstrated its usefulness as a tool for fundamental studies of non-equilibrium behavior.

Appendix I
Properties of the Model Reacting Gas Mixture

The non-equilibrium mode considered here is represented by the dissociation-recombination reaction of dinitrogen tetroxide (N_2O_4) into nitrogen dioxide (NO_2) in the presence of nitrogen and is given by

$$N_2 + N_2O_4 \underset{k_R}{\overset{k_D}{\rightleftharpoons}} N_2 + 2NO_2. \qquad (I.1)$$

where k_D and k_R are the dissociation and recombination reaction rate constants, respectively. The thermodynamic properties of this gas mixture are well known and are reviewed by Grey and Yoffe (20). The equilibrium constant is also well known from the early work of Bodenstein (37) and later experiments of Giauque and Kemp (38). The best fit to the available data for the equilibrium constant K_p has been provided by Strehlow (39) and is given by

$$K_p = p_* \, e^{-T_*/T'} \qquad (I.2)$$

where T is the temperature, $p_* = 1.538 \times 10^{+9}$ atmospheres, $T_* = 6{,}882°K$ and the prime denotes a dimensional quantity. This reaction takes place in the temperature interval of $200 < T < 400°K$.

From shock tube (21) and nozzle flow (28) experiments, the reaction mechanism for Equation (I.1) is assumed to be given by

$$\frac{d[N_2O_4]}{dt} = k_R \, [NO_2]^2 \, [N_2] - k_D \, [N_2O_4][N_2] \, , \qquad (I.3)$$

where [i] denotes molar concentration of the ith species. For mole fractions up to $n_R = 0.05$, the dissociation rate constant was measured by Carrington and Davidson (21) in the shock tube, and the recombination and dissociation rate constants by Wegener (22, 40) in supersonic nozzle flow studies. The results from both experimental investigations are in agreement and the recombination rate constant is taken to be $k_R = 3 \times 10^{14}$ $cm^6/(mole^2 sec)$. The value of k_R is independent of temperature within measuring accuracy in the temperature range $210 < T < 330°K$. The above reaction mechanism and rate constant have been extended to molar concentrations up to $n_R = 0.15$ by Wegener, Chu and Klikoff (24) in ballistic range studies. The reaction mechanism of Equation (I.3) and the above reaction rate constant will also be assumed to hold in the present case where the molar concentration in the free stream does not exceed $n_R = 0.20$.

The model reacting gas mixture may be regarded as a mixture of three individually thermally and calorically perfect gases. The thermal equation of state for the mixture is written

$$p' = \rho' RT'/\mu \ , \tag{I.4}$$

where p, ρ and T are the pressure, density and temperature, respectively, and R is the universal gas constant. The molecular weight of the mixture is given by

$$\frac{1}{\mu} = \frac{\omega_{N_2}}{\mu_{N_2}} + \frac{\omega_{NO_2}}{\mu_{NO_2}} + \frac{\omega_{N_2O_4}}{\mu_{N_2O_4}} = (1 + \alpha) \frac{\omega_o}{\mu_{N_2O_4}} + \frac{\omega_{N_2}}{\mu_{N_2}} \ , \tag{I.5}$$

where $\omega_i = m_i/m$ is the mass fraction of the ith species and ω_o is the mass fraction of reactants. The degree of dissociation, defined by $\alpha = \omega_{NO_2}/(\omega_{NO_2} + \omega_{N_2O_4})$, applies to the reactants only. The relations

$$\omega_{N_2} + \omega_{NO_2} + \omega_{N_2O_4} = 1 \ ,$$

$$\omega_{NO_2} + \omega_{N_2O_4} = \omega_o \ ,$$

$$\omega_{NO_2} = \alpha\omega_o \ ,$$

and

$$\omega_{N_2O_4} = (1 - \alpha)\ \omega_o \tag{I.6}$$

are self-evident. In terms of the variables p, ρ, T and α, the equation of state becomes

$$p' = \rho' T' [a_1(1 + \alpha) + b_1], \tag{I.7}$$

where $a_1 = R\omega_o/\mu_{N_2O_4}$ and $b_1 = R\ \omega_{N_2}/\ \mu_{N_2}$ are constants for a given environment.

The enthalpy per unit mass of the mixture is given by the sum of the enthalpies of the species

$$h' = \omega_{N_2}\ h'_{N_2} + \omega_{NO_2}\ h'_{NO_2} + \omega_{N_2O_4}\ h'_{N_2O_4}. \tag{I.8}$$

The heat of reaction per unit mass of N_2O_4, $\Delta h_{N_2O_4}$, is defined by

$$\Delta h_{N_2O_4} = h'_{NO_2} - h'_{N_2O_4}. \tag{I.9}$$

The value of the heat of reaction is nearly constant in the temperature range of interest and will be assumed constant here. The caloric equation of state for the mixture of individually calorically perfect gases becomes

$$h' = c_p T' + Q_R \alpha, \tag{I.10}$$

where $c_p = \omega_o c_{p_{N_2O_4}} + \omega_{N_2} c_{p_{N_2}}$ and $Q_R = \omega_o \Delta h_{N_2O_4}$ are constants for a given environment. The data for the specific heats of NO_2 and N_2O_4 and the heat of reaction are taken from the recently corrected JANAF data (41) for the NO_2 and N_2O_4 gases and the specific heat of nitrogen is taken from the published JANAF (42) data.

The law of mass action determines the equilibrium composition of the mixture and it is given by

$$\frac{[NO_2]^2}{[N_2O_4]} = K_c = \frac{K_p}{RT'}, \tag{I.11}$$

where K_c and K_p are the equilibrium constants in units of concentration and pressure, respectively and K_p is given by Equation (I.2). Equation (I.11), rewritten in terms of the working variables α, ρ and T, becomes

$$\frac{\alpha^2}{1 - \alpha} = \frac{T_*}{T'} \frac{\rho_*}{\rho'} e^{-T_*/T'}, \tag{I.12}$$

where $\rho_* = \mu_{N_2O_4} p_*/(4\omega_o R T_*)$ is a constant for a given environment.

The rate equation, Equation (I.3), can be expressed in a more convenient form in terms of the variables ρ, T and α. From the postulated structure of the rate equation it follows that

$$\frac{k_D}{k_R} = K_c = \frac{K_p}{RT'}, \tag{I.13}$$

and with the aid of this equation and the relation $[i] = \omega_i \rho'/\mu_i$, the rate equation becomes

$$\frac{d\alpha}{dt} = \phi_1 \frac{\rho'}{\rho_*} \left[\frac{(1 - \alpha) e^{-T_*/T'}}{T'/T_*} - \frac{\rho'}{\rho_*} \alpha^2\right], \tag{I.14}$$

where $\phi_1 = 4k_R \omega_{N_2} \omega_o \rho_*^2/(\mu_{N_2} \mu_{N_2O_4})$ is a constant for a given environment. Note that at equilibrium $d\alpha/dt = 0$, the right hand side of Equation (I.14) must also be zero and the law of mass action is recovered.

It is convenient now to non-dimensionalize the equations which describe the reacting gas mixture. Let the dimensionless quantities be: $T = T'/T_*$, $\rho = \rho'/\rho_*$, $h = h'/Q_R$ and $p = p'/(\rho_* Q_R)$. The thermal and

caloric equations of state, the law of mass action and the rate equation become:

$$p = \rho T\,[a(1 + \alpha) + b], \tag{I.15}$$

$$h = cT + \alpha\ , \tag{I.16}$$

$$\frac{\alpha^2}{1 - \alpha} = \frac{e^{-1/T}}{\rho T}\ , \tag{I.17}$$

and

$$\frac{d\alpha}{dt} = \theta\rho\ \left[(1 - \alpha)\ \frac{e^{-1/T}}{T} - \rho\alpha^2\right]\ , \tag{I.18}$$

where

$$a = RT_*/(\mu_{N_2O_4}\ \Delta h_{N_2O_4})\ ,$$

$$b = a\ \omega_{N_2}\ \mu_{N_2O_4}\ /(\omega_o\ \mu_{N_2})\ ,$$

$$c = a\ c_p\ \mu_{N_2O_4}/(R\ \omega_o)\ ,$$

and $\theta = 4\ \omega_o\omega_{N_2}k_R\rho_*^2/(\mu_{N_2}\mu_{N_2O_4})$ are all constants for a given environment.

The thermal equation of state and subsequent equilibrium flow calculation in the nozzle can be simplified by the following consideration. For an ideal gas reaction the heat of reaction is related to the equilibrium constant by Van't Hoff's equation

$$\frac{d\ \ell n\ K_p}{dT'} = \frac{\Delta H_*}{RT'^2}\ , \tag{I.19}$$

where ΔH_* is the heat of reaction per mole of N_2O_4. The substitution of the equilibrium constant, Equation (I.2) into the above equation yields

$$\Delta h_{*N_2O_4} = \frac{RT_*}{\mu_{N_2O_4}}\ , \tag{I.20}$$

where $\Delta H_* = \mu_{N_2O_4}\ h_{*N_2O_4}$. The constant "a" which appears in the thermal equation of state, Equation (I.15) can be rearranged with the use of the above relation into the form

$$a = \frac{\Delta h_{N_2O_4}}{\Delta h_{*N_2O_4}} \tag{I.21}$$

which has the value a = 0.988 ≈ 1. In the calculations to be discussed in the following sections, an assumption is made that a = 1, which is equivalent to the use of the heat of reaction $\Delta h_{*N_2O_4}$ obtained from the Van't Hoff's equation.

It is useful to reformulate the rate equation, Equation (I.18), into a more general expression, as given by Vincenti and Kruger (35)

$$\frac{d\alpha}{dt} = L(p, \rho, \alpha) = \frac{x(p, \rho, \alpha)}{\tau(p, \rho, \alpha)} , \tag{I.22}$$

where $L(p, \rho, \alpha)$ is given by the right hand side of Equation (I.18), and the function $x(p, \rho, \alpha)$ is defined by

$$x(p, \rho, \alpha) = - \frac{L}{(\partial L/\partial \alpha)_{p,\rho}} \tag{I.23}$$

In this form of the rate equation, the quantity τ is defined as a local characteristic time of the rate process and is given by

$$\tau(p, \rho, \alpha) = - \frac{1}{(\partial L/\partial \alpha)_{p,\rho}} . \tag{I.24}$$

For the present model gas mixture (see also Ref. 43)

$$\left(\frac{\partial L}{\partial \alpha}\right)_{p,\rho} = -\theta\rho\left\{\frac{e^{-1/T}}{T}\left[1 + \frac{a(1 - \alpha)(1 - T)}{T[a(1 + \alpha) + b]}\right] + 2\rho\alpha\right\} . \tag{I.25}$$

In a non-equilibrium flow two limiting sound speeds occur (44), the frozen a_f, and the equilibrium a_e, which are given by

$$a_f^2 = - \frac{h_\rho}{h_p - 1/\rho} \tag{I.26}$$

and

$$a_e^2 = - \frac{h_\rho + h_\alpha \alpha_\rho}{h_p + h_\alpha \alpha_p - 1/\rho} , \tag{I.27}$$

where the subscript denotes partial differentiation. For the present model gas mixture the above expressions become

$$a_f^2 = \frac{cTA}{c-A} \tag{I.28}$$

and

$$a_e^2 = \frac{T\left\{[A(2 - \alpha) - a\alpha(1 - \alpha)]\, cT^2 + \alpha(1 - \alpha)A\right\}}{[(2 - \alpha)(c - A) + a\alpha(1 - \alpha)]\, T^2 - (a+1)\alpha(1-\alpha)T + \alpha(1-\alpha)} , \tag{I.29}$$

where $A = [a(1 + \alpha) + b]$.

Appendix II
Properties, Calibration, and Detailed Description of the Tube Wind Tunnel and the Experimental Procedure

Properties of the Tunnel

Expressions for the properties ahead of the nozzle and the test time have been derived and discussed by Becker (30) and Cable and Cox (28). The derivations will not be repeated here; only the results for ideal operation will be presented. Ideal operation of the tunnel assumes that the nozzle is represented by a discontinuous area change and that there are no boundary layer effects. Furthermore, the gas flow is assumed to be thermally and calorically perfect. The properties in the undisturbed regions are known and are denoted by the subscript 4. The region behind the expansion fan and ahead of the nozzle is denoted by 4'. The Mach number of the flow ahead of the nozzle, M_4', is determined by the ratio of the tube area to the nozzle throat area and is known for a given tunnel. In terms of the Mach number, M_4', the velocity behind the expansion fan and ahead of the nozzle is given by

$$\frac{u_{4'}}{a_4} = \frac{M_{4'}}{1 + \frac{\gamma_4 - 1}{2} M_{4'}} , \tag{II.1}$$

the speed of sound and temperature by

$$\frac{a_{4'}}{a_4} = \left(\frac{T_{4'}}{T_4}\right)^{1/2} = \frac{1}{1 + \frac{\gamma_4 - 1}{2} M_{4'}} , \tag{II.2}$$

the pressure by

$$\frac{p_{4'}}{p_4} = \left[1 + \frac{\gamma_4 - 1}{2} M_{4'}\right]^{-2\gamma_4/(\gamma_4 - 1)} , \tag{II.3}$$

and the density by

$$\frac{\rho_{4'}}{\rho_4} = \left[1 + \frac{\gamma_4 - 1}{2} M_{4'}\right]^{-2/(\gamma_4 - 1)} , \tag{II.4}$$

where γ is the specific heat ratio. The stagnation conditions in region (4') are given by

$$\frac{T_o}{T_4} = \left(\frac{a_o}{a_4}\right)^2 = \frac{1 + \frac{\gamma_4 - 1}{2} M_4'^2}{\left(1 + \frac{\gamma_4 - 1}{2} M_4'\right)^2}, \tag{II.5}$$

$$\frac{p_o}{p_4} = \left(\frac{a_o}{a_4}\right)^{2\gamma_4/(\gamma_4-1)}, \tag{II.6}$$

and

$$\frac{\rho_o}{\rho_4} = \left(\frac{a_o}{a_4}\right)^{2/(\gamma_4-1)}. \tag{II.7}$$

The steady nozzle flow time, or testing time, is obtained by integration of the equation of motion. If t_t is the test time, then

$$t_t = \frac{2\ell/a_4}{1+M_4'} \left[1 + \frac{\gamma_4 - 1}{2} M_4'\right]^{(\gamma_4+1)/[2(\gamma_4-1)]}, \tag{II.8}$$

where ℓ is the length of the pressure tube.

Thus far, only ideal fluid motion has been considered. For real fluid motion, a boundary layer is formed behind the expansion fan. As the expansion fan proceeds into the tube, the boundary layer grows with time at any given position behind the fan. The effect of the boundary layer on flow properties in the pressure tube has been discussed by Becker (33, 30). Results of his work are summarized below for the case of small boundary layer displacement thickness compared with tube radius.

The growing boundary layer displacement thickness has the same effect on the flow as if the tube were to contract with time. Such a movement generates compression waves which travel in both directions from the disturbance and alter the velocity and pressure in the tube. From the nozzle operational viewpoint, in fact, the supply conditions vary with time for a viscous gas. The velocity and pressure ahead of the nozzle section will be altered by the amounts

$$\frac{\Delta u}{a_4'} = \frac{\delta^*}{r} \frac{7/5\ M_4'}{2+3/5\ M_4'} \frac{1 + 0.108\ M_4'}{1 + 0.311\ M_4'} \tag{II.9}$$

and

$$\frac{\Delta p}{p_4'} = \delta_4 \frac{\Delta u}{a_4'}, \tag{II.10}$$

where δ^* is the displacement thickness at the nozzle section entrance and r is the tube radius.

The growing boundary layer thickness has yet another effect on the flow. As the displacement thickness grows, the effective tube cross sectional area decreases and therefore the ratio of tube to throat area also decreases. This in turn causes the Mach number $M_{4'}$ to increase. The variation of $M_{4'}$ is established by expansion waves which travel from the nozzle section into the tube and again change the velocity and pressure there. The corresponding velocity and pressure changes are given by

$$\frac{\Delta u'}{a_{4'}} = \frac{M_{4'} - \frac{\Delta u}{a_{4'}} - M(t)\left(1 - \frac{1}{5}\frac{\Delta u}{a_{4'}}\right)}{1 + \frac{1}{5}M(t)} \qquad \text{(II.11)}$$

and

$$\frac{\Delta p'}{p_{4'}} = \delta_4 \frac{\Delta u'}{a_{4'}}, \qquad \text{(II.12)}$$

where M(t) is the Mach number in the tube ahead of the nozzle section and calculated with the reduced tube area at that point.

Thus, the net effect of the boundary layer is to reduce the supply pressure of the flow ahead of the nozzle as a function of time. The pressure in the tube ahead of the nozzle becomes $p_4 + \Delta p + \Delta p'$. If the tube is very long the boundary layer will grow to the center of the pipe and cause a fully developed pipe flow. In this case the pressure is reduced still further. The pressure drop may be calculated in the same manner as in ordinary steady pipe flow. The obvious practical solution to this dilemma if long testing times are needed is to have a pressure tube diverge, or at least have sections with increasing diameters away from the nozzle.

The boundary layer displacement thickness for turbulent flow behind an expansion wave (33) is given by

$$\delta^* = \frac{1}{8}\, 0.303 \left(\frac{\nu_{4'}}{u_{4'}t'}\right)^{1/5} u_{4'}t'\left(1 + \frac{7}{9}\frac{u_{4'}}{v}\right)^{-4/5}, \qquad \text{(II.13)}$$

where $\nu_{4'}$ is the kinematic viscosity, $t' = t - x/v$, t is the length of flow and x is the distance along the pressure tube measured from the throat of the nozzle. To simplify the calculation of the boundary layer thickness, the thin expansion fan is replaced by a concentrated expansion wave traveling with velocity v. The velocity v is calculated from an arithmetic average of the head and tail velocities of the original expansion fan, i.e. $v = 1/2\,(a_4 + a_{4'} - u_{4'})$.

In the present design of the tunnel the ratio of the pressure tube area to the nozzle throat area is 5.50. The nozzle is two-dimensional and the current set of nozzle blocks have a 6 in. radius of curvature at the throat, a 4 sq. in. throat and 2° divergence angle with an exit section of 2 by 2.44 inches. A detailed description of the design of the wind tunnel is given in a subsequent section. The specific properties of the present tunnel for operation with a gas such as nitrogen or air with $\gamma = 1.4$ are described below. The specific properties of the tunnel for operation with a reactant gas mixture are considered in Appendices III and IV.

The Mach number of the flow ahead of the nozzle is $M_{4'} = 0.11$ and the Mach number at the geometrical exit section of the nozzle is M = 1.55. The highest possible Mach number at the exit is $M_{3'} = 2.55$. The Mach number $M_{3'}$ may readily be increased if required by a decrease of throat area or increase of dump tube cross-sectional area for new nozzles. The steady computed nozzle flow time is 20×10^{-3} seconds. Quantities computed in Equation (II.1) to (II.7) are given below:

$$u_{4'}/a_4 = 0.104$$

$$a_{4'}/a_4 = 0.979$$

$$T_{4'}/T_4 = 0.959$$

$$p_{4'}/p_4 = 0.863$$

$$\rho_{4'}/\rho_4 = 0.900$$

$$T_o/T_4 = 0.961$$

$$p_o/p_4 = 0.870$$

and

$$\rho_o/\rho_4 = 0.905$$

Based on these standard operating conditions, the boundary layer properties may be found from Equation (II.13). The boundary layer displacement thickness ahead of the nozzle section and just prior to the end of the steady nozzle flow is $\delta^* = 0.06$ in. From this one finds the drop in pressure ahead of the nozzle, i.e. supply pressure, at the end of testing time to be only 1/2 percent lower than initially. These data show that one can expect to be permitted to work with a straight driver section and assume practically constant supply conditions.

Calibration of the Tunnel

Calibration measurements in the tunnel are made with the pressure tube filled with dry nitrogen at atmospheric pressure and at room tempera-

ture. These measurements are made to determine whether the tunnel functions properly and to evaluate the real behavior of the tunnel.

Prediction of idealized behavior is checked by measuring the static pressure in the nozzle sidewall as a function of time with a fast response (3×10^{-6} sec.) pressure transducer. At a fixed area ratio and Mach number, one expects p = constant for constant supply pressure. With the transducer located in the sidewall near the exist of the nozzle, a typical oscilloscope trace is shown in Figure II.1. The flow begins to break down at the last division of the reference grid and the measured running time therefore, is approximately 20 milliseconds. This corresponds remarkably well to the predictions. There are some deviations, however. Note that approximately 4 milliseconds are required to establish steady flow in the nozzle and the flow remains steady, as demonstrated by the constant pressure in the trace, for the remainder of the running time. The starting time reflects the fact that in a real tunnel the area changes at the nozzle are gradual and occur over some distance, and therefore, a complicated flow pattern is developed before steady state conditions become established. Static pressure traces have been also obtained with an expanded scale of the pressure coordinate, and these results indicate that the drop in the supply pressure is of the order of the prediction, i.e. approximately 1/2 percent.

Additional experiments to check the performance and to find the duration of the steady flow have been performed by taking shadowgraph pictures of flows about a sphere. Shadowgraphs have been taken in increments of time starting with no delay and ending where the flow has been observed to break down. The duration of the flow appears to be within a millisecond of the values measured with the pressure transducer. Reproducibility of the flow has been checked by taking a number of shadowgraphs of the same event, i.e. with the same delay setting, and no discrepancy in the flow has been observed. A shadowgraph of the flow over a 1/2 in. diameter sphere at M = 1.5 as well as the entire flow field at the exit test section is shown in Figure II.2. The photographic plate is located approximately 11 in. from the centerline of the sphere. A similar set of reproducibility experiments has been recorded with sharp focus shadowgraphs and the measurements of the stand-off distances from these negatives reveal that the reproducibility is of the order of the reading error.

The entire flow history has been recorded with a high speed Fastax movie camera at 5,000 frames per second which photographed a shadowgraph image of the flow on a frosted screen placed near the window. The starting process, a region of constant flow, and the breakdown of the flow is observed. The movie confirmed what has been found with the pressure measurements and the shadowgraphs. Excerpts of this movie are shown in Figure II.3.

The flow in the nozzle has been calibrated by observing the flow about cones with the axis of the cone parallel to the free stream. For a given cone, the angle between the surface of the cone and the attached

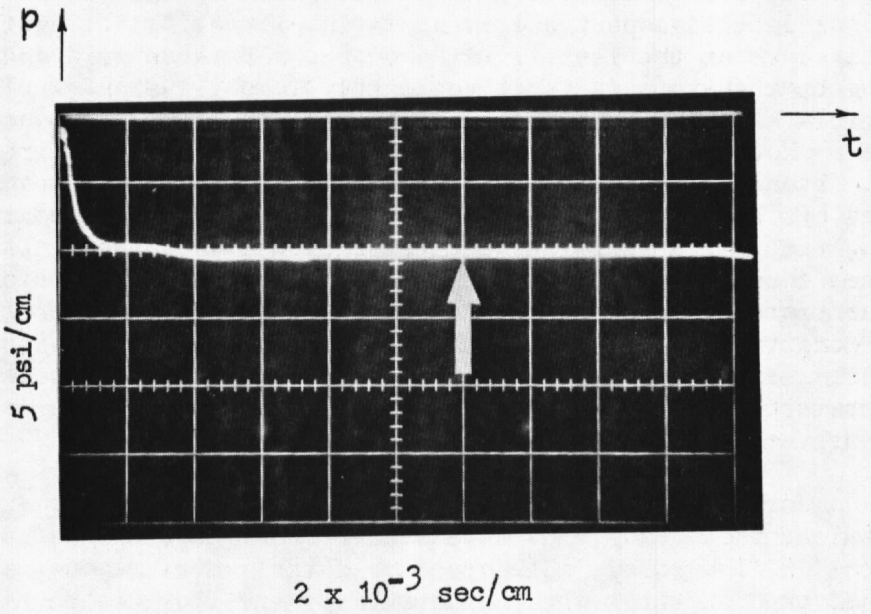

Fig. II.1 Static pressure trace in the nozzle sidewall as a function of time, oscilloscope trace. The arrow indicates the time at which shadowgraphs are taken.

shock wave is sensitive to the free stream Mach number. Numerical calculations of the flow field about cones, the angle between the cone and the shock wave, have been shown to be in excellent agreement with experimental results (45). In the present calibration, shadowgraphs were taken of the flow about 30° and 40° cones. The shock angles have been measured and the corresponding Mach numbers have been obtained from charts prepared by the Ames Research Staff (31). The Mach number, as determined by the above method, is found to be 1.50 and 1.45 for the two testing positions in the nozzle exit and at a test section upstream of the nozzle exit, respectively. An uncertainty of less than 1 percent in these Mach numbers arises from the error in shock angle measurement and interpolation on the chart.

An independent check of the Mach number has been obtained by calculating the effective area ratio in the nozzle. The boundary layer displacement thickness δ^* has been estimated from shadowgraphs via a measurement of the total boundary layer thickness (46). In addition, the displacement thickness has been estimated by a method given by Ruptash (47). Both values of the displacement thickness agree at 0.04 and 0.03 cm for the exit and upstream test sections, respectively. The Mach numbers corresponding to the calculated effective area ratios fall within the values obtained via the cone measurements.

A further check of the performance of the nozzle has been made by measurement of the stand-off distance in dry nitrogen at a number of locations in the tunnel. The results of these measurements are shown in Figures 4 and 12, where the Mach number of the flow has been obtained from the above calibrations. The results of the present measurement lie within the spread of the existing experimental work.

The supersonic nozzle used in the present experiments has a constant angle of divergence and is therefore not a parallel flow nozzle. The extent of the Mach number variation along the axis and perpendicular to the axis due to the divergent flow has been determined. Measurements of the stand-off distance have been first conducted along the nozzle center line. In the region of the two test sections the variation in the dimensionless stand-off distance is nearly linear with the distance along the centerline and is approximately 7 percent per inch. The corresponding variation in Mach number is approximately 3 percent per inch and is nearly the same as the value obtained from the geometric area ratios. Variation of the Mach number in a direction perpendicular to the nozzle axis has been also determined by measurement of the dimensionless stand-off distance. Spheres of 1/16 and 1/8 in. in diameter have been positioned 5/8 in. above, below and along the centerline of the nozzle. These measurements indicate a greater value of the stand-off distance along the centerline position. The variation, however, is small and corresponds to approximately twice the reading error of the negatives. The variation in the non-dimensional stand-off distance is estimated to be less than 1/2 percent.

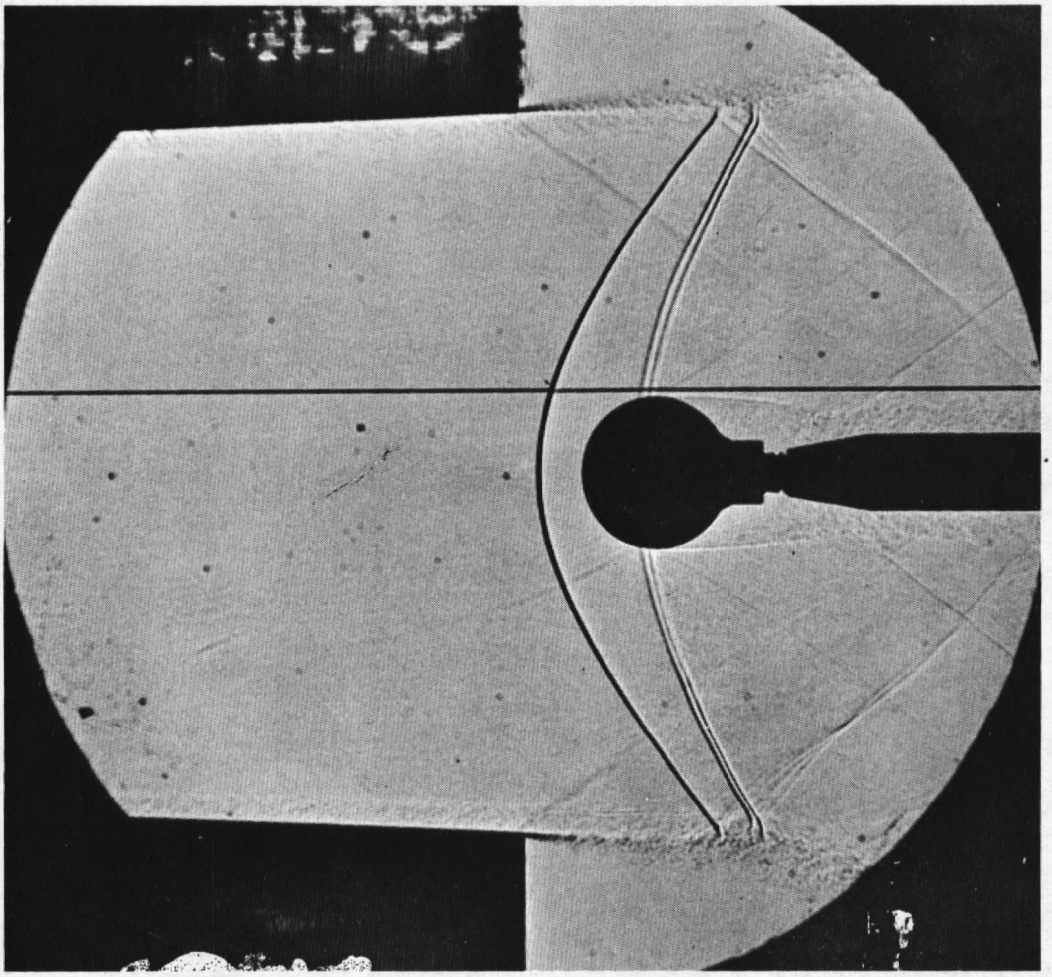

Fig. II.2 Shadowgraph of the flow field about a ½ inch diameter sphere and the entire flow in the exit test section in dry nitrogen at M_∞ = 1.5. The flow is from left to right.

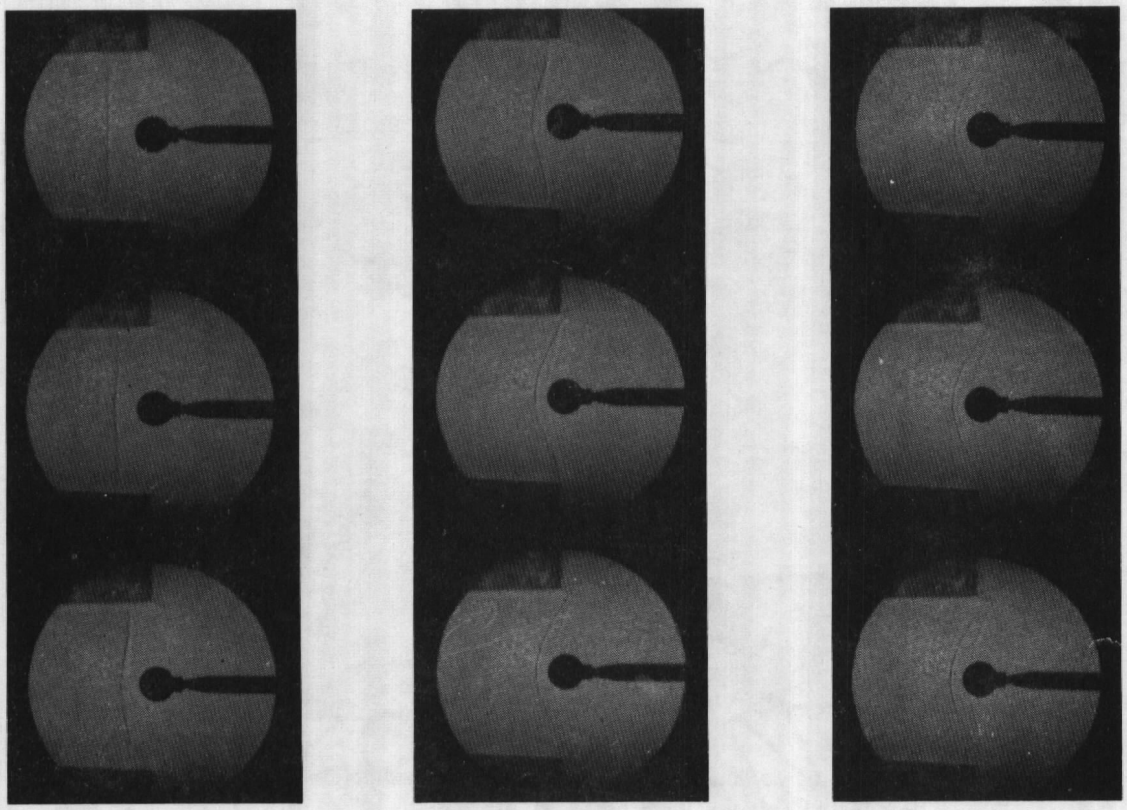

Fig. II-3 Excerpts from a Fastax movie of the flow in the tunnel, M_∞ = 1.47, 1/2 in. diameter sphere. The time interval between successive frames is approximately 1/5 msec.

Detailed Description of the Tunnel

A simplified side view of the tunnel is shown in Figure II.4 and the tunnel is the first piece of equipment in Figure II.5. The overall length of the intermittent tunnel is 26 ft. and it is fabricated entirely out of stainless steel 304. The high pressure end of the tunnel is made from a 10-foot length of seamless tube with 5.295 in. I.D. and 0.134 in. wall thickness. A transition piece made out of 1/8 in. plate and one foot in length connects the tube to a rectangular nozzle section 1-1/2 ft. in length. Screens may be introduced at this point. The nozzle section follows and it will be described in greater detail below. The diaphragm is placed between the nozzle section and another one foot transition section which contains the diaphragm rupturing pin and connects the nozzle section to the low pressure or dump tube. The dump tube is made of seamless tube 3.760 in. I.D. and 0.120 in. wall thickness and consists of two sections. The first section is 2-1/2 ft. long and is connected to the transition piece. The other section is 10 ft. in length. A 2 in. thick insert, the size of a 4 in. pipe flange, is located between these two pipes. The insert contains two quartz windows, 3/4 in. diameter and 1 in. thick, and permits a beam of light to pass through the tube. This arrangement acts as a shock detection station and is used to trigger the electronic instrumentation. The individual sections of the tube are sealed together by inserts containing O-rings placed between the flanges.

The downstream transition section and dump tube assembly is mounted on linear ball bushings which make it possible by a simple hand push to move the entire assembly approximately one foot away from the nozzle section along the tunnel centerline. This permits easy access to the test section as well as insertion and removal of diaphragms. The nozzle section, diaphragm and downstream transition section are held together by a wedge-shaped clamping device. The clamping device permits quick connection and disconnection of the two parts of the tunnel.

The entire tunnel assembly is mounted on a 4 in. I-beam and supported by several 4 in. diameter black pipes. This arrangement is rigid and permits easy access to any part of the tube. A 3 ft. piece of the supporting I-beam flow the test section is removable. The nozzle section and this portion of the I-beam may be lifted and the Mach-Zehnder interferometer, manufactured by the Zeiss Company, positioned in place.

The nozzle section is rectangular with 2 in. by 5 in. inside dimensions and 1-1/2 ft. in length. This section contains the nozzle blocks, test section and model support. The side walls extend to practically the entire length of the section and are sealed to it by means of O-rings. The nozzle blocks are two inches in width and rest on the top and bottom of the rectangular nozzle section. They are held in place by screws and are sealed by O-rings concentric with the screws. The side walls may be easily removed to exchange the nozzle blocks which have been machined out of Plexiglass. The windows are mounted and sealed in

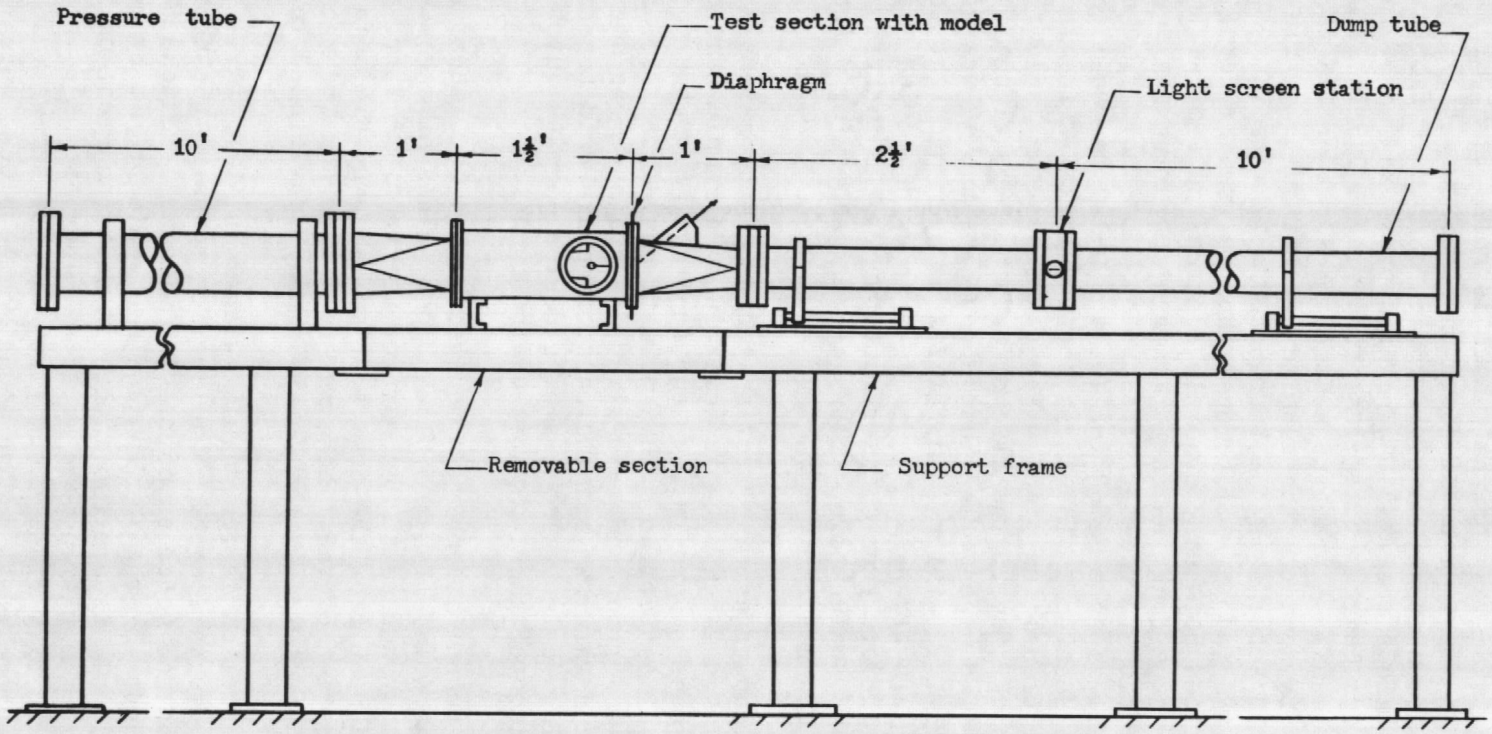

Pressure tube: 5.295 in. I.D., 0.134 in. wall, stainless steel 304 seamless tube.
Dump tube: 3.760 in. I.D., 0.120 in. wall, stainless steel 304 seamless tube.
Nozzle: two dimensional, 2 x 2 in. throat.

Fig. II-4 Sketch of the intermittent tube wind tunnel

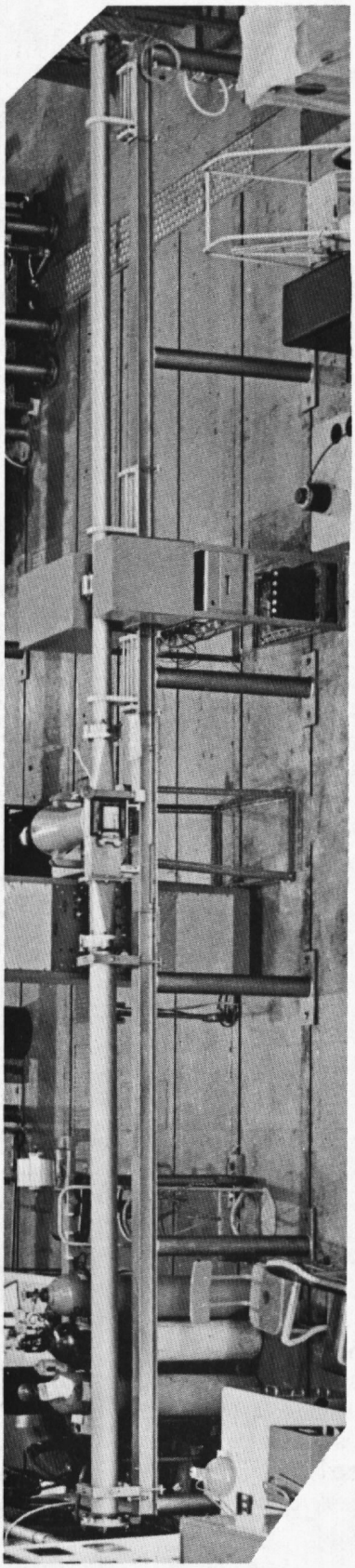

Fig. II-5 The intermittent tube wind tunnel

metal frames which in turn are sealed by means of O-rings into the side walls. Windows are held flush with the inside of the nozzle walls by threaded retaining rings. The windows are 4 in. in diameter, one inch thick, and are made of Schott BK-7 glass ground to 1/8 wave length with a wedge angle not greater than 20'. The location of the windows is at the downstream end of the nozzle blocks and near the diaphragm end of the test section. The model support is mounted in the nozzle section near the diaphragm. Models extend into the nozzle section, as viewed through the window, and are easily changed by reaching into the test section while the diaphragm is being changed. A photograph of the nozzle section is shown in Figure II.6. Portions of the clamping device and the firing pin are also visible in this photograph.

The reacting gas mixtures are prepared in a special separate gas preparation facility. This facility is shown behind the gas bottles on the left of Figure II.5, and a simplified schematic diagram is shown in Figure II.7. The gas mixture preparation takes place in two large stainless steel tanks which are connected to each other. The contents are circulated from one tank to the other by a circulating pump, and thereby, are thoroughly mixed. All lines which connect the tanks and lead to the pressure measuring system and the tunnel are made of 1/4 or 1/2 in. stainless steel tubing. The needle and ball valves used here are also made of stainless steel. The entire gas preparation facility is enclosed in a fume hood which is part of an exhaust system consisting of a 12 in. diameter galvanized steel duct connected to a 3,000 cu. ft. per minute blower which exhausts to the atmosphere outside of the laboratory.

Instrumentation of the Tunnel

The tunnel is instrumented with a temperature and pressure measuring system, a photographic system and a supporting electronic system. Temperatures are read with copper-constantan thermocouples which have been calibrated to within less than 0.2°C. The thermocouples are located in the mixing tank and in the endplate of the pressure tube. A number of thermocouples is also attached to the outside surface of the pressure tube in several different positions and is used to monitor the temperature of the tube during the course of a series of experiments.

The pressure system consists of a precision static pressure measuring system used for the measurement of the pressure during reactant gas mixture preparation and for the tunnel pressure measurement, and a high response pressure transducer for transient pressure measurement in the tunnel nozzle. Due to the corrosive nature of the NO_2 gas, the static pressure system is separated from the reactant gas mixture by a differential stainless steel diaphragm strain gauge pressure transducer (Dynisco model DPT 85-2). A coarse pressure measurement is obtained with

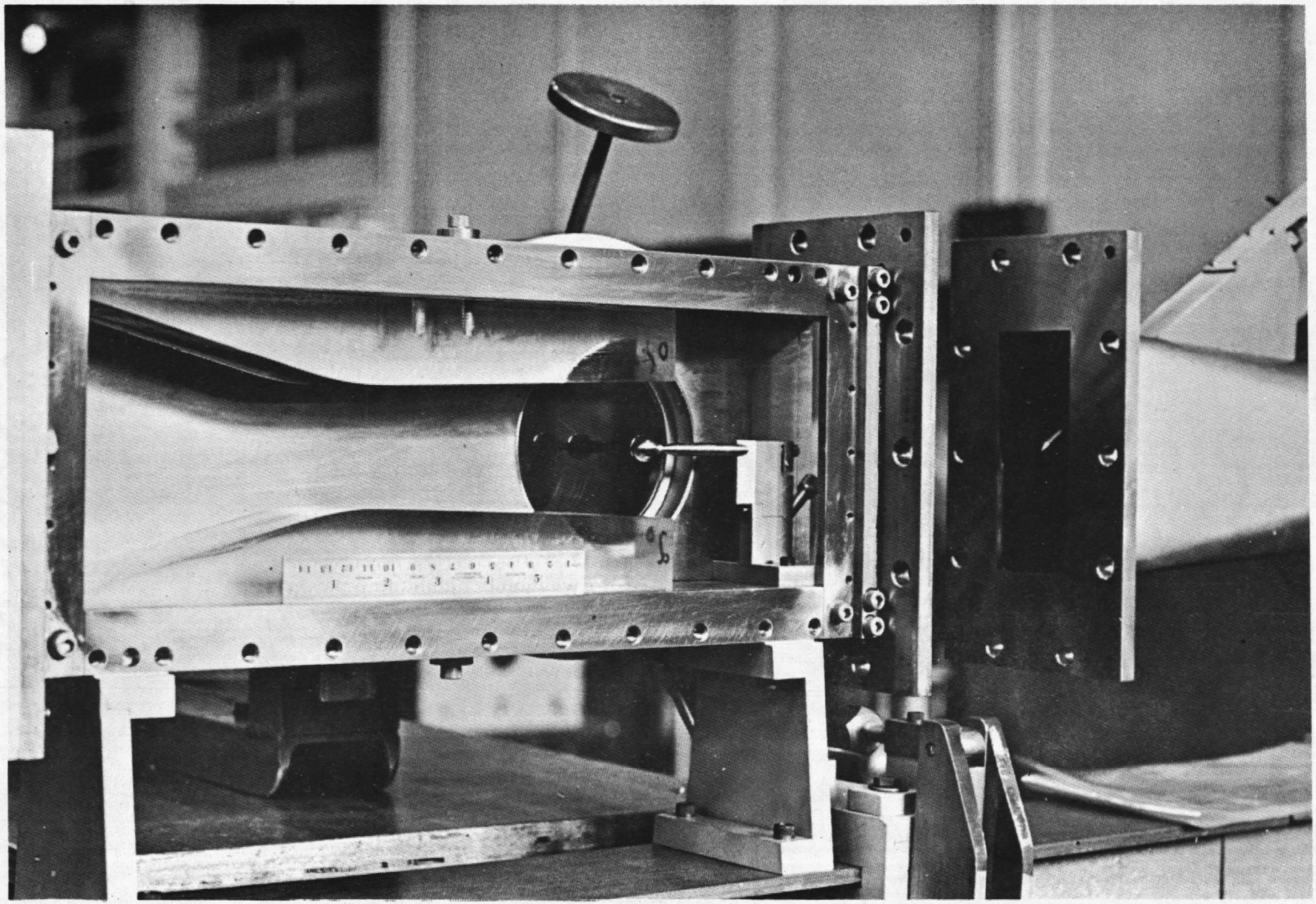

Fig. II-6 Nozzle section, $M_\infty = 1.5$, of the intermittent tube wind tunnel. Sphere model is in the test section. Note diaphragm section in open condition. The flow is from left to right.

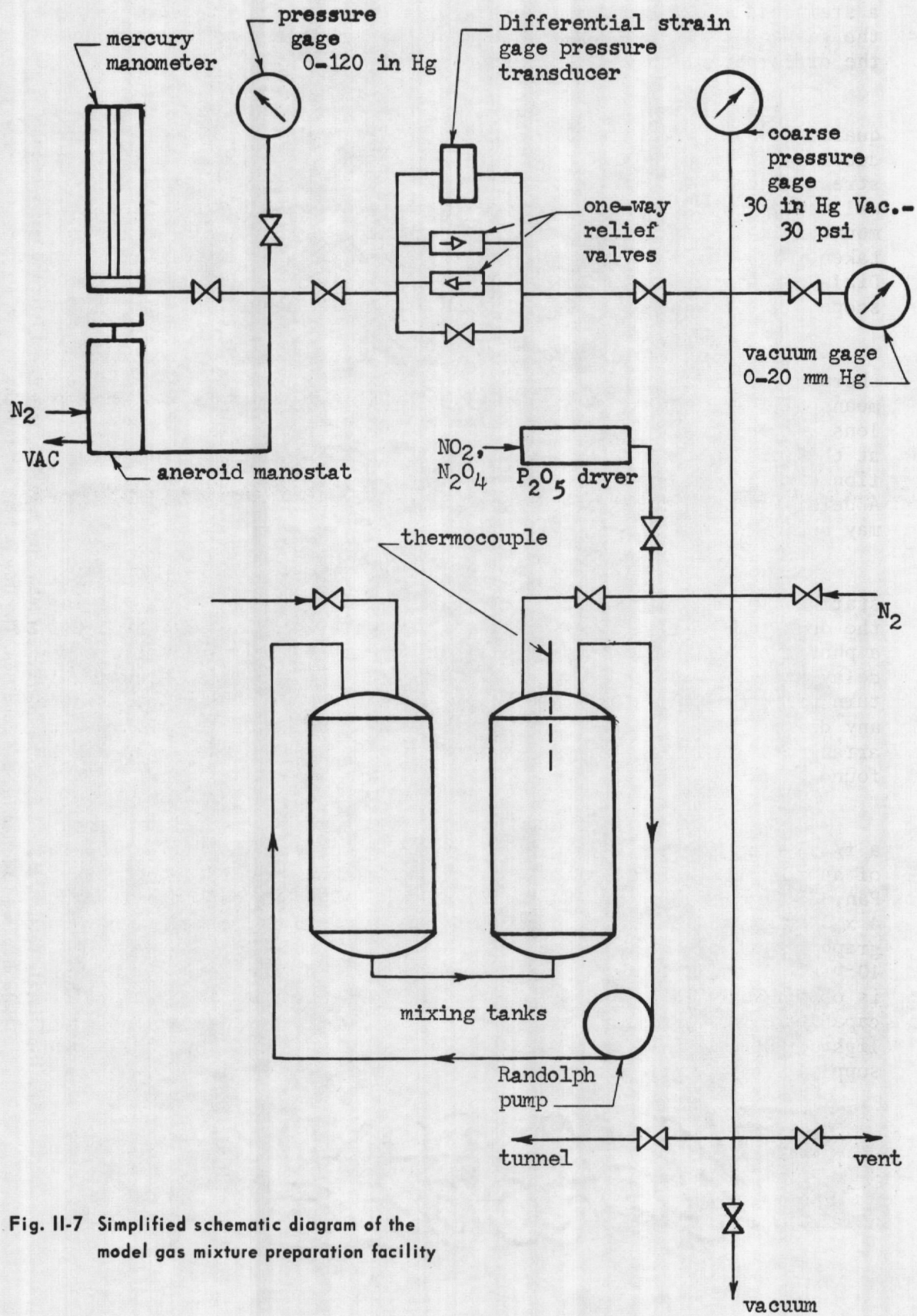

Fig. II-7 Simplified schematic diagram of the model gas mixture preparation facility

a stainless steel Bourdon tube gauge which is in direct communication with the gas and a fine pressure reading is obtained on the reference side of the differential pressure transducer.

Transient pressure recordings are made with a piezo-electric quartz-crystal pressure transducer (Kistler Model 606 L). The transducer may be mounted in an insert between the pressure tube and the upstream transition section and also in the nozzle side wall. The side wall location is near the exit of the nozzle and the transducer is mounted in a blank which replaces the window when pressure readings are taken. The output of the transducer is amplified by a Kistler Universal Dial-Gain Charge Amplifier Model 504 and it is recorded on an oscilloscope. The rise time is given to be 3 microseconds.

The flow field about a sphere is recorded by shadowgraph and sharp focus shadowgraph methods in parallel light which is collimated by means of a f/6, 610 mm focal length Bausch & Lomb Aero Tessar aerial camera lens. A spark light source with a 0.08 cm diameter source is located at the focal point of the lens. The spark light source unit has a duration of 0.5×10^{-6} sec. and is of the type suggested by Kovasznay (48). A detailed description of the spark source and its power supply used here may be found in Klikoff (49).

The spark source is triggered by a light screen shock detection station. After rupture of the diaphragm, the shock wave travels into the dump tube and triggers the light screen by bending a light beam into a phototube. The output of the light screen is then fed into a time delay unit (General Radio Time Delay Generator, Type 1392-A) which in turn triggers a thyratron amplifier and spark source combination after any desired time interval. A detailed description of the light screen arrangement and signal amplification instrumentation used here may be found in Eberstein (50).

The sharp focus shadowgraphs are recorded by a Leica camera with a f/4.5, 135 mm lens with close-up bellows set at a magnification ratio of approximately 1.01. The image of the flow is recorded on Kodak Tri-X Pan, 35 mm film with an ASA rating of 400. Shadowgraphs are recorded on 4 x 5 in. type 52 and 3 x 4 in. type 42 Polaroid film, and in both photographic systems the exposure is determined by the short duration (0.5×10^{-6} sec.) spark source. A shadowgraph movie of the flow in the tunnel is obtained by a Fastax 16 mm Model WF3 high-speed motion picture camera capable of photographing at the rate of 5,000 frames per second and the light source in this case is a mercury arc lamp driven by a D.C. power supply.

Experimental Procedure

The experimental procedure begins with the preparation of a desired reactant gas mixture. First, the entire tunnel and gas mixing apparatus is purged with dry nitrogen and the lines which carry the N_2O_4 and NO_2 gases are purged with the reactant gases. After purging, the mixing apparatus is evacuated to approximately 1 mm Hg abs. and then filled with the test gases. The gas mixture is prepared by first introducing a small quantity of nitrogen (approx. 100 mm Hg), then the gases NO_2 and N_2O_4 are added, and finally nitrogen is again added to the total desired pressure of the entire mixture (3 atmospheres). For each addition, the temperature and pressure of the gas is recorded after a constant temperature and pressure of the mixture is achieved in the tanks. The gases are continuously mixed by recirculation through the mixing tanks during the preparation procedure. The quantity of the gas mixture prepared in this manner is sufficient for two fillings of the tunnel, and three such mixtures are required for each set of experiments. The reactant mass fraction of the mixture can generally be reproduced to within less than 0.001. Mixtures are prepared with average values of the reactant mass fraction of 0.215, 0.300 and 0.400. The gases used in the preparation of the gas mixture are obtained from Matheson cylinders. The nitrogen is the prepurified grade with a minimum purity of 99.996 percent by weight. The nitrogen dioxide has a minimum purity of 95.5 percent by weight, and the following specifications in percent by weight: water equivalent 0.1 max., chloride as nitrosyl chloride 0.08 max., and nonvolatile (ash) 0.01 max. The water vapor is removed by passing the nitrogen dioxide gas through a phosphorus pentoxide drier.

After the preparation of the mixture, the tunnel is readied for filling. A test model is inserted into the test section and a diaphragm is placed between the pressure and dump tubes. The pressure tube is evacuated to approximately 1 mm Hg abs. and then filled with the gas mixture to the desired pressure, 1.1 atmospheres at room temperature. The dump tube is evacuated to 135 mm Hg abs. Next, the shutter to the camera is opened and the pin is released to rupture the diaphragm and initiate the flow in the tunnel. The film in the camera is exposed by the spark light source 10 msec. after the shock wave in the dump tube reaches the light screen station.

At the conclusion of the experiment, the entire tunnel is filled with dry nitrogen to a pressure slightly above an atmosphere and the entire contents of the tunnel are then vented into the exhaust system. The tunnel is repeatedly flushed through with dry nitrogen until the toxic NO_2 gas is removed. Final trace of the gas is eliminated by evacuating and filling the tunnel with dry nitrogen several times.

The exposed negatives are developed in Kodak Microdol-X developer at 70 to 71°F. The fixing, washing and drying of the film follows

the manufacturer's recommended procedure. Developed negatives are read on a Leitz Microscope with a 60 to one magnification ratio. The microscope is used in conjunction with a traveling carriage advanced by precision screws and the negative is held by the carriage with a vacuum frame. The desired coordinates on a negative, as determined by the position of the cross hairs on the image are automatically recorded and readings can be made to 0.0001 cm.

Appendix III
Equilibrium Flow Analysis in the Tube Wind Tunnel

Equilibrium Flow in the Nozzle

The flow in the nozzle is assumed to be inviscid, adiabatic and steady quasi-one-dimensional. The continuity, momentum and energy equations (51) in terms of non-dimensional variables are:

$$\rho u A = \rho^* u^* = m \ , \tag{III.1}$$

$$u \frac{du}{dx'} + \frac{1}{\rho} \frac{dp}{dx'} = 0 \ , \tag{III.2}$$

and

$$h + \frac{1}{2} u^2 = h_o \ . \tag{III.3}$$

Sonic throat quantities are denoted by a superscript asterisk and m and h_o are constants for a given environment. The constant h_o is evaluated at the stagnation condition. The non-dimensional quantities are given by: $T = T'/T_*$, $\rho = \rho'/\rho_*$, $h = h'/Q_R$, $u = u\sqrt{Q_R}$, $p = p'/(\rho_* Q_R)$ and $A = A'/A^*$. The equations of state and the rate equation (Appendix I) are given by:

$$p = \rho T[a(1 + \alpha) + b] \ , \tag{III.4}$$

$$h = cT + \alpha, \tag{III.5}$$

and

$$u \frac{du}{dx} = \theta_1 \rho[(1 - \alpha) \frac{e^{-1/T}}{T} - \rho\alpha^2], \tag{III.6}$$

where a, b, c and $\theta_1 = \theta/\sqrt{Q_R}$ are constants for a given environment and are defined in Appendix I. In a flowing system the derivative $d\alpha/dt$ in the rate equation, Equation I.22, is replaced by the substantial derivative $D\alpha/Dt$ ($D/Dt = \partial/\partial t + u\, \partial/\partial x$), and in Equation II.6 the substantial derivative is replaced by the form $u\, d\alpha/dx$ applicable to steady one-dimensional flow. If the geometry of the nozzle is known

$$A = A(x) \ , \tag{III.7}$$

the system of Equations (III.1) through (III.6) constitute six equations for the six unknowns ρ, u, p, h, T and α, and the non-equilibrium flow is completely specified. This system of equations cannot, in general, be solved analytically. It is possible, however, to obtain analytic solutions for the limiting cases of frozen and equilibrium flows.

For frozen flow $D\alpha/Dt = 0$ and α = constant, and the above system of equations is reduced by one equation. The frozen flow solution for a given nozzle geometry is obtained from the system of five Equations (III.1) through (III.5) and α = constant for the five variables ρ, u, p, h and T.

Equilibrium flow is defined by the expression $x(p, \rho, \alpha) = 0$ at $\tau = 0$, Equation (I.22) and the rate equation, Equation (III.6) is replaced by the algebraic equation $x(p, \rho, \alpha_e) = 0$ which reduces to the equation of the law of mass action and is given by

$$\frac{\alpha^2}{1 - \alpha} = \frac{e^{-1/T}}{\rho T} \quad . \tag{III.8}$$

The equilibrium flow is solved by the system of six equations, Equations (III.1) through (III.5) and Equation (III.8) for the six unknown ρ, u, p, h, T and α where $A = A(x)$ is given. This system of equations may be reduced to a system of algebraic equations if the momentum equation is replaced by the isentropic condition (35). The isentropic relation is obtained as a consequence of the momentum and energy equations in differential form, and hence

$$ds = \frac{dh}{T} - \frac{1}{\rho T} dp = 0. \tag{III.9}$$

Integration of Equation (III.9) is performed in the following manner. The thermal and caloric equations of state and the law of mass action are expressed in their differential forms

$$\frac{dp}{p} = \frac{d\rho}{\rho} + \frac{dT}{T} + \frac{a\, d\alpha}{[a(1 + \alpha) + b]} , \tag{III.10}$$

$$dh = c dT + d\alpha , \tag{III.11}$$

and

$$\frac{d\rho}{\rho} = \left(\frac{1}{T} - 1\right) \frac{dT}{T} - d\left(\ell n \frac{\alpha^2}{1 - \alpha}\right) , \tag{III.12}$$

respectively. Equation (III.9) is expressed in terms of the two independent variables T and α by eliminating the differential quantities dh, dp and $d\rho$ by the use of Equations (III.10) through (III.12), hence

$$ds = c \frac{dT}{T} - [a(1+\alpha) + b] \frac{dT}{T^2} + \left(\frac{1}{T} - a\right) d\alpha + [a(1+\alpha)+b] d\left(\ell n \frac{\alpha^2}{1-\alpha}\right) = 0. \tag{III.13}$$

Equation (III.13) is expressed in a perfect differential form by assuming $a = 1$, as discussed in Appendix I. After extensive algebraic manipulation, Equation (III.13) becomes

$$ds = d\left[c\ \ell nT + \frac{1+\alpha+b}{T} + b\ \ell n\ \frac{\alpha^2}{1-\alpha} + 2\ \ell n\ \frac{\alpha}{1-\alpha}\right] = 0\ , \qquad \text{(III.14)}$$

which is integrated directly to give the isentropic relation

$$c\ \ell nT + \frac{1+\alpha+b}{T} + b\ \ell n\ \frac{\alpha^2}{1-\alpha} + 2\ \ell n\ \frac{\alpha}{1-\alpha} = s_o, \qquad \text{(III.15)}$$

where s_o is a constant evaluated at the stagnation condition. The isentropic relation, Equation (III.15), thus replaces the momentum Equation (III.2) and the system of governing equations becomes a system of algebraic equations. Before the algebraic system of equations can be solved, however, the mass flow rate, constant m in Equation (III.1) must be evaluated. The method of obtaining the mass flow rate follows the outline of the method used by Bray (32) for the ideal dissociating gas.

The differential form of the continuity and energy equations are

$$\frac{d\rho}{\rho} + \frac{du}{u} + \frac{dA}{A} = 0 \qquad \text{(III.16)}$$

and

$$dh + u\ du = 0\ . \qquad \text{(III.17)}$$

An expression for $d\alpha/dA$ is obtained by eliminating the differential quantities $d\rho$, du, dh and dT from the Equations (III.11), (III.12), (III.14), (III.16) and (III.17). Furthermore, since

$$\frac{d\alpha}{dA} = \frac{d\alpha}{dx'} \Big/ \frac{dA}{dx'}\ , \qquad \text{(III.18)}$$

the expression for $d\alpha/dx'$, after extensive algebraic manipulation becomes with a = 1

$$\frac{d\alpha}{dx'} = \frac{1}{A}\frac{dA}{dx'}\ \frac{\alpha(1-\alpha)u^2T[(1+\alpha+b) - cT]}{\phi_1T^3 + \phi_2T^2 + \phi_3T + \phi_4}\ , \qquad \text{(III.19)}$$

where

$$\phi_1 = \alpha(1-\alpha)c + (2 - \alpha)[2c - (1+\alpha+b)]c,$$

$$\phi_2 = 2(2-\alpha)(h_o-\alpha)(1+\alpha+b-c) - 2\alpha(1-\alpha)[2c + h_o - \alpha]\ ,$$

$$\phi_3 = \alpha(1-\alpha)[4(h_o-\alpha) + 2c + 1 + \alpha + b],$$

and

$$\phi_4 = -2\alpha(1-\alpha)(h_o - \alpha)\ .$$

From Equation (III.19) it is seen that $d\alpha/dx' \to 0$ as $dA/dx' \to 0$. The condition $dA/dx' = 0$ denotes the location of the throat. However, for equilibrium flow $d\alpha/dx' \neq 0$ at the throat and, therefore, the following condition must be satisfied.

$$\phi_1(\alpha^*)T^{*3} + \phi_2(\alpha^*)T^{*2} + \phi_3(\alpha^*)T^* + \phi_4(\alpha^*) = 0, \qquad \text{(III.20)}$$

where the starred quantities represent the values at the throat. The isentropic Equation (III.15) is also expressed in terms of the throat values and a simultaneous solution of Equations (III.15) and (III.20) determines α^* and T^*. The mass flow rate m follows from Equations (III.3), (III.5) and (III.7) which are combined into the equation

$$m = \rho^* u^* = \frac{1-\alpha^*}{\alpha^{*2}} \frac{e^{-1/T^*}}{T^*} \sqrt{2(h_o - \alpha^* - cT^*)}. \qquad \text{(III.21)}$$

The system of algebraic equations is now completely determined for a given nozzle geometry and the solution for the variables ρ, u, T and α follows directly from these equations. Due to the transcendental nature of Equation (III.15), however, the solution to this system of algebraic equations is worked out by iteration schemes on Yale's IBM 7094/7040 DCS computer. A rough outline of the computational scheme is given in Appendix VI.

It is recalled that the system of algebraic equations is obtained as a result of the assumption a = 1 (Appendix I). The consequence of this assumption is checked by comparing the results obtained by the above simplified method with the results from a complete solution of the governing equations for the same gas mixture obtained by Wegener and Cole (43). A comparison of the solution obtained from the isentropic relation is shown in Figure III.1 and the agreement is good. Some differences in the comparison also arise due to the slightly different physical constants used by Wegener and Cole (43).

Equilibrium Flow in the Pressure Tube

The flow in the tunnel upstream of the nozzle is given by a solution of the equilibrium flow through a centered expansion fan. The derivation of the changes in gas velocity and gas properties through the expansion fan is identical to the derivation in a non-reacting perfect gas, except that the ordinary sound speed is now replaced by the equilibrium sound speed of the reacting medium. The compatibility relations for the equilibrium flow are given in Ref. (51) as

$$du \pm \frac{dp}{\rho a_e} = 0 \qquad \text{(III.22)}$$

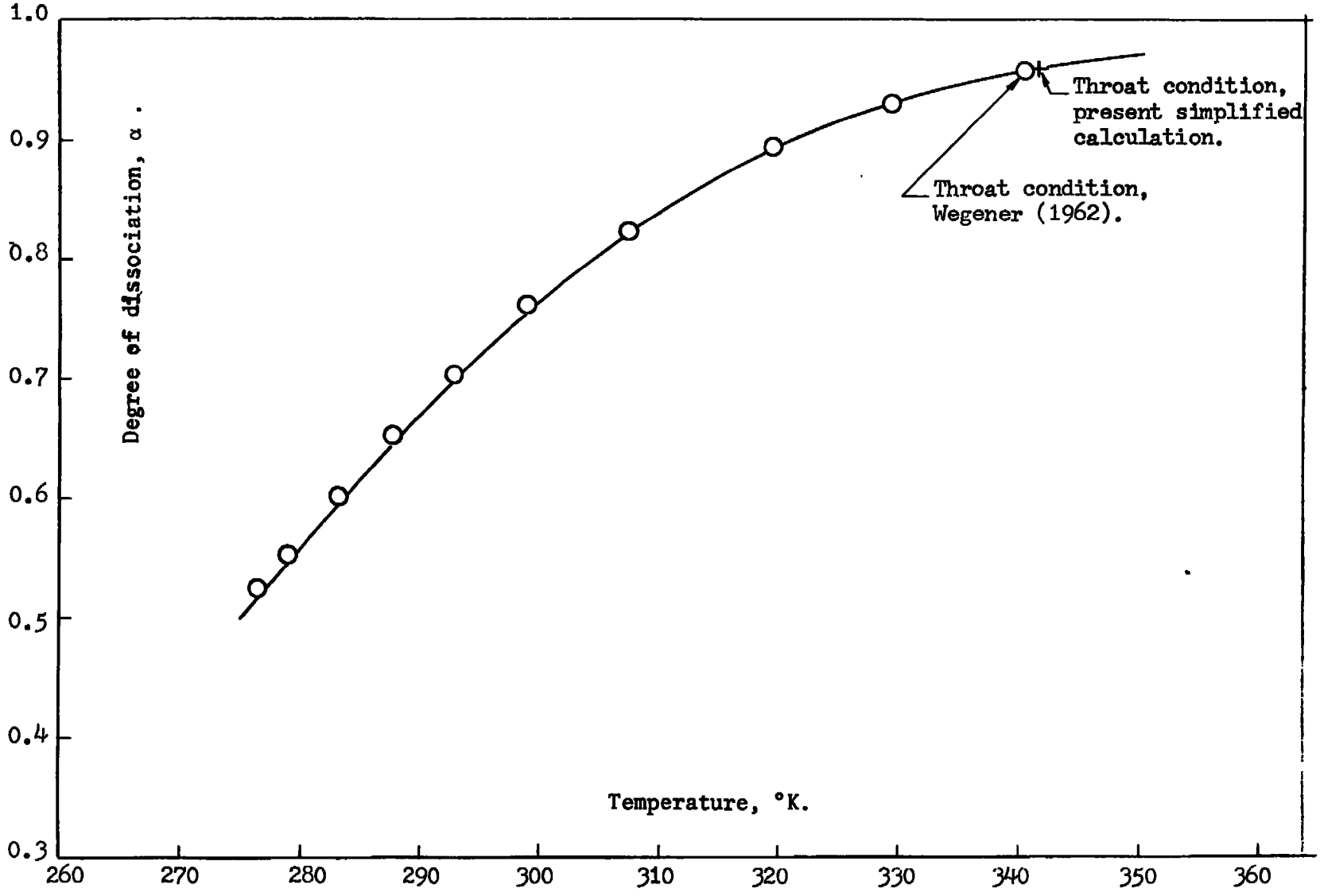

Fig. III.1 Comparison between present simplified calculation with Wegener's (1962) more exact calculation (T_o = 405°K, p_o = 2.2 atmos., ω_o = 0.08)

along the characteristic directions

$$\frac{dx}{dt} = u \pm a_e, \tag{III.23}$$

where the positive and negative signs designate the direction of propagation and a_e is the equilibrium sound speed as given in Appendix I, Equation (I.29). Equation (III.22) is rewritten in a more useable form in terms of the variables u, T and α in the following manner. The differential quantity dp is replaced by the differential quantity dT with the use of the thermal equation of state, Equation (III.4), the law of mass action, Equation (III.7) and the isentropic relation, Equation (III.15). In terms of these new variables, and along the positive direction of propagation across the wave, Equation (III.22) is written in the form

$$du + \frac{1 + \alpha + b - \lambda c T^2}{a_e T(1 - \lambda T)} dT = 0, \tag{III.24}$$

where

$$\lambda = 1 - \frac{(2 - \alpha)(1 + \alpha + b)}{\alpha(1 - \alpha)} .$$

The induced velocity behind the expansion fan $u_{4'}$ is thus given by

$$u_{4'} = - \int_{T_4}^{T_{4'}} \frac{1+\alpha+b-\lambda c T^2}{a_e T(1-\lambda T)} dT . \tag{III.25}$$

where the subscript 4 designates the undisturbed state. The variables α and T in the integrant are related by the isentropic relation, Equation (III.15) and the integral is evaluated numerically due to the implicit functional relationship between α and T and the complicated form of the integrant.

In order that the induced velocity, $u_{4'}$, may be calculated, it is necessary to know the temperature behind the expansion fan, $T_{4'}$. Although the strength of the expansion fan and, therefore, the value of $T_{4'}$, is determined by the ratio of the tube area to nozzle throat area, the actual value of $T_{4'}$ is not known apriori. The value of $T_{4'}$ can be found only by simultaneously solving the entire flow in the tube-nozzle combination. The calculation method consists of matching the flow properties behind the expansion fan with the flow properties at the nozzle entrance. The procedure is outlined below. For a given undisturbed state of the gas in the tube, a guess is made at the stagnation conditions for the nozzle flow. This enables one to calculate all properties and in particular, $T_{4'}$, in the nozzle at the point corresponding to the tube area, and with this value of $T_{4'}$ the induced velocity $u_{4'}$ is calculated by Equation (III.25). The values of $u_{4'}$ obtained from the nozzle

and expansion fan calculations are compared and an iteration scheme is used which repeats the above calculations until agreement to some specified accuracy is found. When the flow behind the expansion fan is matched with the flow in the nozzle, the equilibrium flow in the tunnel and, in particular, at the nozzle test section, becomes completely determined.

Appendix IV
Non-Equilibrium Flow Analysis in the Nozzle and Non-Equilibrium Flow Through a Shock Wave

Non-Equilibrium Flow in the Nozzle

The assumption that the flow in the nozzle is in equilibrium may not always be justified and an independent method must be developed which can check for possible departures from equilibrium flow. The method to be described below follows closely the method proposed by Bray (32).

Non-equilibrium nozzle flow has the following characteristics. Initially, the flow is ordinarily at equilibrium. Departure from equilibrium may take place anywhere in the nozzle, usually downstream of the throat. Once departure occurs, it takes place in a narrow region and may be assumed to occur at a point, the "sudden freezing" point. The flow downstream of this location is assumed to be frozen (32). The rate equation can be expressed in the form

$$\frac{d\alpha}{dt} = r_D - r_R, \tag{IV.1}$$

where r_D and r_R, are the recombination and dissociation rate functions implied in Equation (I.18). The "sudden freezing" point is given by the condition

$$-\frac{d\alpha}{dt} = Kr_D , \tag{IV.2}$$

where K is a constant taken to be of order unity by Bray. Since at equilibrium the condition $r_D = r_R$ is closely satisfied, Equation (IV.2) may also be written as

$$-\frac{d\alpha}{dt} = Kr_R , \tag{IV.3}$$

where it is simpler to compute r_R since k_R is taken as a constant for the reaction. For steady flow, the left hand side of the equation is expressed by $d\alpha/dt = u'd\alpha/dx'$, and the criterion for the "sudden freezing" point becomes

$$-\left(\frac{d\alpha}{dx'}\right)_e = K\,\theta_1\,\frac{\rho_e^2\,\alpha_e^2}{u_e} , \tag{IV.4}$$

where $\theta_1 = 4\omega_o\omega_{N_2}K_R\rho_*^2/(\mu_{N_2}\mu_{N_2O}\sqrt{Q_R})$, the subscript e denotes the equilibrium values, and the expression for the left hand side is given by Equation (III.19). Since the equilibrium properties along the nozzle have already been calculated, both sides of Equation (IV.4) are known and the point at which the flow departs from equilibrium is found when

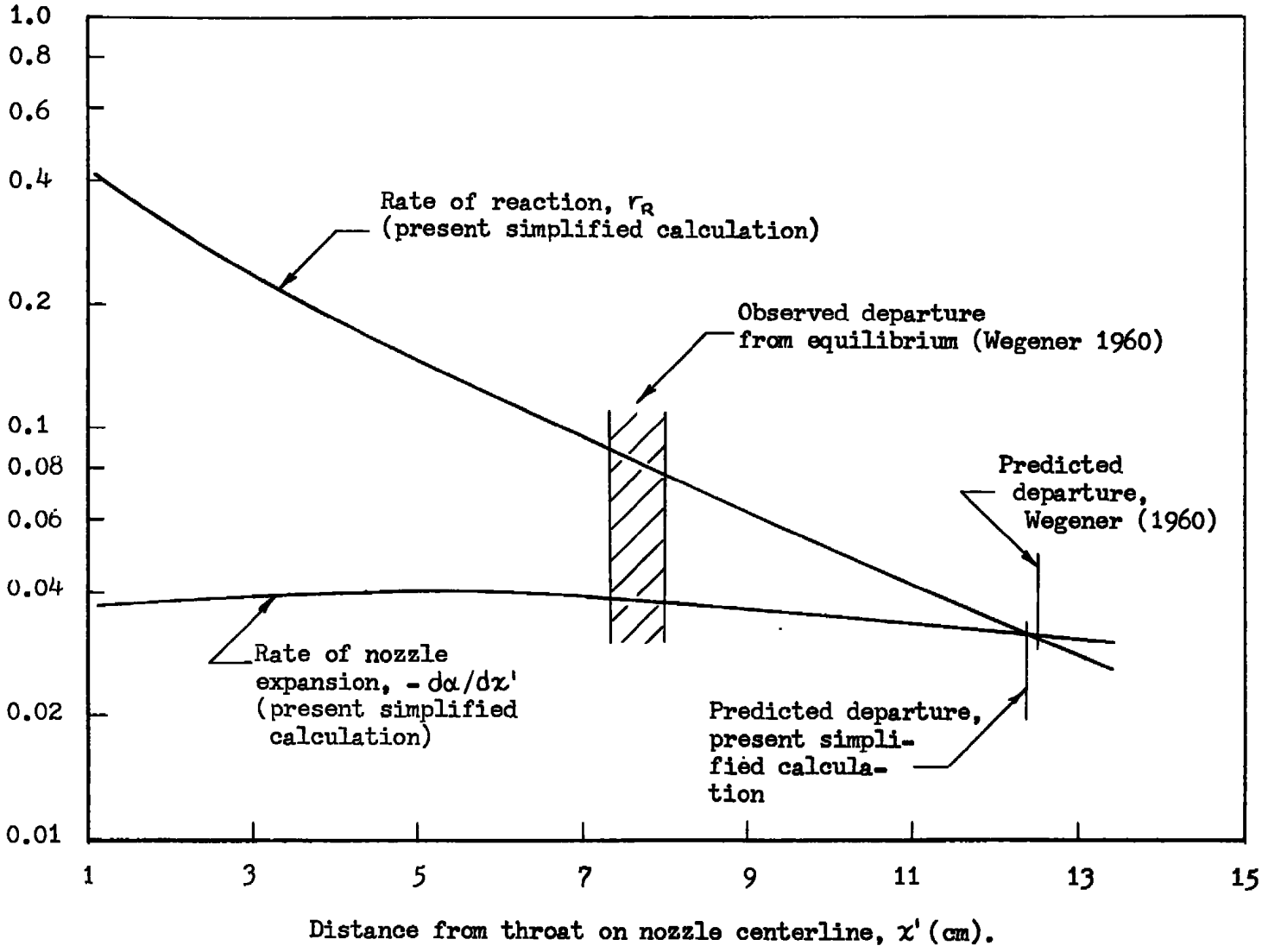

Fig. IV-1 Comparison of observed departure from equilibrium with predicted points of departure (T_o = 402 °K, p_o = 2.16 atmos., ω_o = 0.04)

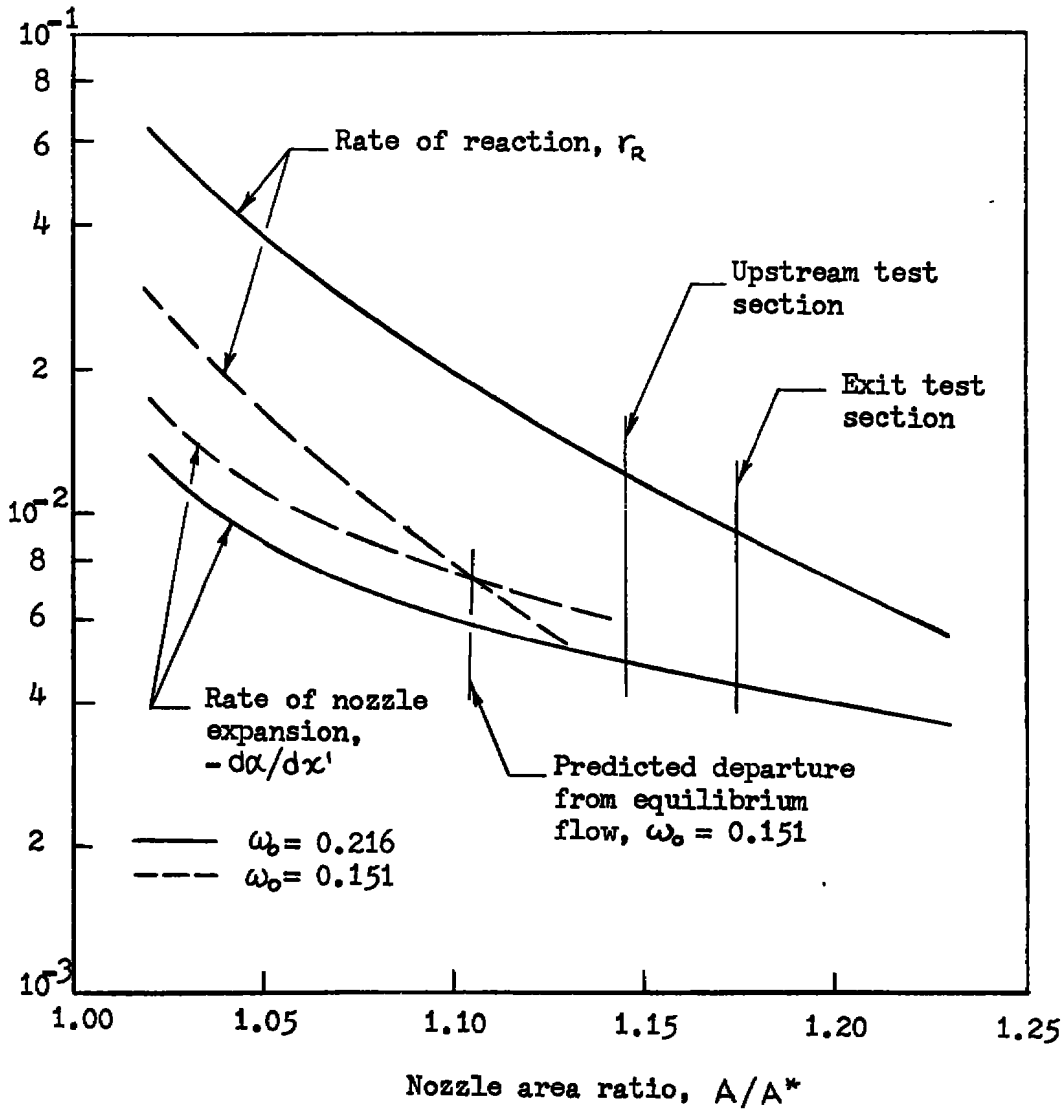

Fig. IV.2 Prediction of the point of departure from equilibrium flow in the nozzle

the condition expressed by Equation (IV.4) is satisfied.

The applicability of the sudden freezing analysis to nozzle flow was first experimentally demonstrated by use of the present reacting gas model (40). A comparison of the approximate method developed for the current purpose with Wegener's more exact calculations is shown in Figure IV.1. For all practical purposes, the two predictions of the point of departure from equilibrium are the same.

The "sudden freezing" criteria is used in all nozzle flow calculation to insure that the flow in the free stream is in equilibrium. A representative result of such a calculation is shown in Figure IV.2 for the reactant mass fraction $\omega_o = 0.216$ with the pressure tube filled to atmospheric pressure at room temperature. This result indicates that the free stream can be assumed to be in equilibrium for $\omega_o \geq 0.216$. A calculation has been also made to determine the reactant mass fraction which would result in a departure from equilibrium and such a result is shown in Figure IV.2 for $\omega_o = 0.151$.

Non-Equilibrium Flow Through a Normal Shock Wave

Consider a standing normal shock wave. The equations of continuity, momentum and energy in terms of dimensionless variables are (51)

$$\rho_\infty u_\infty = \rho u \ , \tag{IV.5}$$

$$p_\infty + \rho_\infty u_\infty^2 = p + \rho u^2 \ , \tag{IV.6}$$

and

$$h_\infty + \frac{1}{2} u_\infty^2 = h + \frac{1}{2} u^2 \ , \tag{IV.7}$$

where the subscript ∞ denotes the conditions upstream of the shock wave which are known and the unsubscripted variables denote conditions downstream of the shock wave. The rate equation for one-dimensional steady flow is given by (Appendix I),

$$u \frac{d\alpha}{dx'} = \theta_1 \rho \left[(1 - \alpha) \frac{e^{-1/T}}{T} - \rho \alpha^2 \right] \ , \tag{IV.8}$$

where $\theta_1 = \theta / \sqrt{Q_R}$ is a constant for a given environment, and primes denote dimensional quantities. The caloric and thermal equations of state are given by (Appendix I)

$$h = cT + \alpha \tag{IV.9}$$

and

$$p = \rho T \left[a(1 + \alpha) + b \right] \ . \tag{IV.10}$$

The expressions for the constants appearing above and the definitions of the dimensionless variables are given in Appendix I. The above system of equations, Equation (IV.5) through (IV.10), constitute six equations for the six unknown variables ρ, u, p, h, T and α. The solution to this system of equations is obtained by rearranging Equations (IV.5) through (IV.7), (IV.9) and (IV.10) into the form

$$\frac{u}{u_\infty} = \frac{\rho_\infty}{\rho} = \frac{1+p_\infty/\rho_\infty u_\infty^2}{2-A/c}\left[1-\sqrt{1-\frac{A/c[2-A/c][1+2(h_\infty-\alpha)/u_\infty^2}{[1+p_\infty/\rho_\infty u_\infty^2]^2}}\right] \quad \text{(IV.11)}$$

and

$$T = \frac{u_\infty^2}{2c}\left[1 + \frac{2}{u_\infty^2}(h_\infty - \alpha) - \left(\frac{u}{u_\infty}\right)^2\right], \quad \text{(IV.12)}$$

where $A = a(1 + b) + c$. The rate equation is written in the form

$$\frac{d\alpha}{dx'} = F_1(\alpha), \quad \text{(IV.13)}$$

where $F_1(\alpha)$ is given by

$$F_1(\alpha) = \theta_1 \frac{\rho}{u}\left[(1-\alpha)\frac{e^{-1/T}}{T} - \rho\alpha^2\right], \quad \text{(IV.14)}$$

and the quantities ρ, u and T are expressed in terms of α by Equations (IV.11) and (IV.12). The variation of α with distance downstream of the shock wave is given by

$$x' = \int_{\alpha_s}^{\alpha} \frac{d\alpha}{F_1(\alpha)}, \quad \text{(IV.15)}$$

where α_s is the value of α immediately behind the shock wave, and $\alpha_s = \alpha_\infty$. Once the function $x' = x'(\alpha)$ is known, the solution for the other values with x' is obtained from Equations (IV.6), (IV.7), (IV.11) and (IV.12) by direct substitution.

An estimate of the time required to reach equilibrium may be obtained by considering the time required for the dissociation to reach 95% of its equilibrium value (1). Hence, a characteristic time of the reaction may be defined by

$$\tau_r = \int_0^{\tau} dt = \int_{\alpha_s}^{0.95\alpha_e} \frac{d\alpha}{F(\alpha)}, \quad \text{(IV.16)}$$

where $F(\alpha) = u' F_1(\alpha)$, and α_e is the equilibrium value of α and is obtained from the equilibrium solution of the shock wave.

The equilibrium solution of the shock wave is obtained by replacing the rate equation with the equation of the law of mass action, i.e. the

equation

$$\frac{\alpha^2}{1-\alpha} = \frac{e^{-1/T}}{\rho T} \quad , \tag{IV.17}$$

and the solution is given by the system of five equations, Equations (IV.6), (IV.10) through (IV.12) and (IV.17) for the five unknown variables ρ, u, p, T and α. The frozen solution of the shock wave is obtained by replacing the rate equation by the condition $\alpha = \alpha_\infty$ and the solution is given directly by Equations (IV.11) and (IV.12) for the unknown variables ρ, u and T.

Appendix V
Reduction of Experimental Data

Stand-off distance measurements are obtained from sharp focus shadowgraph negatives of the flow field. The camera is focused on a plane 0.01 in. from the centerline of the sphere toward the camera and the image of the flow field is recorded in a parallel light beam. On a photograph or a screen, the shock wave appears as a narrow dark line followed by a bright edge, Figure 10, and is caused by the refraction of the light beam in a narrow zone adjacent to the shock front.

Measurements are made with a traveling microscope at a 60 to 1 magnification ratio. The negative is attached to a traveling vacuum carriage and the direction of the flow and the cross hairs in the microscope sights are lined up parallel to each other. The direction of the flow is indicated by the image of an external guide wire which is parallel to the nozzle centerline. The carriage is advanced by precision screws relative to the cross hairs and the desired position of the carriage as marked by the cross hairs is recorded automatically. Positions of the carriage can be resolved to 0.0001 cm and the cross hairs appear 0.0003 cm thick on the projection of the image. A reading of the stand-off distance, i.e. the shortest distance between the shock wave and the body, is made along the centerline of the flow field. First the position of the apparent shock wave is recorded and then the position of the tip of the sphere. The stand-off distance is taken as the distance from the tip of the sphere to the midpoint of the apparent shock wave, i.e. the dark line. The apparent shock thickness is approximately 0.002 cm. The actual thickness of the shock wave as determined from experiments in nitrogen at room temperature and pressure and at $M = 1.4$ is approximately 6×10^{-5} cm (52) and is negligible with respect to the apparent thickness of the shock wave. The apparent shock thickness cannot be decreased further by focusing closer to the centerline since the shock image of the 1/32 in. diameter sphere becomes too faint and the location of the shock cannot be seen on the negative. A measurement of the sphere diameter is made in a direction perpendicular to the flow axis and the stand-off distance is made dimensionless with respect to the radius of the sphere. Readings of the diameter of the sphere at several inclinations to the axis do not reveal any significant distortion of the image.

The stand-off distance and the dimensionless stand-off distance for a series of experiments in dry nitrogen is shown in Table (V.1). Each measurement in this table as well as all measurements given here represent an average of five readings of the same negative. Measurements of the same length are generally within 0.0003 cm of each other. Errors in the readings arise primarily due to optical and photographic limitations of the experimental technique. Diffraction, scattering of light within the film and the grain size of the film cause the image of

a sharp edge or a narrow line to appear as a diffused region. The light scattering effect and the grain size can be related to the resolution of the film. The Kodak Tri-X Pan film used here has a medium resolving power corresponding to 0.001 cm per line which is one half the apparent shock thickness. The width of the diffused region varies between 0.0005 and 0.0010 cm for the largest and smallest spheres, respectively. In the present readings the edge is judged to be approximately in the center of the diffused region. Although readings can be made with high precision, their accuracy depends on the reader's judgment of the edge of the sphere and the apparent shock wave. To reduce the effect of reading errors, all measurements presented here have been obtained during one reading session. Measurements of the negatives also have been made by an independent reader and the difference in measurements between the two readers has been generally less than 0.0005 cm. Based on a uncertainty of ±0.0005 cm, a fractional standard deviation of the dimensionless stand-off distance is 2.4 percent for the 1/32 in. diameter sphere and proportionately less for the larger spheres with 0.2 percent for the largest sphere.

The dimensionless stand-off distance remains constant within reading error for the smaller spheres and decreases systematically by approximately 2.5 percent as the size of the sphere is increased, (Table (V.1)). This decrease is a consequence of the non-uniform flow in the nozzle. It is recalled that a Mach number gradient exists along the centerline of the nozzle and that there is also a slight variation in Mach number in a direction perpendicular to the centerline. For each set of experiments the sphere is positioned in the nozzle such that the tip of the bow shock wave is in approximately the same location in the free stream for all spheres. Thus, the free stream at the tip of the bow shock wave is always reproduced. However, as the size of the sphere is increased, the increased subsonic region becomes exposed to an increasingly larger portion of the non-uniform free stream and the stand-off distance responds accordingly. The subsonic region of the flow field can be approximated by a method developed by Moeckel (53). The subsonic region for a flow at M = 1.5 in nitrogen has been calculated and the results of the calculation are demonstrated in Figure V.1. The point at which the sonic line intersects the detached shock wave is approximately 2.1R above the axis of symmetry and approximately 0.6R behind the position of the tip of the bow wave. For the 5/8 in. diameter sphere the Mach number increases by approximately 1 percent along the nozzle centerline in the distance from the tip to the sonic point on the detached shock wave. The corresponding decrease in the dimensionless stand-off distance is approximately 2 percent. Since the major variation in the dimensionless stand-off distance observed in the present experiments occurs with the larger spheres, it can be attributed to the non-uniform free stream in the nozzle.

A systematic error and additional variation in the stand-off distance can also be introduced by viscous effects in the shock layer. An apparent increase in the stand-off distance can be observed due to an effective displacement caused by a boundary layer on the sphere in the

stagnation region. A rough approximation of the displacement thickness can be calculated with a relation derived by Homann (54) for incompressible flow over a sphere. The displacement thickness Δ^* due to the boundary layer is given by

$$\frac{\Delta^*}{R} = \frac{0.46}{\sqrt{R_e}} \quad , \tag{V.1}$$

where R_e is the Reynolds number based on the radius of the sphere. This displacement effect is less than 1 percent of the dimensionless stand-off distance for the 1/32 in. diameter sphere and less than 0.2 percent for the 5/8 in. diameter sphere. The relative variation of the dimensionless stand-off distance from the 1/8 to the 5/8 in. diameter spheres, where the greatest variation occurs due to the non-uniform free stream, is only 0.3 percent due to the viscous effect.

Table (V.1) Shock Stand-Off Distance Measurements in Dry Nitrogen

Experiment Number	Nominal Sphere Dia. (in.)	Δ (cm)	$\frac{\Delta}{R}$
240	1/32	0.024	0.628
241	1/16	0.048	0.629
242	1/8	0.097	0.628
243	1/4	0.194	0.623
244	1/4	0.194	0.623
245	1/2	0.384	0.617
246	1/2	0.384	0.616
247	5/8	0.478	0.614

Δ - Stand-off distance.

R - Radius of sphere.

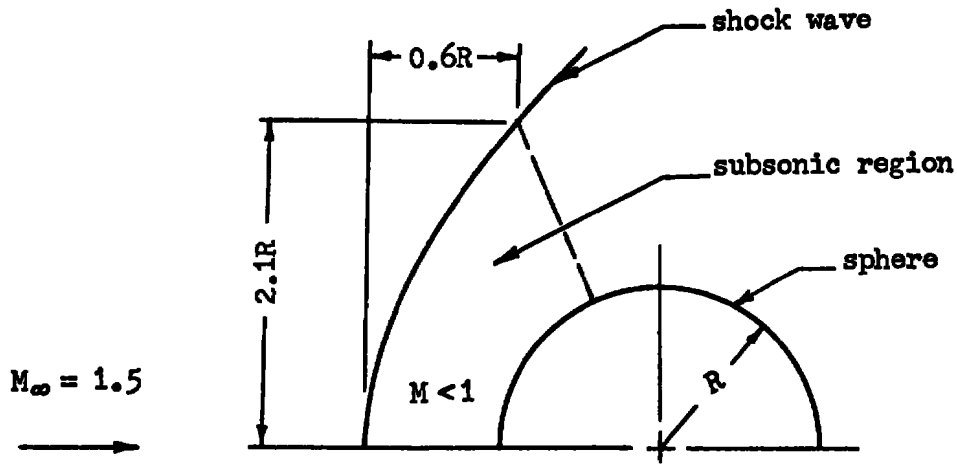

Fig. V.1 An Approximation of the subsonic region in supersonic flow over a sphere at a free stream Mach number of 1.5

Appendix VI
Numerical Calculations

An outline of the computational method used with Yale's IBM 7094/7040 DCS computer is given below. Three computational programs are described: the calculation of the reactant mass fraction of the model reacting gas mixture, the flow in the tunnel and the flow through a normal shock wave. The computational scheme consists of a main program and a large number of short subroutines. All calculations are performed in the subroutines. The main program serves to read the initial data, call the appropriate subroutines, print out the desired results and perform minor calculations such as conversion of units.

Consider first the calculation of the reactant mass fraction. The preparation of the reactant gas mixture takes place in three steps, i.e. the addition of a small quantity of nitrogen, a quantity of an equilibrium mixture of NO_2 and N_2O_4 gases and a final charge of nitrogen. For each addition, the total temperature and pressure is recorded, and from this data the reactant mass fraction is calculated. The initial pressure and temperature is denoted by p_1 and T_1 and the total temperature and pressure after the addition of reactants by p_2 and T_2. Since the temperature of the gas mixture may change during the addition of reactants, the new partial pressure of the nitrogen is given by

$$p_{N_2} = p_1 \frac{T_2}{T_1} \quad . \tag{VI.1}$$

The partial pressure of reactants, p_{r2}, is given by

$$p_{r2} = p_2 - p_{N_2}, \tag{VI.2}$$

the degree of dissociation by

$$\alpha_2 = \sqrt{\frac{K_p(T_2)}{K_p(T_2) + 4p_{r2}}} \quad , \tag{VI.3}$$

and the reactant mass fraction by

$$\omega_{o2} = \frac{1}{1 + \frac{\mu_{N_2}}{\mu_{N_2O_4}} \frac{p_{N_2}}{p_{r2}} (1 + \alpha_2)} \quad , \tag{VI.4}$$

where $K_p(T_2)$ is the equilibrium constant given by Equation (I.2). After the final charge of nitrogen is introduced the temperature of the gas

system may change again and the partial pressure of the constituents must be recalculated accordingly. If the final pressure and temperature is denoted by p and T, the new partial pressure, p_{N3}, of the initial charge of nitrogen becomes

$$p_{N3} = p_1 \frac{T}{T_1} \quad . \tag{VI.5}$$

The partial pressure of the reactants is given by

$$p_r = \frac{K_p(T)(1 - \alpha^2)}{4\alpha^2} \quad , \tag{VI.6}$$

where

$$\alpha = \frac{B}{2A} \left[- 1 + \sqrt{1 + 4A/B} \right] \quad , \tag{VI.7}$$

and $A = 4p_{N3}/K_p(T)$ and $B = (1-\omega_{o2})\mu_{N_2O_4}/(\omega_{o2}\mu_{N_2})$.

The reactant mass fraction of the gas mixture is then given by

$$\omega_o = \frac{1}{1 + \frac{\mu_{N_2}}{\mu_{N_2O_4}} \left(\frac{p}{p_r} - 1\right)(1 + \alpha)} \quad . \tag{VI.8}$$

The above calculation is performed by the subroutine INTANK (p_1, T_1, p_2, T_2, p, T, α, ω_o).

A simplified flow chart of the main program for the calculation of the flow properties in the wind tunnel is shown in Figure (VI.1). The notation used in the flow chart is the same as used throughout the text. The temperature and pressure of the undisturbed gas in the pressure tube and the reactant mass fraction serve as the input data. All the physical constants of the given gas mixture are evaluated in the subroutine CON. Subroutine MATCH matches the solution of the flow through the expansion fan with the solution of the flow through the nozzle at the point where the pressure tube meets the nozzle entrance. This subroutine gives the values of the properties at the entrance to the nozzle, the stagnation enthalpy conditions at the throat and the mass flow rate. Subroutine NUSTAG calculates the new stagnation conditions for the nozzle flow. Next, the area ratio of the test section is read into the program. The subroutine DOWNST calculates the T and α at the test section and the subroutine VAR2 calculates the remainder of the properties there. The subroutine GEOM provides information of the geometry of the nozzle (nozzle expansion rate, dA/dx') and the properties associated with the geometry of the nozzle. A test for the freezing point (i.e. departure from equilibrium flow) is made by the subroutine FREEZ2.

The simplified flow chart of the main program for the calculation of the flow properties through the shock wave is shown in Figure (VI.2).

The temperature, pressure, reactant mass fraction and velocity in the free stream serve as the input data. The physical properties of the mixture are again given by the subroutine CON. The symbol A_i in Figure (VI.2) denotes a group of subroutines: PROP, SOUND and RELAX which are used to calculate the sound speeds, Mach numbers, and relaxation times at a given reference state. Thus, the group A_1 calculates these properties in the free stream. Subroutine FROZ gives the frozen conditions behind the shock wave and the group A_2 is used to calculate Mach number, local relaxation time, etc., there. The equilibrium solution of the shock wave is given by the subroutine HUGOS and the group A_5 gives the appropriate Mach number, etc., there. The reaction profile behind the normal shock wave as a function of time and, in particular, the time required for the degree of dissociation to reach 95 percent of its equilibrium value, is calculated by the subroutine NOLIRE. Once the variation of the degree of dissociation with time is known, the corresponding variation of the remaining variables are given by the subroutine SOFA.

In the calculation of both the tunnel and shock wave flows a number of subroutines are needed which do not appear explicitly in these main programs but do appear in the subroutines mentioned in them. These additional subroutines, some of which are common to both programs, are listed below with a brief description of each subroutine. The variables which are needed by the subroutine appear on the left of the argument and the variables which are calculated by the subroutine are separated by a space and appear on the right.

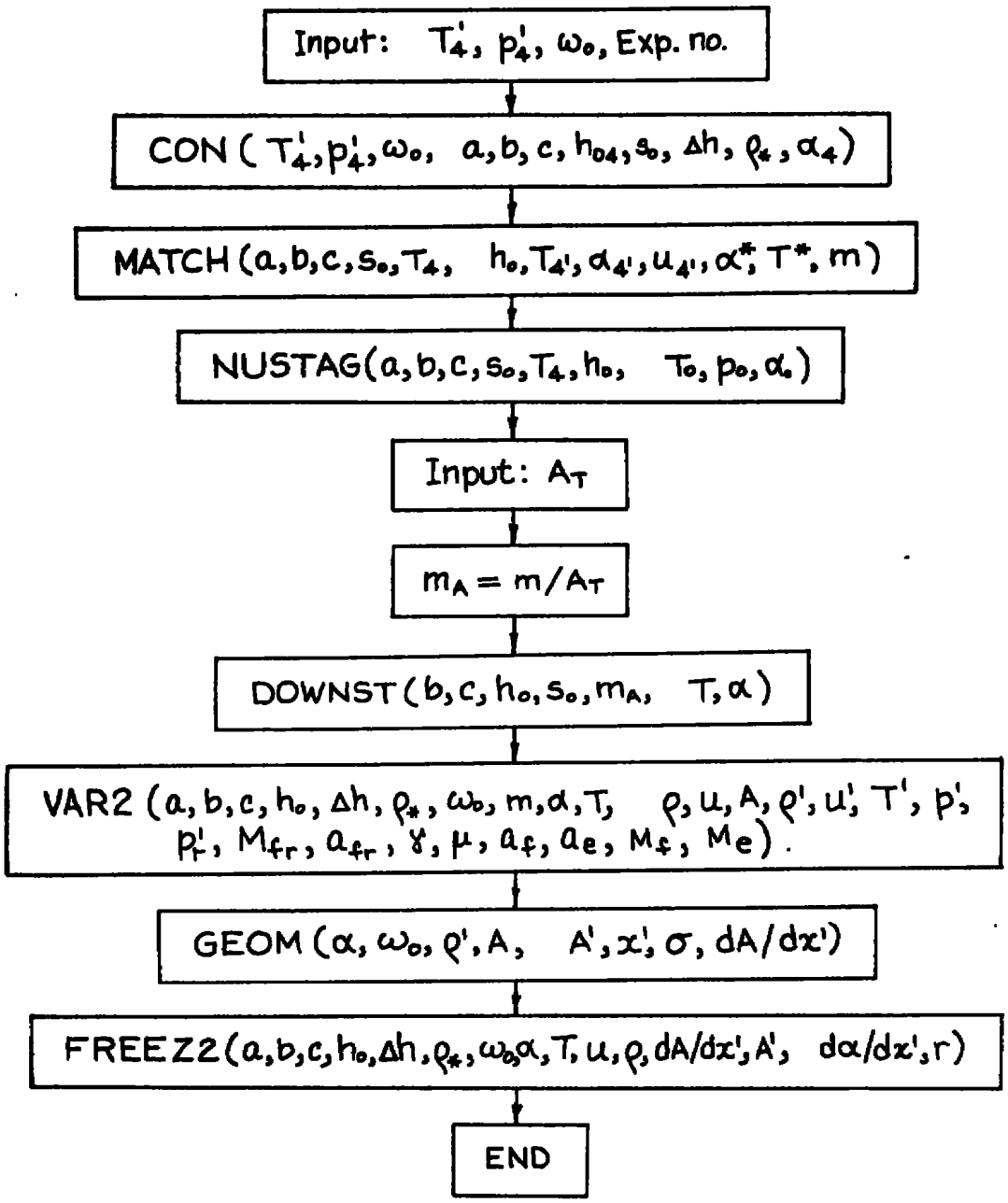

Fig. (VI.1) Simplified flow chart of the main program for the calculation of flow properties in the wind tunnel

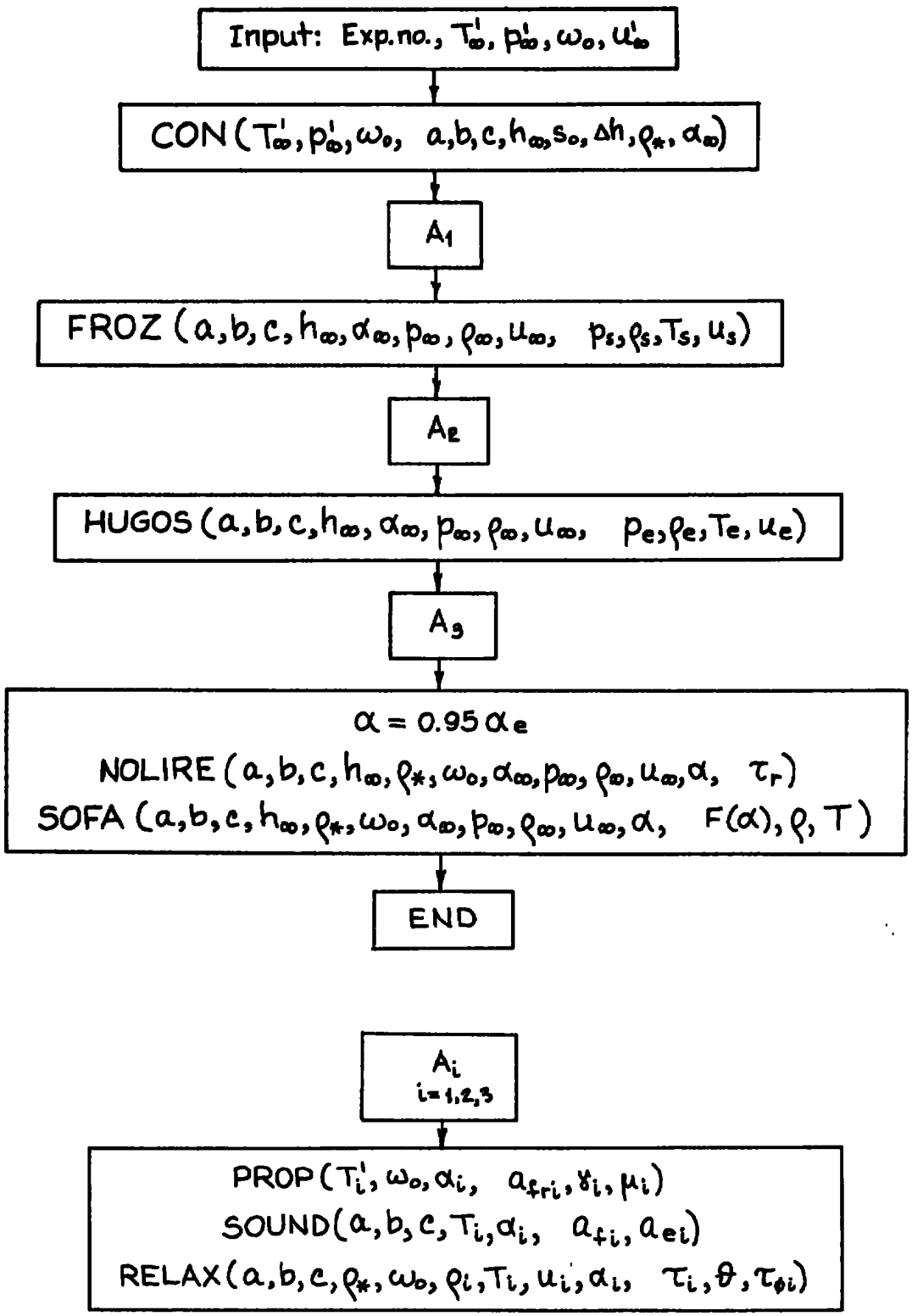

Fig. (VI.2) Simplified flow chart of the main program for the calculation of the flow properties through a normal shock wave

XISENT (b, c, s_o, T, α) - A solution of the isentropic relation, Equation (III.15). For a given gas mixture and at a given temperature the corresponding degree of dissociation is found.

XISAT (b, c, s_o, α, T) - The same as XISENT, except the corresponding temperature is found for a given degree of dissociation.

THROAT (b, c, s_o, α_o, α^*, T^*, m) - The mass flow rate and the conditions at the throat are found. This subroutine gives the simultaneous solution to Equation (III.20) and Equation (III.15) evaluated at the throat.

CUBIX (b, c, h_o, α, T) - The solution of the cubic Equation (III.20) used in the subroutine THROAT.

ALPHCO (b, c, h_o, α, ϕ_1, ϕ_2, ϕ_3, ϕ_4) - Evaluation of the coefficients appearing in the cubic Equation (III.19).

UPSTR (b, c, h_o, s_o, T_o', m_A, T, α, u) - Solution of the flow properties in the nozzle at a point upstream of the throat.

UPTWO (h_o, c, m_A, T, α) - Solution of an equation of the form of Equation (III.21). The degree of dissociation is found for a given gas mixture, mass flow rate and temperature.

YALP (h_o, c, G, Y, T, α) - Solution of a cubic equation which appears in the subroutine UPTWO. The variables G and Y are defined in subroutine UPTWO.

DOWN (c, h_o, m_A, α, T) - This subroutine is similar to sub-UPTWO except that the temperature is found for a given gas mixture, mass flow rate and degree of dissociation.

SOUND (a, b, c, T, α, a_f, a_e) - The frozen and equilibrium sound speeds are evaluated for a given gas mixture, temperature and pressure.

PROP (T', ω_o, α, a_{fr}, γ, μ) - The specific heat ratio γ, the molecular weight μ, and the frozen sound speed a_{fr}, of the mixture are evaluated. The frozen sound speed in this subroutine is obtained from an equation of the form $a_{fr}^2 = \gamma RT'/\mu$.

INTEG (a, b, c, s_o, $T_{4'}$, T_4, $u_{4'}$) - The integral which appears in Equation (III.25) is evaluated by Simpson's rule. The flow chart for this subroutine is taken from Southworth and Deleeuw (55).

XOFOT (a, b, c, s_o, T, F(T)) - The integrant F(T), of the integral appearing in Equation (III.25) is evaluated.

References

1. Freeman, N. C. 1958 Non-equilibrium flow of an ideal dissociating gas. J. Fluid Mech. 4, 407.

2. Conti, R. J. 1966 A theoretical study of non-equilibrium blunt-body flows. J. Fluid Mech. 24, 65.

3. Lick, W. 1960 Inviscid flow of a reacting mixture of gases around a blunt body. J. Fluid Mech. 7, 128.

4. Van Dyke, M. D. 1966 The blunt-body problem revisited. Fundamental Phenomena in Hypersonic Flow. Ithaca: Cornell University Press.

5. Schwartz, R. N. & Eckerman, J. 1956 Shock location in front of a sphere as a measure of real gas effects. J. Appl. Phys. 27, 169.

6. Eckerman, J. 1961 The measurement of the rate of dissociation of oxygen at high temperatures. NAVORD Report 6724.

7. Lobb, K. R. 1963 Experimental measurement of shock detachment distance on spheres fired in air at hypervelocities. High Temperature Aspects of Hypersonic Flow. New York: Pergamon Press.

8. Serbin, H. 1958 The high speed flow of gas around blunt bodies. The Aeronautical Quarterly 9, 313.

9. Hayes, W. D. & Probstein, R. F. 1966 Hypersonic Flow Theory Volume 1. New York: Academic Press.

10. Van Dyke, M. D. 1958 The supersonic blunt-body problem - review and extension. J. Aero-Sciences. 25, 485.

11. Van Dyke, M. D. & Gordon, H. D. 1959 Supersonic flow past a family of blunt axisymmetric bodies. NASA TR R-1.

12. Kendall, J. M., Jr. 1959 Experiment on supersonic blunt-body flows. Prof. Rep. 20-372, Jet Propulsion Lab., Pasadena, California.

13. Zeldovich, Ya. B. & Raiser, Yu. P. 1966 Physics of Shock Waves and High-Temperature Hydrodynamic Phenomena. New York: Academic Press.

14. Chernyi, G. G. 1961 Introduction to Hypersonic Flow. New York: Academic Press.

15. Damköhler, G. 1936 Einflüsse der Strömung, Diffusion und des Wärmeüberganges auf die Leistung von Reaktionsöfen. I Allgemeine Gesichtspunkte für die Übertragung eines chemiches Prozesses aus dem Kleinen ins Grosse. Ztschr. Electrochem. 42, No. 12, 846.

16. Lighthill, M. J. 1957 Dynamics of a dissociating gas. Part I equilibrium flow. J. Fluid Mech. 2, 1.

17. Gibson, W. E. & Sowyrda, A. 1962 An analysis of non-equilibrium inviscid flows. AEDC-TDR-62-172.

18. Hall, J. F., Eschenroeder, A. Q. & Marrone, P. V. 1962 Blunt-nose inviscid airflows with coupled non-equilibrium processes. J. Aerospace Sci. 29, 1038.

19. Wood, W. W. & Kirkwood, J. G. 1957 Hydrodynamics of a reacting and relaxing fluid. J. Appl. Phys. 28, 395.

20. Gray, P. & Yoffe, A. D. 1955 The reactivity and structure of nitrogen dioxide. Chem. Rev. 55, 1069.

21. Carrington, R. & Davidson, N. 1953 Shock waves in chemical kinetics: the rate of dissociation of N_2O_4. J. Phys. Chem. 57, 418.

22. Wegener, P. P. 1958 Measurement of rate constants of fast reactions in a supersonic nozzle. J. Chem. Phys. 28, 724.

23. Wegener, P. P. 1961 A review of investigations of stationary supersonic nozzle flow with reacting gas mixture. Combustion and Propulsion - Fourth AGARD Colloquium. Oxford: Pergamon Press.

24. Wegener, P. P., Chu, B.-T., & Klikoff, W. A. 1965 Weak waves in relaxing flows. J. Fluid Mech. 23, 787.

25. Ludwieg, H. 1955 Der Rohrwindkanal. Zeitschrift für Flugwissenschaften, Jahrgang 3, Heft 7, 206.

26. Ludwieg, H. 1957 The tube wind tunnel - a special type of blow-down tunnel. AGARD Report 143.

27. Hottner, T. H. 1965 Untersuchungen an einem Modell-Rohrwindkanal bei Machzahlen von Ma = 3 bis 6. Zeitschrift für Flugwissenschaften, Jahrgang 13, Heft 7, 237.

28. Cable, A. J. & Cox, R. N. 1963 The Ludwieg pressure-tube supersonic wind tunnel. The Aeronautical Quarterly, 14, Part 2, 143.

29. Alpher, R. A. & White, D. F. 1957 Flow in shock tubes with area change at the diaphragm section. J. Fluid Mech. 3, 457.

30. Becker, E. 1958 Reibungswirkungen beim Rohrwindkanal. Mitteilungen aus dem Max-Plank-Institut für Strömungsforschung und der Aerodynamischen Versuchsanstalt, No. 20.

31. Ames Research Staff 1953 Equations, tables, and charts for compressible flow. NACA Report 1135.

32. Bray, K. N. C. 1959 Atomic recombination in a hypersonic wind tunnel nozzle. J. Fluid Mech. 6, 1.

33. Becker, E. 1957 Grenzschichteffekte beim Rohrwindkanal. Jahrbuch 1957 der WGL, 232.

34. Hall, T. C., Jr. & Blacet, F. T. 1952 Separation of the absorption spectra of NO_2 and N_2O_4 in the range of 2400-5000 Å. J. Chem. Phys. 20, 1745.

35. Vincenti, W. G. & Kruger, C. H., Jr. 1965 Introduction to physical gas dynamics. New York: John Wiley & Sons, Inc.

36. Clarke, J. F. & McChesney, M. 1964 The dynamics of real gases. Washington: Butterworths.

37. Bodenstein, M. 1922 Bildung und Zersetzung der höheren Stickoxyde. Zeitschrift für physicalische Chemie, 100, 68.

38. Giauque, W. F. & Kemp, J. D. 1938 The entropies of nitrogen tetroxide and nitrogen dioxide. The heat capacity from 15°K to the boiling point. The heat of vaporization and vapor pressure. The equilibrium $N_2O_4 = 2NO + O_2$. J. Chem. Phys. 6, 40.

39. Strehlow, R. A. 1964a Private communication.

40. Wegener, P. P. 1960 Experiments on the departure from chemical equilibrium in a supersonic flow. ARS Journal, 30, 322.

41. Strehlow, R. A. 1964b Unpublished communication from H. A. Prophet, Dow Chemical Co.

42. JANAF 1961 Interim Thermochemical Tables. Dow Chemical Company.

43. Wegener, P. P. & Cole, J. D. 1962 Experiments on propagation of weak disturbances in stationary supersonic nozzle flow of chemically reacting gas mixtures. Eighth Symposium (International) on Combustion. Baltimore: Williams and Wilkins Co.

44. Broer, L. J. F. 1958 Characteristics of the equation of motion of a reacting gas. J. Fluid Mech. 4, 276.

45. Maccoll, J. W. 1937 The conical shock wave formed by a cone moving at a high speed. Proceedings of the Royal Society of London, Series A. 159, 459.

46. Persh, J. & Lee, R. 1956 Tabulation of compressible boundary layer parameters. NAVORD Report 4282.

47. Ruptash, J. 1953 Growth of boundary layer in supersonic nozzles. Symposium on High-Speed Aerodynamics, Summary of Proceedings, NAE, Ottawa, 42.

48. Kovasznay, L. S. G. 1949 High power short duration spark discharge. Rev. of Sci. Inst. 20, 696.

49. Klikoff, W. A. 1965 Propagation of Weak Conical Disturbances in Relaxing Supersonic Flows. D. Eng. Thesis. Yale University, New Haven.

50. Eberstein, I. J. 1966 Evaluation of light deflection technique for detection of transient shock waves. Rev. of Sci. Inst. 37, 959.

51. Liepman, H. W. & Roshko, A. 1957 Elements of Gasdynamics. New York: John Wiley & Sons, Inc.

52. Greene, E. F. & Hornig, D. F. 1953 The shape and thickness of shock fronts in argon, hydrogen, nitrogen and oxygen. J. Chem. Phys. 21, 617.

53. Moeckel, W. E. 1949 Approximate method for predicting form and location of detached shock waves ahead of plane or axially symmetric bodies. NACA TN 1921.

54. Homann, F. 1936 The effect of high viscosity on the flow around a cylinder and around a sphere. NACA TM 1334.

55. Southworth, R. W. & Deleeuw, S. L. 1965 Digital Computation and Numerical Methods, p. 376. New York: McGraw-Hill Book Company.

56. Heberle, J. W., Wood, G. P. & Gooderum, P. B. 1950 Data on shape and location of detached shock waves on cones and spheres. NACA TN 2000.

57. Nagamatsu, H. T. 1949 Theoretical investigation of detached shock. Ph.D. Thesis. California Institute of Technology, Pasadena.

58. Jenkins, A. H., Jenkins, B. Z. & Johnson, L. H. 1966 Transonic and low supersonic shock shape solutions. AIAA, 4, 1483.

UNCLASSIFIED

Security Classification

DOCUMENT CONTROL DATA - R & D

(Security classification of title, body of abstract and indexing annotation must be entered when the overall report is classified)

1. ORIGINATING ACTIVITY (Corporate author)	2a. REPORT SECURITY CLASSIFICATION
Yale University New Haven, Connecticut 06520	UNCLASSIFIED
	2b. GROUP N/A

3. REPORT TITLE

EXPERIMENTS ON NON-EQUILIBRIUM SUPERSONIC FLOW SHOCK STAND-OFF DISTANCE OF SPHERES CARRIED OUT IN A NEW TYPE OF INTERMITTENT WIND TUNNEL

4. DESCRIPTIVE NOTES (Type of report and inclusive dates)

July 1, 1965 to December 31, 1966 - Final Report

5. AUTHOR(S) (First name, middle initial, last name)

George Buzyna and Peter P. Wegener, Yale University

6. REPORT DATE	7a. TOTAL NO. OF PAGES	7b. NO. OF REFS
May 1969	110	58

8a. CONTRACT OR GRANT NO.	9a. ORIGINATOR'S REPORT NUMBER(S)
AF40(600)-1133	
b. PROJECT NO. 8952	AEDC-TR-69-81
c. Program Element 62201F	9b. OTHER REPORT NO(S) (Any other numbers that may be assigned this report)
d. Task 895208	N/A

10. DISTRIBUTION STATEMENT

This document has been approved for public release and sale; its distribution is unlimited.

11. SUPPLEMENTARY NOTES	12. SPONSORING MILITARY ACTIVITY
Available in DDC.	Arnold Engineering Development Center Arnold AF Station, Tennessee 37389

13. ABSTRACT

An experimental investigation of the non-equilibrium behavior of the shock stand-off distance ahead of spheres is described. Wind tunnel experiments using a well understood reacting model gas mixture with a single relaxation process are performed. A marked variation of the dimensionless shock stand-off distance as a function of a non-equilibrium parameter patterned after that proposed by Damköhler is observed. Qualitatively, the results are found to be in agreement with theoretical predictions in the literature. A new application of the Ludwieg tube intermittent supersonic wind tunnel to the study of non-equilibrium flow is presented in the process of this work. The behavior of the intermittent tunnel as a tool is non-equilibrium flow research is calculated in some detail. Experimental results on the facility performance are included for comparison.

DD FORM 1 NOV 65 1473

UNCLASSIFIED

Security Classification

14. KEY WORDS	LINK A		LINK B		LINK C	
	ROLE	WT	ROLE	WT	ROLE	WT
spheres						
shock waves						
supersonic flow						
wind tunnel testing						